

THESIS ON CIVIL ENGINEERING F33

Development of Accelerating Pipe Flow Starting from Rest

IVAR ANNUS

TUT
PRESS

TALLINN UNIVERSITY OF TECHNOLOGY
Faculty of Civil Engineering
Department of Mechanics

**Dissertation was accepted for the defence of the degree of Doctor of
Philosophy in Engineering on September 28, 2011**

Supervisor: Professor Tiit Koppel, Department of Mechanics, Tallinn
University of Technology

Opponents: Professor Bruno Brunone, Department of Civil and Environmental
Engineering, University of Perugia, Italy

PhD Rein Ruubel, Science and Innovation Investment Fund,
Zagreb, Croatia

Defence of the thesis: November 8, 2011

Declaration:

Hereby I declare that this doctoral thesis, my original investigation and
achievement, submitted for the doctoral degree at Tallinn University of
Technology has not been submitted for any academic degree.

/Ivar Annus/

Copyright: Ivar Annus, 2011
ISSN 1406-4766
ISBN 978-9949-23-183-6 (publication)
ISBN 978-9949-23-184-3 (PDF)

EHITUS F33

**Paigalseisust algava kiireneva voolamise
areng torus**

IVAR ANNUS

TABLE OF CONTENTS

LIST OF TABLES	7
LIST OF FIGURES.....	8
NOMENCLATURE.....	10
INTRODUCTION.....	12
Motivation.....	12
Aim of investigation	13
Acknowledgements.....	14
1. LITERATURE REVIEW.....	15
1.1 Historical review.....	15
1.2 Hypotheses describing the development of flow and the transition to turbulence in accelerating pipe flows starting from rest.....	23
1.3 Summary.....	34
2. MATHEMATICAL MODEL FOR FLOW WITH CONSTANT ACCELERATION	37
2.1 Equations for compressible fluid on a long pipe	37
2.2 One dimensional model	41
2.3 Equations for start-up flows.....	44
2.4 Dynamical boundary layer in a pipe	45
2.5 Flow with constant acceleration.....	48
3. EXPERIMENTAL APPARATUS AND INSTRUMENTATION	50
3.1 Description of the test facility.....	50
3.2 Description of instrumentation	52
3.3 Shear stress sensor calibration and PIV settings.....	54
4. EXPERIMENTAL RESULTS.....	62
4.1 Experimental program	62
4.2 Experimental results.....	66
4.3 Analysis of different criteria on transition to turbulence.....	83
4.4 Comparison between model and experimental results: the development of velocity profiles	88
4.5 Summary.....	95
5. CONCLUSIONS.....	98
5.1 Summary of findings.....	98
5.2 Recommendation for future research.....	100
BIBLIOGRAPHY	101
Papers presented by the candidate	101
List of references.....	102
ABSTRACT	110
KOKKUVÕTE.....	111
CURRICULUM VITAE	112

ELULOOKIRJELDUS.....	115
APPENDIX A	117

LIST OF TABLES

<i>Table 4. 1 – List of experiments in A1 test series</i>	62
<i>Table 4. 2 – List of experiments in A1A test series</i>	63
<i>Table 4. 3 – List of experiments in B test series</i>	64
<i>Table 4. 4 – Variation of forces in time</i>	82
<i>Table 4. 5 – Dependence between τ^* and α</i>	85
<i>Table A. 1 – Experimental results, A1 test series</i>	117
<i>Table A. 2 – Experimental results, A1A test series</i>	117
<i>Table A. 3 – Experimental results, B test series</i>	118
<i>Table A. 4 – Sequence in reaction to turbulence, A1 test series</i>	119
<i>Table A. 5 – Sequence in reaction to turbulence, A1A test series</i>	120
<i>Table A. 6 – Sequence in reaction to turbulence, B test series</i>	121

LIST OF FIGURES

Figure 1. 1 - The regions in which slugs and puffs occur in transitional pipe flow as a function of the disturbance level (Wyganski and Champagne, 1973)	25
Figure 1. 2 – Outcomes of experiments using a single-jet disturbance as a function of disturbance amplitude and Re (Darbyshire and Mullin, 1995).....	25
Figure 1. 3 – Laminar to turbulent transition modes in accelerating pipe flows (Moss, 1989)	26
Figure 1. 4 – Surface shear stress sensor output exhibiting a turbulent slug (Lefebvre and White, 1991)	28
Figure 1. 5 – Wavy appearance of the spots of turbulence (Kask and Koppel, 1987)	29
Figure 1. 6 – Time-wise evolution of local mean velocity and turbulence intensity at three radial positions (Viola and Leutheusser, 2004) ...	32
Figure 1. 7 - Variation of forces in the flow by the one-dimensional equation of motion. \square - Frictional force on the wall; \blacklozenge - Pressure force (Ruubel, 1991).....	33
Figure 3. 1 – Test rig for accelerating flows (reversible and non-reversible) (Vardy et. al., 2009)	51
Figure 3. 2 – Test section	52
Figure 3. 3 - Layout of dynamic instruments in a test rig for non-reversing and reversing accelerating flows (Vardy et. al., 2009)....	53
Figure 3. 4 – Positions of the hot-films	54
Figure 3. 5 – Calculated shear stress versus the Reynolds number	55
Figure 3. 6 – Calibration curves for hot-film 2, steady state run Group0A020	57
Figure 3. 7 – Calculated velocity vector field, test A1A076, $Re_l = 0$, $Re_f = 400\,000$, $t_v = 2\,s$	59
Figure 3. 8 – Image for PIV calibration	60
Figure 3. 9 – Example of an air pocket causing erroneous vectors.....	61
Figure 4. 1 – Case A1A007; a – variation of the flow rate, b – variation of shear stresses.....	67
Figure 4. 2 - Dependence between the acceleration rate and transition period	68
Figure 4. 3 – Case A1027; a – variation of the flow rate, b – variation of pressure, c – variation of hot-film output.....	70
Figure 4. 4 – Case A1A014; a – variation of the flow rate, b – variation of pressure, c – variation of hot-film output.....	72

<i>Figure 4. 5 – Variation of the mean flow rate.....</i>	<i>74</i>
<i>Figure 4. 6 – Variation of mean pressure</i>	<i>74</i>
<i>Figure 4. 7 – Variation of mean wall shear stress</i>	<i>75</i>
<i>Figure 4. 8 – Variation of RMS of wall shear stress.....</i>	<i>75</i>
<i>Figure 4. 9 – Development of the velocity profile in accelerating flow... </i>	<i>77</i>
<i>Figure 4. 10 – Development of turbulent intensity in accelerating flow.. </i>	<i>78</i>
<i>Figure 4. 11 – Variations of axial velocity components in three different radial positions and shear stress at the wall.....</i>	<i>79</i>
<i>Figure 4. 12 – Variation of the radial velocity component in accelerating flow; a – case A1A031; b – case A1A058; c – case A1A061; d – case A1A069; e – ensemble average</i>	<i>80</i>
<i>Figure 4. 13 – Propagation of the radial velocity component in time in accelerating flow</i>	<i>81</i>
<i>Figure 4. 14 – Equilibrium of forces</i>	<i>82</i>
<i>Figure 4. 15 – Correlation of the critical Reynolds number.....</i>	<i>83</i>
<i>Figure 4. 16 – Variation of dimensionless transition time τ^* versus dimensionless acceleration α</i>	<i>84</i>
<i>Figure 4. 17 – Dependence between the critical Reynolds number and acceleration in logarithmic scale</i>	<i>86</i>
<i>Figure 4. 18 – Dependence between the critical Reynolds number and dimensionless acceleration in logarithmic scale</i>	<i>87</i>
<i>Figure 4. 19 – Theoretical and measured ensemble averaged dimensionless velocity profiles, a – $A = \text{const}$; b – $A \neq \text{const}$.....</i>	<i>89</i>
<i>Figure 4. 20 - Comparison between numerical and ensemble averaged dimensionless pressures p_1 and p_2.</i>	<i>92</i>
<i>Figure 4. 21 - Modeled and measured ensemble averaged dimensionless velocity profiles</i>	<i>93</i>
<i>Figure 4. 22 – The development of modeled dimensionless radial velocity over the radius in different time-steps.....</i>	<i>94</i>
<i>Figure 4. 23 – Comparison between measured and modeled mean velocities.....</i>	<i>95</i>

NOMENCLATURE

a	Dimensionless pressure gradient
A	Acceleration [m/s^2]
c	Speed of sound in fluid [m/s]
D	Pipe diameter [m]
Dn	Dissipation number
Eu	Euler number
I_n	Modified Bessel function of the first kind of order n
k	Pipe roughness [mm]
L	Pipe length [m]
$L(\tau)$	Weighting function
M	Mach number
N	Number of repeated runs
p	Fluid pressure [Pa]
P_0	Reference value of pressure [Pa]
q	Dimensionless pressure
r	Radial coordinate [m]
R	Pipe radius [m]
Re	Reynolds number
Re_l	Initial Reynolds number
Re_f	Final Reynolds number
s	Laplace parameter
Sh	Strouhal number
t	Time [s]
t_v	Valve opening time [s]
T_0	Reference value of time [s]
u	Dimensionless axial velocity
u_r	Radial velocity [m/s]
u_z	Axial velocity [m/s]
U	Dimensionless mean velocity
U_0	Reference value of velocity [m/s]
v	Dimensionless radial velocity
V	Mean velocity [m/s]
z	Axial coordinate [m]

Greek

α	Dimensionless acceleration
β_k	Zeros of the modified Bessel function of the first kind of order zero $I_0(\beta)$
γ_k	Positive zeros of the modified Bessel function of the first kind of order two $I_2(\gamma)$
ε	Dimensionless ratio

η	Dimensionless radial coordinate
ϑ	Dimensionless distance from the pipe wall
ε	Dimensionless wall shear stress
μ	Dynamic viscosity [Pa·s]
ν	Kinematic viscosity [m ² /s]
ζ	Dimensionless axial coordinate
ρ	Fluid density [kg/m ³]
τ	Dimensionless time
τ_w	Wall shear stress [N/m ²]

Subscripts

* Values at the moment of transition

Abbreviations

CFD	Computational Fluid Dynamics
LDV	Laser Doppler Velocimetry
PIV	Particle Image Velocimetry
RMS	Root Mean Square

INTRODUCTION

Motivation

Unsteady flows in pipes and ducts have been the source for experimental and theoretical investigations for over a century. From a theoretical point of view, unsteady pipe flows have remained an enigma, as the mathematical models available are not suitable to describe all the aspects of dynamic flow patterns. From a practical point of view, unsteady flows can be the source of many unwanted phenomena – sudden valve closure, pump failure, water-turbine emergency shutdown etc can cause water hammer events and therefore be responsible for numerous pipe failures (in water, waste water, oil-hydraulic, hydro-power systems) and for unacceptable noise in workplaces.

In recent years interest in transient problems in pipeline systems has substantially increased. Unsteady flow models have been developed to describe transitional processes like water-hammer, two-phase flow in pipes etc more precisely (for example employing unsteady friction into the models) and to reduce the risk of pipe rupture. In addition to that, transient models are also employed as diagnostic tools. Pressure waves in a pipe system are used to obtain information about the physical characteristics of the system. Inverse transient analysis methods are proposed for the hydraulic model calibration and for the location of system leakage (Ferrante and Brunone (2003), Kapelan et. al. (2004)).

Developers and users of models of unsteady skin friction and transient pipe flow need full-scale data with which to compare and justify their models. Experimental data for model validation is limited and available mainly for low Reynolds number flow cases. Therefore, there is a strong need for detailed measurements in flows at higher Reynolds numbers. In addition, there is a need for a wider range of well-controlled acceleration/deceleration rates and detailed visualization of flow structures and profiles. To address these needs, a large-scale pipeline apparatus at Deltares, Delft, the Netherlands, was recently used for unsteady skin friction experiments including acceleration, deceleration and acoustic resonance tests. The project “Unsteady friction in pipes and ducts” was divided into three groups and the author of the thesis was directly involved with one of them – accelerating pipe flows starting from rest. This included the planning of the test program, procedure and carrying out the experiments. It should be noted that the development of flow and transition to turbulence in accelerating pipe flows has been a subject of an ongoing research in Tallinn University of Technology for the past forty years.

In the thesis the start-up unsteady flow as a special case of transient flow is taken under investigation in the light of new experimental findings gained in a large-scale pipeline system in Deltares. Accelerated pipe flow starting from rest can be considered as an everyday practical problem – it occurs every time we

start a pump, open a valve etc. Therefore in this thesis the main emphasis is put on the practical point of view – how mid and high acceleration rates influence mean flow, pressure and friction in the system. Flow visualization (PIV measurements) is used to describe the unsteady processes at the transition to turbulence. The aim is to analyze integrally the propagation of turbulence over the cross-section of the pipe and how the radial velocity component is developing in the flow.

In the first chapter of the thesis a historical overview of theoretical and experimental findings regarding the flow development and transition to turbulence in steady and unsteady flow (including accelerating start-up flow) in pipes is given. Experimental work in this field has been very active over the past half a century. Different hypothesis posed in those investigations are brought forth.

The second chapter focuses on a mathematical model that is used to calculate the velocity profiles in constant accelerating pipe flows starting from rest. The novelty of the model is that it is derived emanated from the initial and boundary conditions used in experiments carried out in Deltares – describing the development of constant accelerating pipe flow starting from rest. The model is based on Navier-Stokes equations and derived for a one-dimensional case. The third chapter of the thesis gives an overview of the test rig used in experimental work. It includes a description of instrumentation, calibration methods and drawbacks faced in the experimental process.

In the fourth chapter experimental results and conclusions are given. It includes an overview of the experimental program carried out, interpretation of the experimental results, comparison between the 1D and 2D model and experimental results. Different criteria describing the transition to turbulence posed in earlier studies are analyzed. New experimental findings are analyzed in the light of the hypothesis brought forth in earlier investigations.

The final chapter gives a summary of the findings and recommendations for future research.

Aim of investigation

The thesis will focus on accelerating pipe flows starting from rest. The study involves the analysis of the development of accelerating flow and transition to turbulence in start-up constant accelerating flows. The aim is to validate the existing hypothesis and model results in the light of new experimental data gained in a large-scale pipeline. The specific objectives can be outlined as follows:

- ◆ To analyze the effect of transition to turbulence in accelerating pipe flows from a practical point of view – the effects on mean flow rate, pressure and friction.

- ◆ To modify an existing 1D unsteady flow model to describe the development of velocity profiles in constant accelerating flows starting from rest and to compare different model results with experimental data.
- ◆ To validate the existing hypothesis about accelerating pipe flow based on new experimental data.
- ◆ To analyze different criteria based on mean values proposed in earlier studies describing transition to turbulence in accelerating pipe flow.
- ◆ To describe the development of the radial velocity component, flow structures and the transition process itself based on the 2D model, flow visualization and other measurements.

Acknowledgements

I would like to thank my supervisor Prof. Tiit Koppel for his guidance and advice throughout the PhD studies.

The help of Prof. *emeritus* Leo Ainola and PhD Laur Sarv is greatly appreciated for the assistance with mathematical models and numerical calculations. Thanks to all colleagues from the Department of Mechanics for the support, motivation and fruitful discussions.

I would like to give my gratitude to all the researchers involved with the project “Unsteady friction in pipes and ducts”. Thank you for the opportunity to participate in the project and to carry out an experimental investigation in start-up pipe flows. Special thanks to the staff from Deltares for their contribution to setting up the test rig and measurement system.

Finally, I would like to thank my family and friends for the support throughout my studies.

This work has been supported by the European Community's Sixth Framework Program through the grant to the budget of the Integrated Infrastructure Initiative HYDRALAB III within the Transnational Access Activities, Contract No. 022441. The financial support by the Estonian Science Foundation (Grant No. 7646) is greatly appreciated.

1. LITERATURE REVIEW

A literature review of experimental and numerical investigations carried out in unsteady pipe flow over the past half a century is given in this chapter. In Section 1.1 a more general historical overview of studies on flow development and transition to turbulence in steady laminar, periodic and turbulent flow, including the main results, is presented. In addition, a brief synopsis of the development of mathematical models based on Navier-Stokes and continuity equations used in applied engineering problems of transient pipe flow is brought forth.

Section 1.2 focuses on the experimental studies that have investigated the flow development and transition to turbulence in accelerating start-up pipe flows. From the main results of these studies a list of hypothesis is drawn describing the processes in start-up accelerating flows. These conjectures are examined later on in the light of new experimental results.

1.1 Historical review

Historically the first widely known experimental investigations, describing the flow transition from laminar to turbulent motion were carried out by Reynolds (1883) and Taylor (1923). In a well-known paper published by Reynolds in 1883, he introduced a parameter, known as the Reynolds number $Re = VD/\nu$, which predicted the transition from laminar to turbulent regime. It was found that the lower critical Reynolds number for transition to turbulence is typically about 2260 and upper about 12 000 but it can vary depending on the disturbances in the inlet of the pipe. Indeed, he suggested that the instability which initiates the turbulence might require a perturbation of a certain magnitude, for a given value of Re , for the unstable motion to take root and turbulence to set in (Davidson, 2006).

Many series of experiments to investigate the transition to turbulence from fully developed laminar pipe flow (for example Wygnanski and Champagne, 1973; Wygnanski et. al., 1975; Eliahou et. al., 1998, Han et. al., 2000, Hof et. al., 2004, Mullin and Peixinho, 2006) have been carried out afterwards and various test results show that the lower critical Reynolds number is in the range of $1800 < Re < 2300$ and upper critical value of the Reynolds number accesses to 100 000 (Darbyshire and Mullin, 1995). So in practice pipe flow becomes turbulent even at moderate velocities. In contrast to other laminar – turbulence transitions, where primary and secondary instabilities of the laminar flow provide guidance, the transition process in pipe flow has remained a near total mystery. In pipes turbulence sets in suddenly and fully, with no intermediate states and without a clear stability boundary (Hof et. al., 2004).

A thorough historical overview of transitional pipe flow in Hagen-Poiseuille flows has been given by Kerswell (2005) looking back to 1686 to trace the earliest studies in fluid mechanics and summarizing recent

understandings about the transition to turbulence in a pipe introducing new traveling wave solutions. The same coherent structures have been widely discussed in another review paper by Eckhardt et. al. (2007).

In transition from laminar to turbulent state in the Hagen-Poiseuille pipe flow two different states are described – puffs and slugs. A thorough experimental study was carried out by Wygnanski and Champagne (1973) who stated that slugs are caused by the instability of the boundary layer to small disturbances in the inlet region of the pipe and puffs are generated by large disturbances at the inlet ($L/D < 15$). While slugs are associated with transition from laminar to turbulent flow, puffs represent an incomplete relaminarization process (therefore not present in accelerating pipe flows). Air was used as the working fluid and disturbances generated with air jets were introduced through slots milled in the pipe wall. Measurements were done using a multichannel hot-wire anemometer system. A similar test rig was used by Wygnanski et. al. (1975), Eliahou et. al. (1998) and Han et. al. (2000). Eliahou et. al. (1998) investigated a bypass transition to turbulence generated by controlled disturbances. Eight acoustic drivers were used to provide periodic blowing and suction through eight slots in the pipe wall. Most of the experiments were carried out by simultaneous generation of two opposing helical modes. It was found that transition to turbulence occurs when vortices develop due to a nonlinear interaction of helical modes, distorting the time-averaged velocity profile. Han et. al. (2000) evoked the transition to turbulence in Hagen-Poiseuille flow by simultaneous excitation of different helical modes. The breakdown to turbulence was noticed with the appearance of spikes in the temporal traces of the velocity. In time the spikes not only propagated downstream but also propagated across the flow. Based on these experimental findings and boundary conditions Reuter and Rempfer (2005) performed a direct numerical simulation using an accurate hybrid finite-difference code for the simulation of unsteady incompressible pipe flow. Modeling results corresponded closely to the self-sustaining process suggested in previous studies – a base flow that is deformed by superimposed high- and low-speed streaks exhibits a linear instability which gives rise to vortices. In addition, it was found that energy transfer changes inside the flow in different time steps of the transition process play a vital role. Hof et. al. (2004) used a 3D PIV system to capture the full three-component velocity field and turbulent structures developing at the transition. A series of tests to identify the propagation of turbulent puffs and slugs were carried out that showed similar streak patterns that appeared close to the solutions of travelling waves. Fully developed laminar flow was destabilized 350 pipe diameters (pipe $D = 40$ mm) from the inlet by means of injecting an impulsive jet through a small hole in the pipe wall. Experimental results were compared with the numerical studies of Faisst and Eckhardt (2003) and Wedin and Kerswell (2004) and good agreement between the two was found. The observations supported a theoretical scenario in which the turbulent state is organized around a few dominant traveling waves. It must be noted that

travelling waves were computed in short pipes (only a few diameters long) while puffs were as long as 20 pipe diameters. Therefore Viswanath and Cvitanović (2009) raised an appropriate question – “*Do the experimentally observed structures correspond to the computed travelling waves?*” Mullin and Peixinho (2006) investigated the stability of Hagen-Poiseuille flow using impulsive perturbations (by either injecting or sucking small amounts of fluid through holes in the pipe wall). Flow visualization (with a travelling camera) and single point LDV measurements were conducted. A definite scaling law for the threshold (amplitude of perturbation) versus the Reynolds number for transition to turbulence was suggested. Ben-Dov and Cohen (2007) suggested a theoretical explanation for the critical Reynolds number based on the minimum energy of an axisymmetric deviation. Linearized Navier-Stokes and continuity equations for small disturbances in an incompressible fluid were used. It was shown that for $Re > 1840$ the minimum energy of the deviation, associated with the central part of the pipe, becomes a global minimum for triggering secondary instabilities. These findings correlated well with previous experimental studies by Wygnanski and Champagne (1973), Wygnanski et. al. (1975), Darbyshire and Mullin (1995) and Mullin and Peixinho (2006). In another study by Ben-Dov and Cohen (2007) it was demonstrated that very small finite-amplitude three-dimensional deviations from the developed base flow in a pipe render instabilities. Numerical simulations showed similar symmetries of streamwise rolls that were presented for travelling wave solutions by Faisst and Eckhardt (2003) and Wedin and Kerswell (2004). Schneider et. al. (2007) showed in their numerical studies that at transition the global structure of the flow field is simple and dominated by two high-speed streaks and a corresponding pair of strong counter-rotating vortices which are located off the center. It showed no discrete rotational symmetry like the traveling waves described in previous studies by Faisst and Eckhardt (2003) and Wedin and Kerswell (2004).

In addition to the above mentioned studies, in recent years numerical simulations for transitional pipe flow have been carried out in short pipes (Viswanath and Cvitanović, 2009) and in ducts of square cross-section (Biau et. al., 2008).

Theoretically laminar flow in pipes is linearly stable for all Reynolds numbers and sufficiently small perturbations will decay. Therefore, to trigger a transition to turbulence in Hagen-Poiseuille flow the velocity of the fluid has to be sufficiently large and the perturbation has to be strong enough. Many studies have investigated the border on the perturbation of which the flow swings up to the turbulent region or decays to the laminar profile. During the last two decades the main interest has shifted from the traditional question of how turbulence is initiated to answering the question of how turbulence maintains itself. The general conclusion is that achievable numerical solutions of the Navier-Stokes equations are starting to reproduce at least qualitatively what is seen and measured in experiments. The major difficulty is to ensure that the computational pipe is long enough so that transitional structures could evolve

without being influenced by artificial numerical boundary conditions (Kerswell, 2005). The main difference between the transition process in fully developed laminar flow and accelerated pipe flow is the source of the transition – in the first case transition to turbulence is triggered artificially, in the second case it bursts naturally. The transition process in Hagen-Poiseuille flows is usually studied in $Re < 3500$, while in accelerating flows transition to turbulence is delayed up to $Re = 500\,000$. Zhao et. al. (2007) showed that the method of normal modes applied with the quasi-steady assumption failed to predict the flow instability in accelerated pipe flow started from rest. The comparison with data gained from Lefebvre and White (1989) indicated that the instability could not be explained by the exponential growth of a mode.

In a last half a century transition to turbulence has been a subject of research in oscillatory pipe flow. Experimental investigations by Merkli and Thomann (1975), Hino et. al. (1976), Ohmi et. al. (1982), Akhavan et. al. (1991), Eckmann and Grotberg (1991) et. al. can be described as cycles of accelerating and decelerating tests without a steady state between two cycles. Merkli and Thomann (1975) used hot wire probes and flow visualization to detect the transition to turbulence. These experiments revealed that along the tube wall there exist vortex patterns which are too weak to be observed by normal pressure measurements. Transition to turbulence occurs in the form of periodic bursts which are followed by relaminarization in the same cycle and they do not lead to turbulent flow during the whole cycle (Merkli and Thomann, 1975). Hino et. al. (1976) used a hot-wire anemometer to measure the velocity and classified the flows into four types with respect to the Reynolds number as follows:

- ◆ Region I – laminar flow;
- ◆ Region II – small amplitude perturbations appear in the early stage of the accelerating phase at the central portion of the pipe;
- ◆ Region III – small amplitude perturbations exist in the phase of higher velocity;
- ◆ Region IV – turbulent bursts occur in the decelerating phase.

Ohmi et. al. (1982) introduced a fifth region emanated from their test results stating that turbulent bursts occur in the accelerating phase as well as in the decelerating phase (except the early stage of accelerating and the latest stage of the decelerating phase). Velocity measurements were made in 16 or 17 (depending on the test) radial points by using a hot wire anemometer. Turbulence appeared “explosively” towards the end of the acceleration phase of the cycle and was sustained throughout the deceleration phase in all flows studied (using LDV) by Akhavan et. al. (1991) as well, leading to the conclusion that there is a rapid buildup of turbulent shear stresses in the near-wall region of the pipe towards the end of the acceleration phase. Eckmann and Grotberg (1991) used LDV and a hot-film anemometer to study whether there exists a flow regime near the transition in which the boundary layer is unstable, while in the viscous core region remains turbulence free. Three different experiments were conducted to study the phenomena. New experimental results differed from the

previous studies, showing that the instability near the transition was confined to an annular region near the wall rather than dispersing across the entire cross-section.

Studies on the transition to turbulence in oscillatory flows have been carried out at quite low velocities and final Reynolds numbers ($Re \leq 65000$). Therefore, the transition takes place mainly in the deceleration phase rather than in the acceleration phase. The process is more similar to ramp-type flows. The initial forces and velocity histories that are present at the beginning of the accelerating phase in oscillatory flows but not present in flows starting from rest have to be taken into account (it can be considered as a more basic flow system). In the case of start-up transient flow the mean velocity changes monotonously between zero and a steady value. Therefore, not only a sectional velocity profile but also the origination and development of turbulence and the transition from laminar to turbulent are considered to be much different from those in an oscillating and pulsating flow (Kurokawa and Morikawa, 1986).

According to Lam and Leutheusser (2002) transition from laminar to turbulent in an accelerating pipe flow was experimentally first investigated by Carstens (1956) and Rotta (1956). Experimental work in the field has been very active in the past half a century. The development of the flow and transition to turbulence in accelerating pipe flows has been investigated experimentally by Maruyama et. al. (1976), Koppel and Liiv (1977), Leutheusser and Lam (1977), Maruyama et. al. (1978), Kask (1980), Ainola et. al. (1981), Lamp (1983), Lamp and Liiv (1983), Daniel et. al. (1985), Daniel and Koppel (1985), Kurokawa and Morikawa (1986), Kask and Koppel (1987), Lefebvre and White (1989), Moss (1989), Lefebvre and White (1991), Ruubel (1991), Das and Arakeri (1998), Lam and Leutheusser (2002), Greenblatt and Moss (2003), Viola and Leutheusser (2004), Koppel and Ainola (2006), Nakahata et. al. (2007), Nishihara et. al. (2008), Vardy et. al. (2009). The hypotheses brought forth in these studies are closely examined in the next chapter.

Accelerated and decelerated pipe flows and transitional processes between two turbulent steady states (ramp-up and ramp-down flows) have been investigated for example by Viola et. al. (1984), Shuy (1996), Greenblatt and Moss (1999), He and Jackson (2000), He et. al. (2008) and Vardy et. al. (2009). Shuy (1996) compared experimental results of a series of ramp-up (linearly accelerating) and ramp-down (linearly decelerating) tests with quasi-steady values and it was found that in accelerating pipe flows measured unsteady wall shear stress was consistently lower than the quasi-steady shear stress. In rapidly decelerated flows the phenomena were observed to behave vice versa. In slowly changing flow conditions the wall shear stress was found to have a quasi-steady behavior. Based on the measurements empirical equations for unsteady friction were derived in terms of the acceleration parameter. Greenblatt and Moss (1999) investigated the relaminarization process in temporally accelerated pipe flows under initially turbulent conditions. They concluded that relaminarization was identified when the imposed unsteady pressure gradient was of the order of that

required for relaminarization under steady conditions. In the pipe core-region the turbulence fluctuations were effectively frozen. A detailed investigation of fully developed transient flow was undertaken by He and Jackson (2000) who did a series of ramp-up (linearly accelerating) and ramp-down (linearly decelerating) tests. LDV was used to measure all three velocity components and to analyze the development of mean flow, propagation of turbulent energy, inertial effects etc. Their study identified three different delays in the response of turbulence to the imposed acceleration – delay in the response of turbulence production, delay in the radial propagation of turbulence and delay in turbulent energy redistribution. To compare the test results He et. al. (2008) introduced a CFD model to study the influence of turbulence and inertia on wall shear stresses. It was shown that the wall shear stress initially overshoots the corresponding quasi-steady value and this was attributed to inertial causes. Thereafter, the wall shear stress undershot the quasi-steady value because inertial effects were more than counterbalanced by the cumulative influence of delays in the response of turbulence to flow changes. Recent experimental investigations carried out on ramp-up and ramp-down pipe flows were described by Vardy et. al. (2009).

The transition process in accelerating flow between two turbulent steady states is in many aspects similar to start-up accelerating flows. The propagation of unsteady shear stresses (in comparison with quasi-steady values) and turbulent intensities are found to be in a good agreement. Still, the difference at initial conditions (initial velocity, velocity histories, turbulence and equilibrium of forces present at the start of the acceleration phase) compared to the accelerating flow starting from rest, makes the processes somewhat different.

Studies published over the past few years have investigated the effect of initial constant acceleration on the transition to turbulence (Nishihara et. al., 2009; Iguchi et. al., 2010). Air was used as the working fluid and a series of tests were carried out in low-, mid- and high-acceleration rates to judge the influence of initial constant acceleration on the transition to turbulence. Empirical equations to predict the time from the start of the constant velocity flow to the initiation of turbulence (Nishihara et.al, 2009) and the time lag for the appearance of the turbulent slug after the cross-sectional mean velocity of the flow had reached the constant value (Iguchi et. al., 2010) were proposed.

For practical solutions of applied engineering problems of transient pipe flow Navier-Stokes and continuity equations are very troublesome both analytically and numerically. Therefore, the use of approximate one- and two-dimensional mathematical models is inevitable. Several approximate models given by Brown (1962), D'Souza and Oldenburger (1964), Holmboe and Rouleau (1967), Zielke (1968), Letelier and Leutheusser (1976), Achard and Lespinard (1981), Vardy and Hwang (1991), Shuy (1995), Vardy and Brown (1995), Brereton (2000), Brereton and Jiang (2005) have been used. Brown (1962) and D'Souza and Oldenburger (1964) attempted solutions for transient flow including the effect of the varying velocity distribution over the cross-section. Their work was limited to laminar flow and neglected all nonlinear

effects. Zielke (1968) incorporated the influence of viscous dispersion effects into the one-dimensional model of transient pipe flow and used the Laplace transformation to solve the Navier-Stokes equation for fully developed pipe flow. Zielke derived an expression for the momentary wall shear stress as a convolution integral of the history of the bulk-flow acceleration. Zielke's approach is assigned for transient laminar flow cases and is based on solid theoretical fundamentals. The model was tested with numerous experiments and showed good conformity between the calculated and measured results (Adamkowski nad Lewandowski, 2006). Letelier and Leuthesser (1976) studied the establishment of Poiseuille flow and laminar U-tube oscillations analytically and experimentally. Based on their findings they concluded that neither the assumption of a constant friction coefficient in a quadratic resistance law nor of quasi-steady flow was justified in the treatment of unsteady laminar pipe flow subjected to significant acceleration. Achard and Lespisrand (1981) developed and studied the fidelity and range of applicability of several compact approximations to Zielke's solution. Vardy and Hwang (1991) and Vardy and Brown (1995) used Zielke's solution to analyze fast transients in both laminar and turbulent flow. Approximate analytical solutions were developed, leading to relationships for the decay of the wall shear stress following a sudden velocity change. Shuy (1995) derived an approximate equation for the wall shear stress in unsteady laminar pipe flows in terms of instantaneous values of section mean velocity and acceleration. The proposed equation is exact for an initially steady flow undergoing a constant acceleration or deceleration. The main advantage of the simple approximate equation which expresses the unsteady wall shear stress explicitly in terms of the instantaneous section mean velocity and acceleration is that it does not involve complex expressions (compared for example to Zielke's (1968) and Achard and Lespisrand's (1981) solutions). Therefore, it suits better for wider engineering applications. New relationships in parallel/laminar flow in channels/pipes of arbitrary unsteadiness between flow rates, pressure gradients and wall friction were derived by Brereton (2000).

Recent reviews of the various forms of one- and two-dimensional water hammer equations and assumptions inherent in these equations were given by Ghidaoui (2004) and Ghidaoui et. al. (2005).

Models for laminar transient flows were extended to turbulent unsteady flows by Brunone et. al. (1991), Vardy and Brown (1995), Pezzinga (2000), Bergant et. al. (2001), Vardy and Brown (2003) et. al.. The pre-described models are mainly used in different water-hammer applications where unsteady friction plays an important role to predict precisely the pressure wave dumping in the system. Adamkowski and Lewandowski (2006) analyzed the selected unsteady friction model calculations with their own experimental results and found to have good agreements in laminar flows and at low Reynolds numbers ($Re < 16\ 000$). They concluded that it is required to broaden the assessment of the unsteady friction models for a wider range of Reynolds numbers. This clearly

indicates that there is a need for new experimental data gained at higher Reynolds numbers to validate and justify the existing models.

Models describing the development of the axial velocity distribution in accelerating transitional pipe flow were given by Ainola et. al. (1981), Ainola and Liiv (1985) and Koppel and Ainola (2006). One-dimensional models based on non-dimensional Navier-Stokes equations are proposed to describe the development of axial velocity distribution in different initial conditions. In addition, a criterion is proposed to describe the dependence between the dimensionless pressure gradient and dimensionless transition time (time when transition to turbulence takes place) in start-up flows. Using experimental results from a previous study, Koppel and Ainola (2006) showed that the logarithms of the time of transition, the mean, and friction velocities are the linear functions of the logarithm of the pressure gradient. Similar linear functions can be obtained, theoretically, based on the turbulence spreading through the unsteady boundary layer at the friction velocity. The different time interval, which allows for the turbulence to dissipate through the unsteady boundary layer, determines the differences in the delay in the transition time.

A two-dimensional model describing the transitional processes in pipes for compressible fluids is given by Ainola et. al. (1979) and Ainola et. al. (1981). A dissipative model based on Navier-Stokes equations was solved using the variational principle. Under certain initial conditions numerical calculations were carried out making use of the finite difference method. The modeled results were compared with experimental findings and found to be in a good agreement.

Existing transient pipe flow models are derived under the premise that no helical type vortices emerge (i.e. the flow remains stable and axisymmetric during a transient event). Ghidaoui (2001) analyzed the stability of velocity profiles in water-hammer flows. Emanated from the comparison of modeling and published experimental work he confirmed that water-hammer flows can become unstable and the instability (which develops in a short timescale) is asymmetric. Some strong asymmetries in water-hammer flows were reported in experimental studies carried out by Brunone et. al. (2000). Experiments showed that at some time steps forward flow took place only in the lower part of the pipe and a small backward flow occurred in much of the upper portion. It should be noted that the authors indicated that the two test results analyzed in their study were too small a sample to be definitive. Similar results have been gained in recent experimental (e.g. Das and Arakeri, 1998) and theoretical works indicating that flow instabilities, in the form of helical vortices, can develop in transient flows. These instabilities lead to the breakdown of flow symmetry with respect to the pipe axis (Ghidaoui et. al., 2005).

Despite the amount of experimental work in this field the physical understanding of the transition process in accelerating flows stays blurry. Some people doubt whether transition from laminar to turbulent flow can ever be treated as a well posed mathematical problem (Bradshaw, 1982). The essence of the problem was well described by Swinney and Gollub (1978) – “*Fluid flows*

have been studied systematically for more than a century and their equations of motion are well known, yet the transition from laminar flow to turbulent flow remains an enigma. The difficulty lies in the intractability of the nonlinear hydrodynamic equations that express the conservation of mass, momentum and energy for fluid continuum. Although these equations can be linearized and readily solved for a system near thermodynamic equilibrium, the solutions of the nonlinear equations – required to describe fluids far from equilibrium – are generally neither unique nor obtainable.” In early stages of transition studies it was believed that a laminar flow changes to turbulent flow at a certain Reynolds number as ice changes to water at a certain temperature (Sato, 1980). Nowadays it has been made clear that this concept is not true. Experimental studies and modeling have given different approaches to describe the transition process from laminar flow (or from rest) to turbulent flow. The next chapter will mainly concentrate on the transition to turbulence in accelerating pipe flows starting from rest and give an overview of the hypotheses on transition process raised over the years.

1.2 Hypotheses describing the development of flow and the transition to turbulence in accelerating pipe flows starting from rest

Transition to turbulence has been theoretically and experimentally investigated mostly in Hagen-Poiseuille flow and in periodic (oscillating, pulsating) flows. Experimental investigations dating back to 1883 showed that most of the time transition takes place at Reynolds numbers between 2000 and 4000. In laboratory conditions Hagen-Poiseuille flow has been stable even at Reynolds numbers up to 100 000 although linear stability theory applied to Hagen-Poiseuille flow indicates that the parabolic velocity profile is stable at all values of the Reynolds number (Tritton, 1977). This is due to the fact that Hagen-Poiseuille flows are known to be stable to infinitesimal disturbances while their response to finite amplitude disturbances is unresolved and still the subject of ongoing research (Greenblatt and Moss, 2003).

A thorough overview of the transition process from laminar flow was given by Wygnanski and Champagne (1973) who described the rise of turbulent slugs and puffs in transition to turbulence. In their interpretation slugs are caused by the instability of the boundary layer to small disturbances in the inlet region of the pipe and puffs are generated by large disturbances at the inlet. While slugs are associated with transition from laminar to turbulent flow, puffs represent an incomplete relaminarization process (therefore not present in accelerating pipe flows). Puffs can only be seen at $2000 \leq Re \leq 2700$, while slugs occur at any $Re \geq 3200$ as shown in Figure 1.1. The authors stated that because of the presence of a core of constant velocity one would expect turbulent spots to originate near the wall where the mean shear is high, just as in a boundary layer. Another study by Kovaszny et al. (1962) showed that regions of highly concentrated vorticity occur near the outer edge of a boundary layer at the initial stages of transition.

Wynanski and Champagne (1973) described these vorticities as spikes that may burst into turbulent spots if the amplitude is high enough. As a turbulent spot travels downstream it may increase in size and its dimensions become comparable with the pipe radius (Lindgren, 1969). This results in a turbulent slug, temporally filling the entire cross-section of the pipe with turbulent flow. As the slug is restricted by the pipe diameter it can only grow in axial direction causing the pipe to be fulfilled with turbulent flow. Lindgren (1969) showed that only the turbulent regions of natural origin increase in length as they proceed down the pipe. Turbulent regions created by large disturbances at the inlet tend, sometimes, to split and decay.

Subsequently Rubin et. al. (1979) concluded by studying the effects of large disturbances on fully developed pipe flow that slugs were comprised of a succession of merged puffs – irrespective of the means by which the turbulence was initiated. Maruyama et. al.'s (1978) observations appear to confirm the proposal – despite the fact that the turbulence they observed was initiated by a large inlet disturbance, the nature of the structure and its interface velocity were consistent with a turbulent slug rather than a turbulent puff (Moss, 1989).

Darbyshire and Mullin (1995) observed transitional pipe flow in a constant-mass-flux device and compared their test results with earlier work done in pressure-driven systems. The results were qualitatively the same but some doubts were raised in distinguishing between puffs and slugs in the pipe flow. On the basis of their test results critical finite amplitude of disturbance required to cause transition was suggested. In Figure 1.2 the line AB was drawn to guide the eye since there is not a sharp divide between the two possible outcomes (whether transition to turbulence takes place or decays).

The latest numerical simulations carried out by Willis and Kerswell (2009) showed that there is a possibility that puffs exist as solutions of the Navier-Stokes equations beyond the Re at which they are observed in experiments.

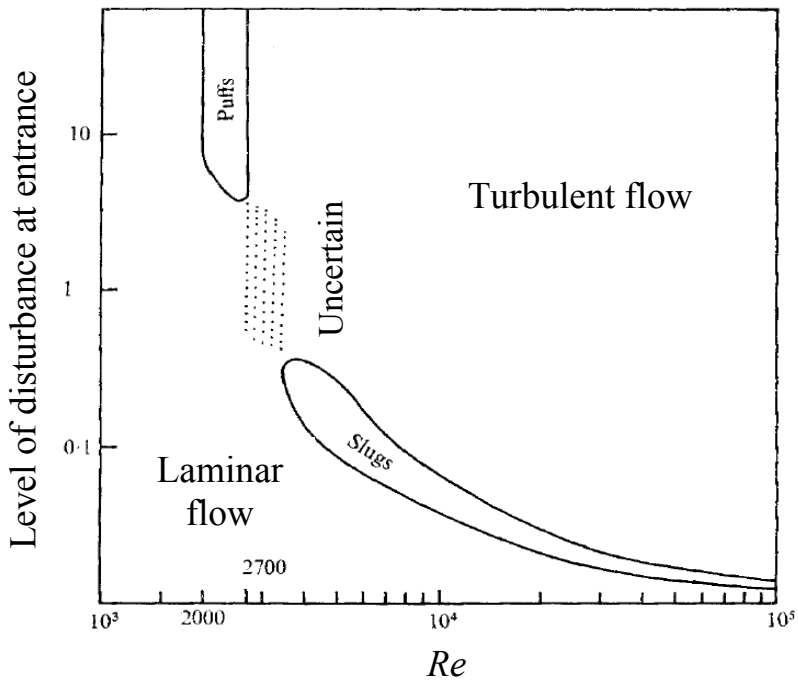


Figure 1. 1 - The regions in which slugs and puffs occur in transitional pipe flow as a function of the disturbance level (Wyganski and Champagne, 1973)

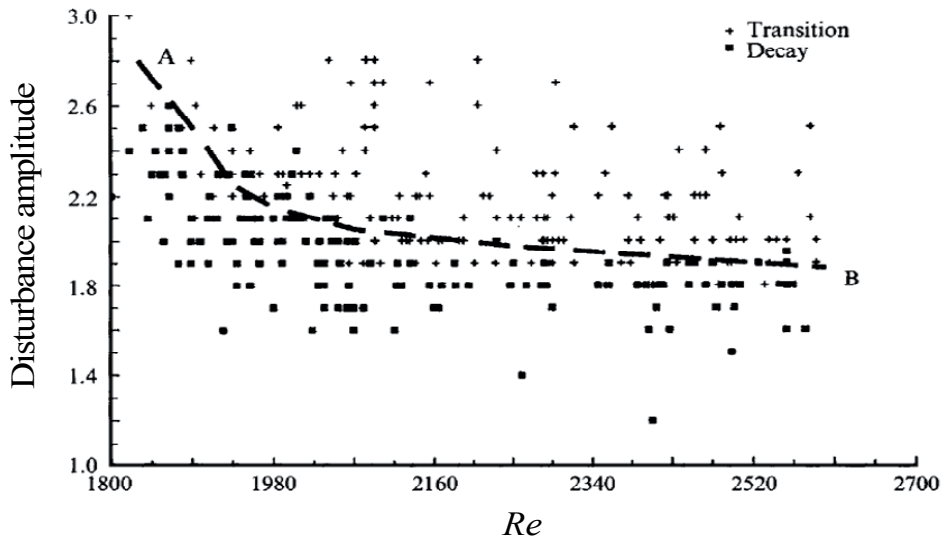


Figure 1. 2 – Outcomes of experiments using a single-jet disturbance as a function of disturbance amplitude and Re (Darbyshire and Mullin, 1995)

The propagation and occurrence of slugs and puffs are investigated and noticed in accelerating pipe flows (Moss, 1989; Lefebvre and White, 1989, 1991) and in initially constant-acceleration pipe flows (Iguchi et. al., 2010). Moss used kerosene as a working fluid and experiments were carried out on a vertical tube under a constant head. Flow was initiated by opening a solenoid valve and a wall shear stress probe was used to capture the transition process in accelerating flow. Two transition events were recorded, separated by the passage of a turbulent to laminar front and a period of laminar flow dividing the initial laminar flow into three discrete events. Figure 1.3 is a map, incorporating approximately 250 test runs, of the times t corresponding to different final Reynolds numbers at which the above occur. As Re increases the time interval between the trailing edge of the first (turbulent slug) and the leading edge of the second turbulent structures reduces. When $Re > 11\,000$, continuous turbulence is observable at all times after its initial occurrence (Moss, 1989). Moss described the first laminar-turbulent transition as a occurrence of natural transition once local conditions are met (mode II in Figure 1.3) followed by a passing of a turbulent to laminar interface and followed by a final laminar to turbulent interface carried down from the inlet (mode I in Figure 1.3).

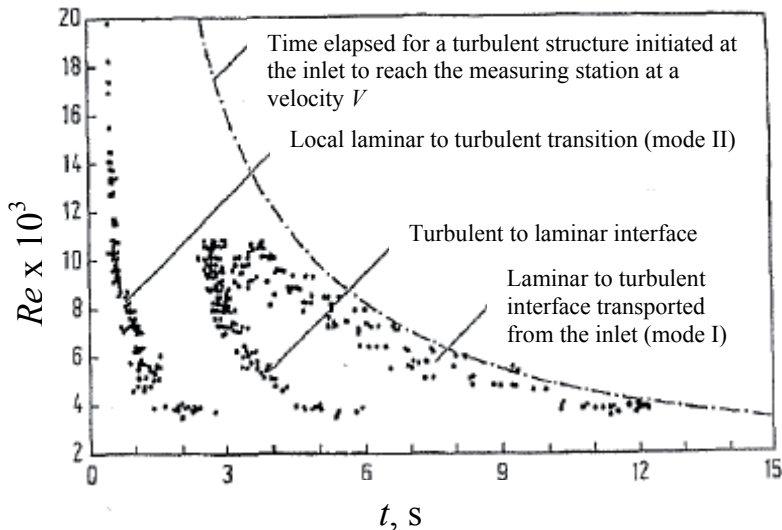


Figure 1. 3 – Laminar to turbulent transition modes in accelerating pipe flows (Moss, 1989)

Lefebvre and White (1991) used several different parameters to correlate their test results and stated that the transition time and the Reynolds number in constant acceleration flow are dependent on the pipe diameter and acceleration. They used LDV and surface shear stress sensors to define the transition time. As the maximum deviation in transition time was very similar (transition times in

the test section between different hot-films varied about 3 % or 50 milliseconds), they concluded that for constant acceleration pipe startup flow the entire flow in the test section undergoes a kind of global instability with transition being essentially independent of axial position, which meant that flow remained laminar in all three measurement stations until final transition to turbulence occurred. Still, at some test runs turbulent slugs preceded final transition. Figure 1.4 shows the uncalibrated voltage output signal from two surface shear stress sensors for two different runs – the upper frame at an acceleration of 7.1 m/s^2 and the lower one at 5.65 m/s^2 . The turbulent slug is captured only by one sensor at both cases while the transition to turbulence is seen at the same time by both of the sensors. As the slug appeared only during a few test runs, and even then at different sensor locations, it is believed that the cause of the slug is more likely a relatively small disturbance within the test section or a natural instability in the velocity profile. Furthermore, the observance of the slug was believed to be intermittent because, under the accelerations tested, the flow tends to become unstable at even slight disturbances, including vibrations, which can occur randomly (Lefebvre and White, 1991).

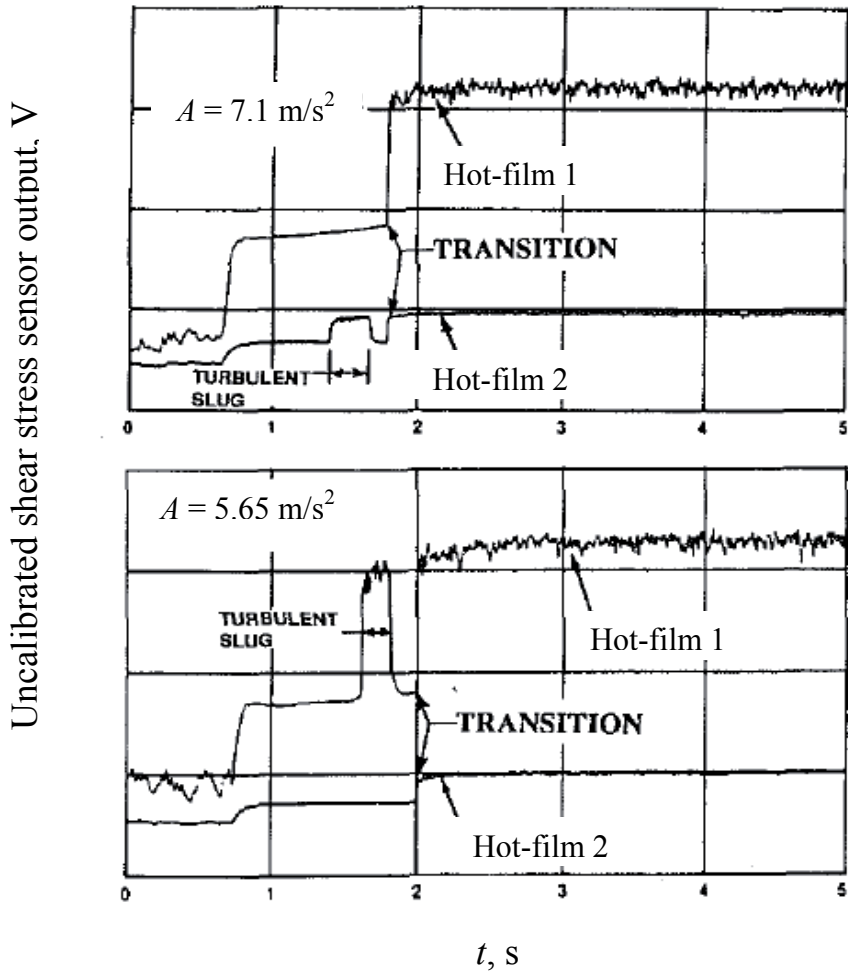


Figure 1. 4 – Surface shear stress sensor output exhibiting a turbulent slug (Lefebvre and White, 1991)

Kask and Koppel (1987) described the process of turbulization of the flow in accelerating flow as a wavy appearance of the spots of turbulence (Figure 1.5). These turbulent structures (spots) will spread downstream, enlarge, and merging in, fill all the flow. In their tests at initial moments only the bottom of the pipe was covered with color. After a rapid opening of the downstream end valve fluid was accelerated from rest and turbulent structures were developed in the pipe merging the color into the water. Eventually color was transported out of the system and the pipe was filled only with water. Visualization of the accelerated flow from rest in pipes with diameters $D = 0.036 \text{ m}$ and $D = 0.05 \text{ m}$ showed as the turbulization started at the bottom of the pipe and propagated downstream in

waves eventually filling the whole pipe diameter. They concluded that the wavelength of the spots depends on the initial pressure in the pressure tank. The timescale in Figure 1.5 is changing from top to bottom with a time step of $t = 0.04$ s and fluid is moving from right to left.

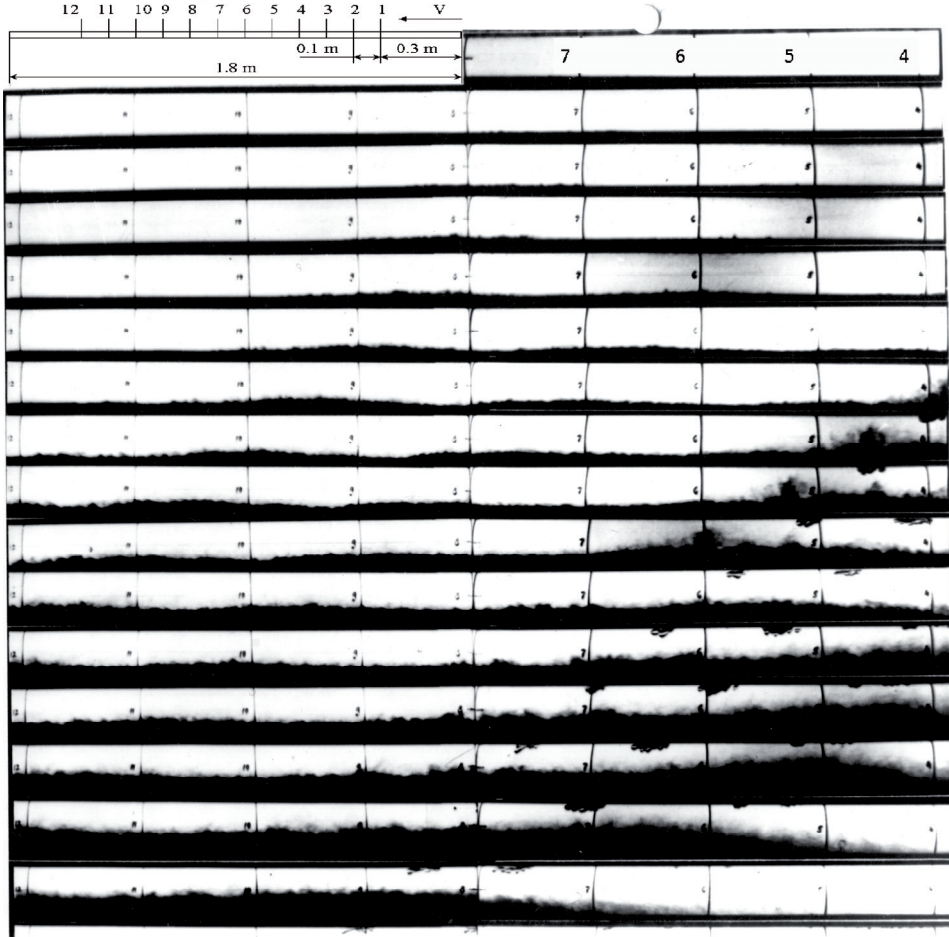


Figure 1. 5 – Wavy appearance of the spots of turbulence (Kask and Koppel, 1987)

Similar tests as Lefebvre and White (1991) did, were carried out by Nakahata et. al. (2007) too. The transition to turbulence was judged on the basis of the output signal of a hot-wire anemometer or LDV. Same parameters introduced by Lefebvre and White (1991) were used to study the correlation between the two test series. As a result, Nakahata et. al. proposed an empirical equation for the critical Reynolds number:

$$Re_* = 1.33 \cdot \left[D \cdot \left(\frac{A}{v^2} \right)^{1/3} \right]^{1.86} \quad (1.1)$$

where D is the pipe diameter, A is acceleration and ν is kinematic viscosity. They stated that in accelerated flows the critical Reynolds number (the Reynolds number at transition) is highly increased compared to steady pipe flows. The same tendency that transition to turbulence in accelerating flow is delayed, was earlier experimentally showed by Leutheusser and Lam (1977), Koppel and Liiv (1977) and Lefebvre and White (1989). Critical Reynolds numbers (depending on the final Reynolds number and acceleration) can be as high as $Re_* > 500\,000$ (Lefebvre and White, 1989).

Kurokawa and Morikawa (1986), Lefebvre and White (1989, 1991) and Nakahata et. al. (2007) analyzed the dependence between the critical Reynolds number (Re_*) and acceleration rate. In all studies it was found that the increase in acceleration rate inflicts the increase in the critical Reynolds number and the dependence between the two variables in the logarithmic scale is almost linear. Changes in the pipe diameter directly affect the change of the critical Reynolds number – with the increase of the pipe diameter, at the same acceleration rates, Re_* also increases. Kurokawa and Morikawa (1986) found that the critical Reynolds number is nearly proportional to the square root of acceleration. Lefebvre and White (1991), on the other hand, stated that Re_* is proportional to the cube root of acceleration.

In another study Nakahata et. al. (2007) investigated the propagation of turbulence in accelerating flow. They judged the transition to turbulence on the basis of the history of the axial velocity and stated that turbulence is generated near the wall in the entrance region and then propagates towards the centerline while traveling in the downward direction. Nakahata et. al. (2007) showed that the acceleration rate plays an important role in the propagation while at smaller acceleration, the propagation of turbulence is similar to steady pipe flow. When acceleration exceeds a certain critical value, turbulence propagates to the centerline even near the entrance of the pipe. Kurokawa and Morikawa (1986) also divided the transition from laminar to turbulent into two types. At relatively high acceleration rates the transition takes place before the viscous effects extend over the inner region of the pipe and at the transition the flow is suddenly decelerated near the wall and accelerated in the core region. Changes in the mean velocity at the moment of transition were not recorded. The analysis of the equilibrium of forces indicated that before the transition inertial and pressure forces are almost equal. After the transition the shear forces increase suddenly and inertial forces start to diminish. The same flow behavior at transition was noted in an experimental study by Ainola et. al. (1979). When the acceleration is comparatively small, the transition takes place after the viscous effects extend over the whole region and at the transition the flow is suddenly accelerated near the wall and decelerated in the inner region. This causes a change in the mean velocity as well. Before the transition the mean flow acceleration decreases and suddenly increases after the transition to turbulence. The first type of transition was investigated by Daniel and Koppel (1985) and Koppel and Ainola (2006)

who supported the hypothesis that in accelerating flow the transition to turbulence spreads simultaneously over the entire length of the pipe.

Kurokawa and Morikawa (1986) also investigated friction coefficients in accelerated pipe flows and stated that in the case of laminar flow the friction coefficient was found to be greater than the corresponding value of quasi-steady flow. On the contrary, it was found to be smaller under the conditions of turbulent flow. Shuy (1996) and Vardy et. al. (2009) came to similar conclusions in flows accelerated from an initially turbulent steady state to another.

Viola and Leutheusser (2004) stated that in boundary shear flows it is a widely held belief that turbulence starts at the wall whence it diffuses gradually into the flow. They did a series of tests in a 20 m long horizontal 0.0402 m diameter PVC pipe that was connected to a 1 m diameter constant head tank at the upstream end and a spring-loaded exit valve at the downstream end. Local velocities were evaluated using LDV installed 1.5 m upstream from the exit valve. A series of tests confirmed the aforesaid statement indicating that turbulence starts at the wall. In the case of flow establishment from rest, the local mean velocities in the core of the pipe exhibit a distinct overshoot, which leads to the development of transient annular ring-type velocity distributions during the establishment process, i.e. the velocity in the core region is momentarily larger than in the final turbulent steady-state. The reasons for this are the time-wise evolution of turbulence, which starts at the wall and proceeds toward the pipe center; and the difference in speed between laminar (initially faster) and turbulent (initially slower) flow establishment (Viola and Leutheusser, 2004). In Figure 1.6 the temporal mean velocity and turbulence intensity are shown at different radial locations. It can be seen that turbulence first occurs at the wall at about 7 s and reaches the center of the pipe at approximately 14 s. The wall shear stress measurements showed that initially shear stress was a very smooth function of time, increasing rapidly at $t = 14$ s. The time-wise concurrence between the turbulent bursts in the pipe center and shear stress sensor were found to be striking. This pointed out that wall shear stress is a very sensitive indicator of transition to turbulence.

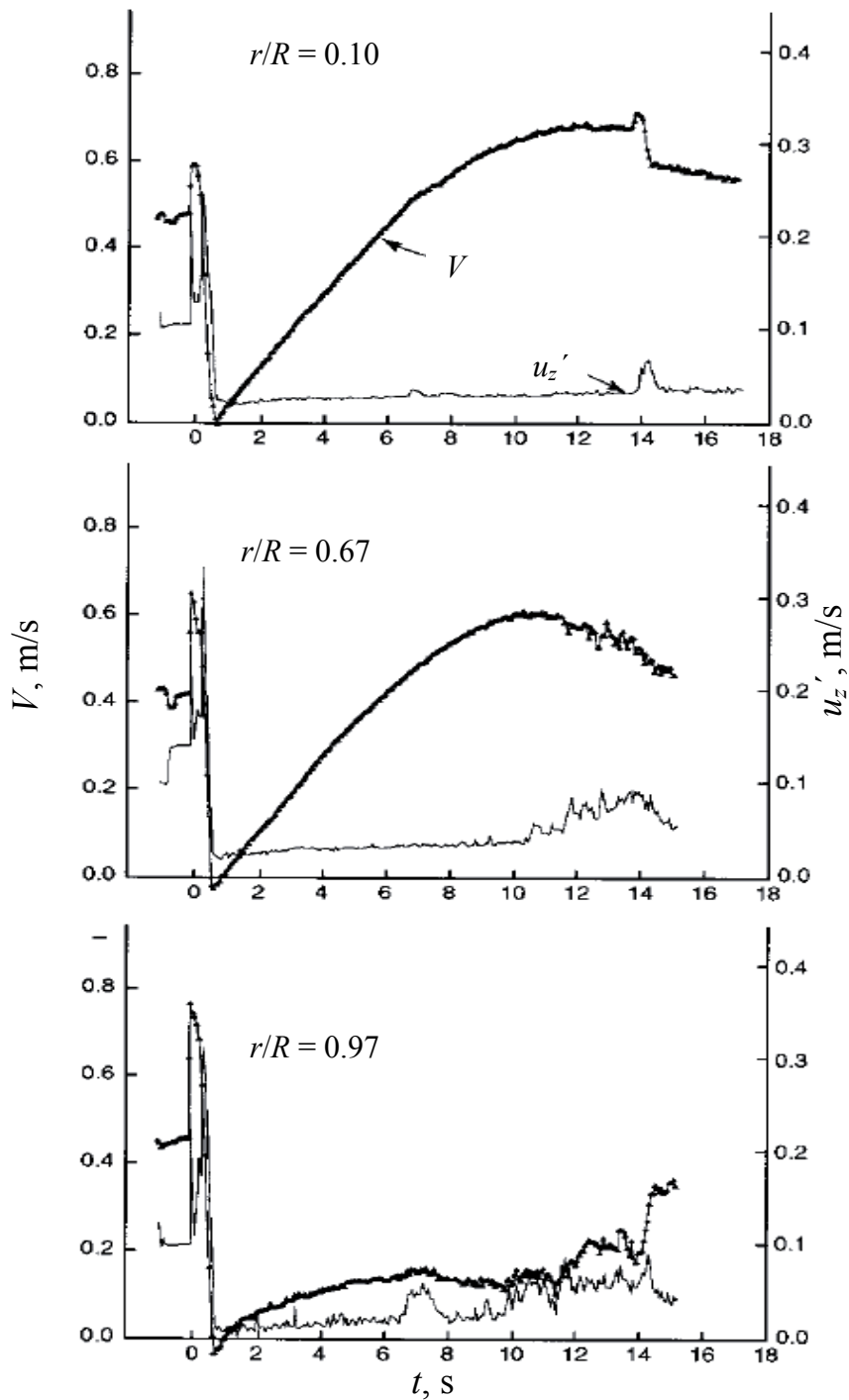


Figure 1. 6 – Time-wise evolution of local mean velocity and turbulence intensity at three radial positions (Viola and Leutheusser, 2004)

The same conclusion about the turbulence propagation from the wall region towards the center of the pipe has been given by Kask (1980), Lamp (1983), Koppel and Ainola (2006).

Ruubel (1991) showed that in accelerated flows transition to turbulence can be described through the equilibrium of forces. At the start of the process the dominating forces in the system are inertia and pressure. As the fluid flows downstream inertial forces start to decrease while frictional forces on the wall increase. Transition to turbulence occurs practically momentarily after the frictional forces on the wall become larger than the pressure forces (see Figure 1.7). It must be noted that the study of Kurokawa and Morikawa (1986) does not support the hypothesis. Therefore, the equilibrium of forces can be considered to be dependent on the test rig and initial conditions.

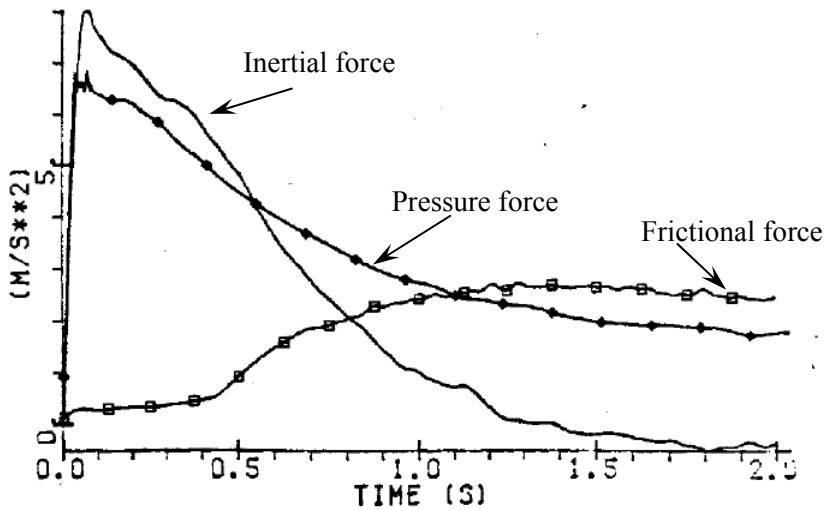


Figure 1. 7 - Variation of forces in the flow by the one-dimensional equation of motion.
 □ - Frictional force on the wall; ◆ - Pressure force (Ruubel, 1991)

Ruubel (1991) did a series of tests in accelerating transient flows using 2D LDV and shear stress sensors to capture the transition process. In an ensemble averaged test series of 30 repeats he measured the shear stress at the same position in pipe length but in different radial locations concluding that turbulence propagates in a pipe like a three-dimensional wavy vorticity structure as the shear stress sensors captured turbulence propagation in the same sequence for all repeated cases. Similar ideas can be found in a study carried out by Zhao et. al. (2007). The authors investigated perturbed unsteady laminar flows in pipes and induced the linear growth of the amplitude of perturbation by tilting vorticity by the radial component of the velocity perturbation. Energy growth at the transition became more pronounced for perturbations with longer wavelength along the stream wise direction (i.e. perturbations growth is independent of the

stream wise coordinate). They compared the model results with the experimental data gained by Lefebvre and White (1989) and found good agreement between the model and test results. In conclusion it was stated that the transient growth mechanism may play an important role in the development of instability for flows accelerated from rest (Zhao et. al., 2007).

1.3 Summary

Over the years the studies of flow development and transition to turbulence in accelerating flows have given quite a number of hypotheses describing the transition process. These conjectures are examined later on in the light of new experimental results. In conclusion the aforementioned hypotheses are brought forth:

- ◆ At some initial conditions turbulent slugs precede final transition to turbulence.
- ◆ Transition time and the Reynolds number in constant acceleration flow are dependent on the pipe diameter and acceleration.
- ◆ Transition to turbulence in high acceleration flows takes place simultaneously over the entire length of the pipe.
- ◆ Wavy appearance of the spots of turbulence occurs in the turbulization process in accelerating flows. These turbulent structures will spread downstream, enlarge, and merging in, fill all the flow.
- ◆ An empirical equation for the critical Reynolds number was proposed (Eq. 1.1).
- ◆ Transition to turbulence in accelerating flows is delayed (up to $Re_* = 500\,000$).
- ◆ Increase in the acceleration rate inflicts the increase in the critical Reynolds number. Changes in the pipe diameter directly affect the change of the critical Reynolds number (Re_*) – at the same acceleration rates, with the increase of the pipe diameter Re_* also increases.
- ◆ The critical Reynolds number is nearly proportional to the square root (Kurokawa and Morikawa, 1986) or cube root of the acceleration (Lefebvre and White, 1991).
- ◆ At low acceleration rates at the point of transition the flow is suddenly accelerated near the wall and decelerated in the inner region. At relatively high accelerations at the point of transition the flow is suddenly decelerated near the wall and accelerated in the core region.
- ◆ At low acceleration rates the acceleration of the mean velocity decreases before transition to turbulence and increases afterwards. At relatively high accelerations changes in the mean velocity were not observed.

- ◆ In accelerating flows the friction coefficient compared to a quasi-steady value is greater in the laminar region and smaller in the turbulent region.
- ◆ In accelerating flows turbulence is generated near the pipe wall and then propagates towards the centerline of the pipe.
- ◆ Transition to turbulence occurs at the point where a sudden growth of shear forces takes place and the frictional forces near the wall become larger than the pressure forces.
- ◆ Turbulence propagates in the pipe as a three-dimensional vorticity structure.

Experimental findings gained in earlier studies have posed many hypotheses describing the flow development and transition to turbulence in accelerating pipe flows. Although there are many similarities in the results, some aspects have still remained rather contradicting and blurry. Different results are dependent on the set-up of the test rig (how vibrations and other exterior irritations affect the measurements), initial and boundary conditions, instruments used in the measurements etc. The development of technology has created an opportunity to measure more precisely, with higher sampling rates and therefore to have more information about the process.

It must be noted that all the available experimental results have been gained in rather small-scale pipeline systems. Therefore, the thesis concentrates on the same issues that were raised in earlier similar studies but in the light of new experimental findings gained in a large-scale pipeline. The experimental work was carried out in Deltares, Delft, the Netherlands as a part of an international project “Unsteady friction in pipes and ducts”. A series of accelerating start-up flow tests was therefore planned in the project’s test program. Approximately 100 different acceleration rates were used to study the transition phenomena in constant acceleration start-up pipe flows and to analyze the effect of transition to turbulence from a practical point of view – the effects on the mean flow rate, pressure and friction. Modern technology (PIV, shear stress sensors) was used to capture the transition process and visualize the flow structures.

The main purpose of the thesis is to study the genesis and the propagation of turbulence in accelerating pipe flows starting from rest. The experimental findings available are quite contradicting – some say that the transition to turbulence takes place simultaneously over the pipe cross-section; others argue that first it sets in at the wall and then proceeds toward the pipe center. The transition to turbulence is mainly captured using single point measurements (LDV) by ensemble-averaging procedure. To estimate the propagation of turbulence in a single test, integral measurement of velocity profile is necessary. In this study it is attempted to describe the developing structures and the transitional process itself in accelerating start-up flows using PIV technique.

A 1D mathematical model is modified to describe the development of velocity profiles in constant accelerating flows. New experimental findings are compared with 1D and 2D model results, experimental results available and empirical equations and criteria proposed in earlier studies describing the transition to turbulence in accelerating pipe flows.

2. MATHEMATICAL MODEL FOR FLOW WITH CONSTANT ACCELERATION

In this chapter a mathematical model describing a uniformly accelerated laminar flow in a pipe, initially at rest, is given. Two- and one-dimensional unsteady flow equations for start-up flow derived from the Navier-Stokes and continuity equations are presented. The dynamical boundary layer in a pipe is described theoretically with the Laplace transformation method for small values of time. A mathematical model describing the development of velocity profile for accelerating flow starting from rest up to the point of transition to turbulence is given.

An exact solution for axial velocity distribution using linearized equations of Navier-Stokes was given by Ainola et. al. (1981). It was indicated that during the starting period the flow remains approximately automodelous until the turbulence is generated. Ainola and Liiv (1985) used Navier-Stokes equations to model laminar unsteady hydrodynamic processes in circular long pipes and presented a criterion for the transition from laminar to turbulent pipe flow starting from rest. Equations for impulsively started flow and flow caused by the Heaviside pressure gradient using Navier-Stokes and continuity equations were derived by Koppel and Ainola (2006). In this chapter Navier-Stokes equations of a compressible viscous fluid are derived for constant accelerated-from-rest start-up flow.

2.1 Equations for compressible fluid on a long pipe

A laminar transient flow of a compressible viscous fluid in a cylindrical pipe which is described by the Navier-Stokes and continuity equations is considered. For the axisymmetric flow these equations in a dimensionless form are given as:

$$Sh \frac{\partial u}{\partial \tau} + u \frac{\partial u}{\partial \xi} + v \frac{\partial u}{\partial \eta} = -Eu \frac{\partial q}{\partial \xi} + \frac{1}{\varepsilon Re} \left(\varepsilon^2 \frac{\partial^2 u}{\partial \xi^2} + \frac{\partial^2 u}{\partial \eta^2} + \frac{1}{\eta} \frac{\partial u}{\partial \eta} \right) + \frac{\varepsilon}{3Re} \frac{\partial v}{\partial \xi}, \quad (2.1)$$

$$\varepsilon^2 Sh \frac{\partial v}{\partial \tau} + \varepsilon^2 u \frac{\partial v}{\partial \xi} + \varepsilon^2 v \frac{\partial v}{\partial \eta} = -Eu \frac{\partial q}{\partial \eta} + \frac{\varepsilon}{Re} \left(\varepsilon^2 \frac{\partial^2 v}{\partial \xi^2} + \frac{\partial^2 v}{\partial \eta^2} + \frac{1}{\eta} \frac{\partial v}{\partial \eta} - \frac{v}{\eta^2} \right) + \frac{\varepsilon}{3Re} \frac{\partial v}{\partial \eta}, \quad (2.2)$$

$$Sh \frac{\partial q}{\partial \tau} + u \frac{\partial q}{\partial \xi} + v \frac{\partial q}{\partial \eta} + \frac{1}{EuM^2} v = 0, \quad (2.3)$$

where

$$v = \frac{\partial u}{\partial \xi} + \frac{\partial v}{\partial \eta} + \frac{1}{\eta} v. \quad (2.4)$$

The dimensionless variables and numbers are defined as:

$$\xi = \frac{z}{L}, \quad \eta = \frac{r}{R}, \quad \tau = \frac{t}{T_0}, \quad (2.5)$$

$$u = \frac{u_z}{U_0}, \quad v = \frac{Lu_r}{RU_0}, \quad q = \frac{p}{P_0}, \quad (2.6)$$

and

$$\varepsilon = \frac{R}{L}, \quad Sh = \frac{L}{T_0 U_0}, \quad Eu = \frac{P_0}{\rho U_0^2}, \quad Re = \frac{U_0 R}{\nu}, \quad M = \frac{U_0}{c}. \quad (2.7)$$

Here z and r are the length coordinates in the axial and radial directions; t is the time; u_z and u_r are the axial and radial velocities; p is the fluid pressure; R is the pipe radius and L is the pipe length; U_0 , P_0 and T_0 are the suitable reference values of velocity (maximum mean velocity), fluid pressure (initial pressure in the tank) and time (duration of the process); ρ is fluid density, ν is the kinematic viscosity, c is the speed of sound in fluid; and Sh , Eu , Re and M are the Strouhal, Euler, Reynolds and Mach numbers, respectively.

For long pipes

$$\varepsilon \ll 1. \quad (2.8)$$

Therefore, Eqs. (2.1) and (2.2) can be simplified and written as

$$Sh \frac{\partial u}{\partial \tau} + u \frac{\partial u}{\partial \xi} + v \frac{\partial u}{\partial \eta} = -Eu \frac{\partial q}{\partial \xi} + \frac{1}{\varepsilon Re} \left(\frac{\partial^2 u}{\partial \eta^2} + \frac{1}{\eta} \frac{\partial u}{\partial \eta} \right), \quad (2.9)$$

$$\frac{\partial q}{\partial \eta} = 0. \quad (2.10)$$

From Eq. (2.10) it follows that in the case of a long pipe the fluid pressure can be considered as independent of the radial coordinate, i.e. $q=q(\xi, \tau)$. Substituting Eq. (2.10) into Eq. (2.3), it can be obtained

$$Sh \frac{\partial q}{\partial \tau} + u \frac{\partial q}{\partial \xi} + \frac{1}{EuM^2} v = 0. \quad (2.11)$$

Thus, the compressible viscous flow in the long pipe can be described by Eqs. (2.9) – (2.11). It is essential that differently from a conventional solution to this system there is no need for the specification of boundary conditions for pressure q on the boundary $\eta = 1$.

For the start-up flow problem more suitable reference scales T_0 , U_0 and P_0 in Eqs. (2.7) can be determined.

Assume that the pressure scale - P_0 is expressed through the velocity scale - U_0 by Joukowsky fundamental relation

$$P_0 = \rho c U_0. \quad (2.12)$$

The time scale - T_0 let be defined through sound speed in fluid as

$$T_0 = \frac{L}{c}. \quad (2.13)$$

Substituting Eqs. (2.12) and (2.13) into Eqs. (2.7), the following expressions for dimensionless numbers can be obtained:

$$Sh = \frac{c}{U_0}, \quad Eu = \frac{c}{U_0}, \quad Re = \frac{U_0 R}{\nu}, \quad M = \frac{U_0}{c}. \quad (2.14)$$

From Eqs. (2.14) it follows

$$Sh = \frac{1}{M}, \quad Eu = \frac{1}{M}. \quad (2.15)$$

Substituting Eqs. (2.15) into Eqs. (2.9) - (2.11):

$$\frac{\partial u}{\partial \tau} + Mu \frac{\partial u}{\partial \xi} + Mv \frac{\partial u}{\partial \eta} = -\frac{\partial q}{\partial \xi} + \frac{M}{\varepsilon Re} \left(\frac{\partial^2 u}{\partial \eta^2} + \frac{1}{\eta} \frac{\partial u}{\partial \eta} \right), \quad (2.16)$$

$$\frac{\partial q}{\partial \eta} = 0, \quad (2.17)$$

$$\frac{\partial q}{\partial \tau} + Mu \frac{\partial q}{\partial \xi} + \nu = 0. \quad (2.18)$$

In practical start-up flow problems $M \ll 1$. Therefore, Eqs (2.16) and (2.18) can be written as

$$\frac{\partial u}{\partial \tau} = -\frac{\partial q}{\partial \xi} + Dn \left(\frac{\partial^2 u}{\partial \eta^2} + \frac{1}{\eta} \frac{\partial u}{\partial \eta} \right), \quad (2.19)$$

$$\frac{\partial q}{\partial \eta} = 0, \quad (2.20)$$

$$\frac{\partial q}{\partial \tau} + \frac{\partial u}{\partial \xi} + \frac{\partial v}{\partial \eta} + \frac{1}{\eta} v = 0, \quad (2.21)$$

where

$$Dn = \frac{Lv}{cR^2}. \quad (2.22)$$

Note that the dissipation number Dn is the only dimensionless parameter in Eqs. (2.19) - (2.21). Equations (2.19) – (2.21) were first given by D’Sousa and Oldenburger (1964).

The form of Eqs. (2.19) – (2.21) depends on the definitions of the scales P_0 and T_0 . The scales can be defined as

$$P_0 = \frac{\rho \nu L}{R^2} U_0, \quad T_0 = \frac{R^2}{\nu}. \quad (2.23)$$

Then instead of Eqs. (2.19) – (2.21) the transformation equations take the form:

$$\frac{\partial u}{\partial \tau} = -\frac{\partial q}{\partial \xi} + \frac{\partial^2 u}{\partial \eta^2} + \frac{1}{\eta} \frac{\partial u}{\partial \eta}, \quad (2.24)$$

$$\frac{\partial q}{\partial \eta} = 0, \quad (2.25)$$

$$Dn^2 \frac{\partial q}{\partial \tau} + \frac{\partial u}{\partial \xi} + \frac{\partial v}{\partial \eta} + \frac{1}{\eta} v = 0. \quad (2.26)$$

For the studying of the start-up flows these equations are more suitable.

2.2 One dimensional model

Integrating Eqs. (2.24) and (2.26) over the cross-section of the circular pipe with the aid of the operator

$$2 \int_0^1 (\dots) \eta d\eta \quad (2.27)$$

and using the following boundary conditions

$$u(\xi, 1, \tau) = 0, \quad \left. \frac{\partial u}{\partial \eta} \right|_{\eta=0} = 0, \quad (2.28)$$

it can be obtained

$$\frac{\partial U}{\partial \tau} + 2\alpha + \frac{\partial q}{\partial \xi} = 0, \quad (2.29)$$

$$\frac{\partial U}{\partial \xi} + \frac{Dn^2 \partial q}{\partial \tau} = 0. \quad (2.30)$$

Here U is the average velocity and α is the wall shear stress:

$$U = 2 \int_0^1 u \eta d\eta, \quad (2.31)$$

$$\mathfrak{a} = -\left(\frac{\partial u}{\partial \eta}\right)_{\eta=1}. \quad (2.32)$$

To express the wall shear stress \mathfrak{a} through the average velocity U Eq. (2.19) is solved with the Laplace transform method.

The time Laplace transform of Eq. (2.19) can be written as

$$\left(\frac{\partial^2 u^*}{\partial \eta^2} + \frac{1}{\eta} \frac{\partial u^*}{\partial \eta}\right) - s u^* = \frac{\partial q^*}{\partial \xi}. \quad (2.33)$$

Here s is the Laplace variable and the asterisks denote the Laplace transform. Equation (2.33) is the Bessel equation. Its solution can be expressed as:

$$u^*(\xi, \eta, s) = \frac{1}{s} \left(\frac{I_0(\sqrt{s}\eta)}{I_0(\sqrt{s})} - 1 \right) \frac{\partial q^*}{\partial \xi}, \quad (2.34)$$

where I_0 is the modified Bessel function of the first kind of order zero.

From Eqs. (2.31) and (2.34) it follows that

$$U^*(\xi, s) = -\frac{I_2(\sqrt{s})}{s I_0(\sqrt{s})} \frac{\partial q^*}{\partial \xi}. \quad (2.35)$$

The Laplace transformation of Eq. (2.29) can be written as

$$s U^* + 2\mathfrak{a}^* + \frac{\partial q^*}{\partial \xi} = 0. \quad (2.36)$$

By the elimination of the term $\frac{\partial q^*}{\partial \xi}$ between Eqs. (2.35) and (2.36) the following relationship can be obtained:

$$\mathfrak{a}^* = \frac{s}{2} L^*(s) U^*, \quad (2.37)$$

where

$$L^*(s) = \frac{2\sqrt{\frac{1}{s}}I_1(\sqrt{s})}{I_2(\sqrt{s})}. \quad (2.38)$$

This result was first given by Zielke (1968).
From Eqs. (2.37) and (2.38) it can be obtained

$$\mathfrak{a}(\xi, \tau) = \frac{1}{2} \int_0^\tau L(\tau - \tau') \frac{\partial U}{\partial \tau'} d\tau', \quad (2.39)$$

where

$$L(\tau) = 8 + 4 \sum_{k=1}^{\infty} e^{-\gamma_k^2 \tau}. \quad (2.40)$$

Here γ_k are the positive zeros of $I_2(\gamma)$. The function $L(\tau)$ is named as a weighting function.

In the final form Eqs. (2.29) and (2.30) can be expressed as

$$\frac{\partial U}{\partial \tau} + \int_0^\tau L(\tau - \tau') \frac{\partial U}{\partial \tau'} d\tau' + \frac{\partial q}{\partial \xi} = 0, \quad (2.41)$$

$$\frac{\partial U}{\partial \xi} + \frac{Dn^2 \partial q}{\partial \tau} = 0. \quad (2.42)$$

The models in this form are named as convolution load models. For the practical application of these models an approximation for the weighting function $L(\tau)$ is needed.

In Eqs. (2.41) and (2.42) the wall shear stress $\mathfrak{a}(\xi, \tau)$ is expressed through average velocity $U(\xi, \tau)$. An alternative possibility where the wall shear stress is expressed through pressure can be considered (Brereton (2000)). Substituting Eq. (2.35) into Eq. (2.37), it can be obtained

$$\mathfrak{a}^* = M^*(s) \frac{\partial q^*}{\partial \xi}, \quad (2.43)$$

where

$$M^*(s) = -\frac{\sqrt{\frac{1}{s}} I_1(\sqrt{s})}{I_0(\sqrt{s})}. \quad (2.44)$$

Respectively

$$\mathfrak{a}(\xi, \tau) = -\int_0^\tau M(\tau - \tau') \frac{\partial q}{\partial \xi} d\tau', \quad (2.45)$$

where

$$M(\tau) = -4 - 2 \sum_{k=1}^{\infty} e^{-\beta_k^2 \tau}. \quad (2.46)$$

Here β_k are the zeros of $I_0(\beta)$.

Using Eqs. (2.45) and (2.46), Eq. (2.29) can be expressed as

$$\frac{\partial U}{\partial \tau} - 2 \int_0^\tau M(\tau - \tau') \frac{\partial q}{\partial \xi} d\tau' + \frac{\partial q}{\partial \xi} = 0. \quad (2.47)$$

Thus, instead of the system (2.41) and (2.42), a system in the alternative form – Eqs. (2.47) and (2.42) – can be obtained.

2.3 Equations for start-up flows

Now the very first motion of the flow in a small time limit is considered.

In the theory of the Laplace transform to the image function at $s \rightarrow \infty$ corresponds the original function at $\tau \rightarrow 0$.

From the series expansion of the modified Bessel function for high values of z one can have

$$I_n(z) = \frac{e^z}{\sqrt{2\pi z}} \left[1 - \frac{4n^2 - 1}{8z} + \frac{(4n^2 - 1)(4n^2 - 9)}{2!(8z)^2} - \dots \right]. \quad (2.48)$$

Using Eq. (2.48), from Eq. (2.38) it can be obtained:

$$L^*(s) = 2\left(\frac{1}{s}\right)^{1/2} + 3\frac{1}{s} + \frac{15}{4}\left(\frac{1}{s}\right)^{3/2} + \dots \quad (2.49)$$

The inverse Laplace transformation of Eq. (2.49) can be expressed as

$$L(\tau) = \left[\frac{2}{\sqrt{\pi}}(\tau)^{-1/2} + 3 + \frac{15}{2\sqrt{\pi}}(\tau)^{1/2} + \dots \right]. \quad (2.50)$$

Therefore Eq. (2.41) can be written in the form:

$$\begin{aligned} \frac{\partial U}{\partial \tau} + \frac{2}{\sqrt{\pi}} \int_0^\tau \frac{1}{\sqrt{\tau - \tau'}} \frac{\partial U}{\partial \tau'} d\tau' + 3U + \\ \frac{15}{2\sqrt{\pi}} \int_0^\tau \sqrt{\tau - \tau'} \frac{\partial U}{\partial \tau'} d\tau' + \frac{\partial q}{\partial \xi} = 0. \end{aligned} \quad (2.51)$$

Note that Zielke (1968) has proposed to use the first five terms in sum for function $L(\tau)$ in Eq. (2.41) at time interval $0.02 < \tau$.

For the alternative equation – Eq. (2.47) – from Eqs. (2.44) and (2.48) the following equations can be obtained:

$$M^*(s) = -\sqrt{\frac{1}{s}} + \frac{1}{2}\frac{1}{s} + \frac{1}{8}\left(\frac{1}{s}\right)^{3/2} + \dots, \quad (2.52)$$

and

$$\begin{aligned} \frac{\partial U}{\partial \tau} - \frac{2}{\sqrt{\pi}} \int_0^\tau \frac{1}{\sqrt{\tau - \tau'}} \frac{\partial q}{\partial \xi} d\tau' + \int_0^\tau \frac{\partial q}{\partial \xi} d\tau' + \\ \frac{1}{2\sqrt{\pi}} \int_0^\tau \sqrt{\tau - \tau'} \frac{\partial q}{\partial \xi} d\tau' + \frac{\partial q}{\partial \xi} = 0. \end{aligned} \quad (2.53)$$

2.4 Dynamical boundary layer in a pipe

Now, using the notation

$$a = -\frac{\partial q}{\partial \xi}, \quad (2.54)$$

the Eq. (2.24) can be written as

$$\frac{\partial u}{\partial \tau} = a + \frac{\partial^2 u}{\partial \eta^2} + \frac{1}{\eta} \frac{\partial u}{\partial \eta}. \quad (2.55)$$

For the start-up flow of a fluid the corresponding initial and boundary conditions by $\eta = 0$ and $\eta = 1$ are

$$u(\xi, \eta, 0) = 0 \quad (2.56)$$

and

$$u(\xi, 1, \tau) = 0, \quad \frac{\partial u}{\partial \eta}(\xi, 0, \tau) = 0. \quad (2.57)$$

Applying the Laplace transform for the governing equation (2.55) with the initial condition (2.56) it can be obtained

$$\frac{\partial^2 \bar{u}}{\partial \eta^2} + \frac{1}{\eta} \frac{\partial \bar{u}}{\partial \eta} - s \bar{u} = \bar{a}. \quad (2.58)$$

Respectively the boundary conditions (2.57) take the form of

$$\bar{u}(\xi, 1, s) = 0, \quad \frac{\partial \bar{u}}{\partial \eta}(\xi, 0, s) = 0. \quad (2.59)$$

The solution of Eq. (2.58) with boundary conditions (2.59) becomes

$$\bar{u}^*(\xi, \eta, s) = a^* K^*(\eta, s), \quad (2.60)$$

where

$$\bar{K}^*(\eta, s) = \frac{1}{s} \left[1 - \frac{I_0(\eta\sqrt{s})}{I_0\sqrt{s}} \right]. \quad (2.61)$$

Here I_0 is the modified Bessel function of the first kind of order zero. For large values of s using Eq. (2.48), Eq. (2.61) can be written as

$$\bar{K}^*(\eta, s) = \frac{1}{s} \left[1 - \frac{e^{-\sqrt{s}(1-\eta)}}{\sqrt{\eta}} \left(1 + \frac{1-\eta}{8\eta} \frac{1}{\sqrt{s}} + \frac{9(1-\eta^2) - 2\eta(1-\eta)}{128\eta^2} \frac{1}{s} + \dots \right) \right]. \quad (2.62)$$

Here it is assumed that $\eta \neq 0$. The inverse Laplace transformation for Eq. (2.62) is

$$K(\eta, \tau) = 1 - \frac{1}{\sqrt{\eta}} \left[\left(1 + \frac{(1-\eta)^2}{8\eta} \right) \text{erfc}\beta - \frac{1-\eta}{4\eta^{3/2}} \sqrt{\frac{\tau}{\pi}} e^{-\beta^2} + \dots \right], \quad (2.63)$$

where

$$\beta = \frac{1-\eta}{2\sqrt{\tau}}. \quad (2.64)$$

Here $\text{erfc}\beta$ is a complementary error function.

For $\eta = 0$ at small values of τ one can have respectively

$$K^*(0, s) = \frac{I_0(\sqrt{s}) - 1}{sI_0(\sqrt{s})}, \quad (2.65)$$

$$K^*(0, s) = \frac{1}{s} - \frac{\sqrt{2\pi}}{s^{3/4}} e^{-\sqrt{s}} + \dots, \quad (2.66)$$

$$K(0, \tau) = 1 - \frac{\sqrt{2}}{\Gamma(1/4)} \int_0^\tau \frac{e^{-\frac{1}{4\tau'}}}{\tau'^2 (\tau - \tau')^3} d\tau' + \dots. \quad (2.67)$$

To describe the unsteady boundary layer on the pipe wall more precisely the distance from the wall ϑ can be defined as

$$\vartheta = 1 - \eta. \quad (2.68)$$

Respectively Eq. (2.63) takes the following form

$$K(\vartheta, \tau) = 1 - \frac{1}{\sqrt{1-\vartheta}} \left[\left(1 + \frac{\vartheta^2}{8(1-\vartheta)} \right) \operatorname{erfc} \beta - \frac{\vartheta}{4(1-\vartheta)^{3/2}} \sqrt{\frac{\tau}{\pi}} e^{-\beta^2} + \dots \right], \quad (2.69)$$

where

$$\beta = \frac{\vartheta}{2\sqrt{\tau}}. \quad (2.70)$$

This result was given by Koppel and Ainola (2006).

The velocity profile near the wall of the pipe is rapidly changing in time. In the central part of the pipe the changes of the velocity profile are small.

2.5 Flow with constant acceleration

In experimental investigations of transient flows mainly two model conditions are used: flows with a constant pressure gradient and flows with constant acceleration. Consider now a flow with constant acceleration. Let

$$\frac{\partial U}{\partial \tau} = \alpha = \text{const.} \quad (2.71)$$

Then from Eq. (2.51) it can be obtained

$$\frac{\partial q}{\partial \xi} = -\alpha \left(1 + \frac{2}{\sqrt{\pi}} \int_0^{\tau} \frac{d\tau'}{\sqrt{\tau-\tau'}} + 3\tau + \frac{15}{2\sqrt{\pi}} \int_0^{\tau} \sqrt{\tau-\tau'} d\tau' \right) \quad (2.72)$$

or

$$\frac{\partial q}{\partial \xi} = -\alpha \left(1 + \frac{4}{\sqrt{\pi}} \sqrt{\tau} + 3\tau + \frac{5}{\sqrt{\pi}} \tau \sqrt{\tau} \right). \quad (2.73)$$

Now the distribution of the velocity of flow in the boundary layer of the pipe is considered. From Eq. (2.60) it follows that for the arbitrary function $a(\tau)$ can be written

$$u(\vartheta, \tau) = \int_0^{\tau} a(\tau - \tau') K(\vartheta, \tau) d\tau'. \quad (2.74)$$

Therefore, from Eqs. (2.63), (2.73) and (2.74) it can be obtained

$$u(\vartheta, \tau) = \alpha \int_0^{\tau} \left(1 + \frac{4}{\sqrt{\pi}} \sqrt{\tau} \right) K(\vartheta, \tau) d\tau. \quad (2.75)$$

3. EXPERIMENTAL APPARATUS AND INSTRUMENTATION

A large-scale pipeline apparatus with Reynolds numbers up to 1 000 000 was used to investigate unsteady flows. Laboratory experiments presented in the thesis were carried out in Deltares, Delft, the Netherlands as a part of the European Community's Sixth Framework Program through the grant to the budget of the Integrated Infrastructure Initiative HYDRALAB III within the Transnational Access Activities, Contract No. 022441. The project “Unsteady friction in pipes and ducts” was divided into three subgroups and the author of the thesis was directly involved with one of them – transition to turbulence in accelerating pipe flows starting from rest. This included the planning of the test program, procedure and carrying out the experiments. Processing and analyzing of the experimental data presented in the thesis was carried out by the author.

In this chapter a description of the test facility, experimental apparatus and instrumentation is given. It has been closely expatiated on choosing PIV settings and hot-film calibrations. Detailed specification of the instrumentation layout and full test program is given in papers by Vardy et. al. (2009), Annus et. al. (2010) and Annus and Koppel (2011).

3.1 Description of the test facility

Laboratory experiments were conducted in the Hydraulics Laboratory of Deltares (formerly Delft Hydraulics). The experimental apparatus depicted in Figure 3.1 consists of a constant head tank at the upstream end (head of 25 m), a horizontal galvanized steel pipe of total length $L = 44$ m with the internal diameter in the main section $D = 207.3$ mm, test section $D = 206.4$ mm and a control valve at the downstream end.

Two types of transient accelerating flows that were investigated in Deltares are presented in this work:

- ◆ Non-reversing accelerating flows (A1 and A1A tests)
- ◆ Reversing accelerating flows (B tests).

For non-reversing acceleration flow tests the downstream-end high-head tank was vented (atmospheric pressure). The test rig was gravity driven and acceleration from zero flow was controlled initially by a downstream-end butterfly type valve (A1 tests) and later by a globe type valve (A1A tests). The reversing accelerating flows were controlled by the pressurized downstream-end tank instead of the globe valve (B tests). Transient events were induced by opening a fast operating on/off valve (Figure 3.1). Therefore, the pressure gradient accelerated an initially zero flow. Flow straighteners were positioned initially at two places – one at the upstream end of the straight pipe section and one just before the control valve. In between the test series the flow straightener before the control valve was uninstalled. The length of the flow straighteners

was 150 mm and they contained tubes with the internal diameter of 12 mm, wall thickness 1 mm.

Water used in the tests was not treated. It was stored in an underground and dark large reservoir with temperature approximately 15° C.

Up to 20 channels were recorded simultaneously using data acquisition software Testpoint. Measured values were flow (2 flow meters), differential pressure (3 differential pressure transducers), pressure (in three locations), shear stress (6 glue-on hot-film sensors), fluid temperature, time, and trigger. A separate PC was used for the PIV measurements using special software DaVis 8,0.

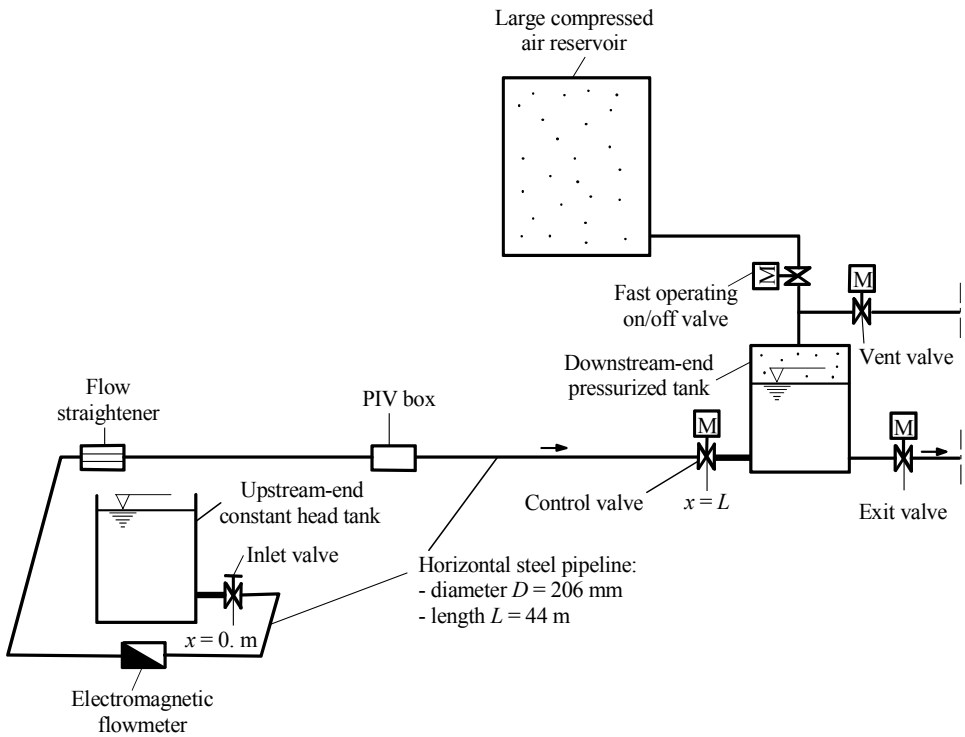


Figure 3. 1 – Test rig for accelerating flows (reversible and non-reversible) (Vardy et. al., 2009)

The test section shown in Figure 3.2 consisted of a galvanized stainless steel pipe of total length $L_t = 3,75$ m, internal diameter $D = 206,4$ mm, wall thickness $e = 6,35$ mm and a Perspex tubing within a glass box for PIV measurements.

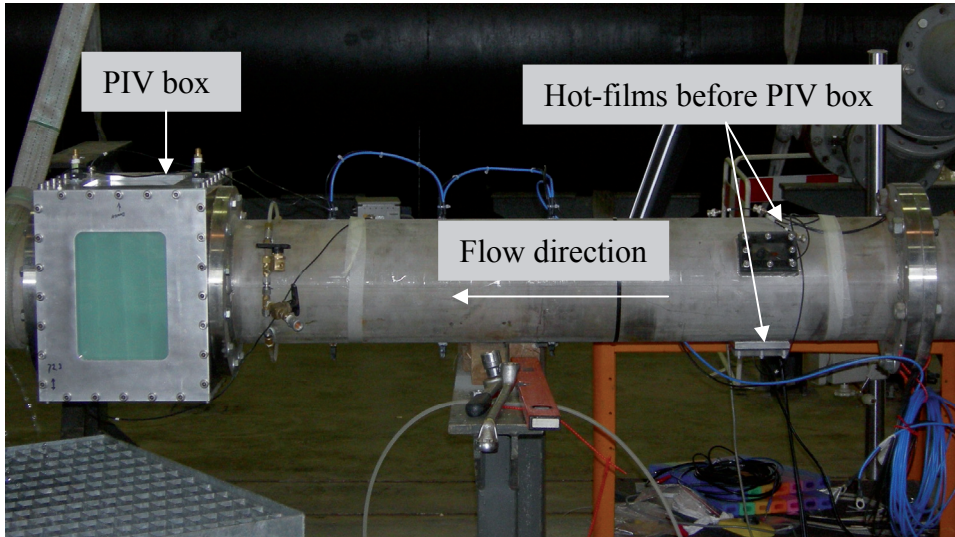


Figure 3. 2 – Test section

3.2 Description of instrumentation

The instrumentation for the unsteady flow tests was carefully selected to have the suitable accuracy and frequency response. Instruments were calibrated before and after the dynamic measurements up to 3 times per day (see Section 3.3). The sampling frequency for each continuously measured quantity (except PIV) was for steady-state calibration $f_s = 100$ Hz and for dynamic measurements $f_s = 1000$ Hz. For high Reynolds number cases, a high-speed PIV camera was set to record at a frequency of $f_s = 3000$ Hz, whereas for lower Reynolds number cases, it was $f_s = 2000$ Hz or $f_s = 1000$ Hz.

The layout of the dynamic instruments in the test rig for accelerating flows from rest (both reversing and non-reversing) is depicted in Figure 3.3. The following quantities were measured continuously:

- ◆ valve position;
- ◆ pressure in three locations:
 - close to the downstream end valve (app. 1/10 of the pipe length from the control valve)
 - close to the PIV box (app. 1/4 of the pipe length from the control valve)
 - app. 2/5 of the pipe length from the control valve
- ◆ differential pressures in two locations
 - within the test length (distance between the taps is app. 3/10 of the pipe length)
 - between the downstream-end pressurized tank and the pipe (reversing flow tests only)

- ◆ velocity profile (PIV box)
- ◆ wall shear stresses in two axial locations
3 sensors at the PIV box
3 sensors app. 1.2 m upstream of the PIV box
- ◆ water temperature
- ◆ flow rate (2 electromagnetic flow meters app. 2/3 of the pipe length from the control valve)
- ◆ flow direction (reversing flow tests only).

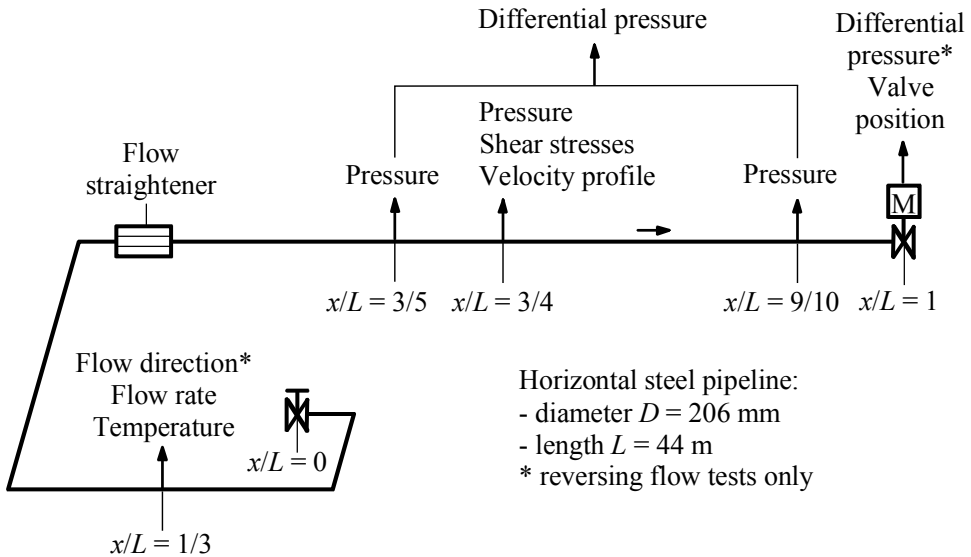


Figure 3.3 - Layout of dynamic instruments in a test rig for non-reversing and reversing accelerating flows (Vardy et. al., 2009)

Two different electromagnetic flow meters were attached to the system (Endress-Hausser and ABB). In A1 test series only flow measurements gained with ABB flow meter were used. In A1A and B tests flow measurements of both flow meters were recorded. Endress-Hausser values were used in the analysis. ABB's working range was 0 - 100 l/s and Endress-Hausser's 0-80 l/s.

3 differential pressure transducers were attached at the same location and their working ranges were 0-7.5 mbar (Rosemounth 3051), 0-60 mbar (Rosemounth 3051) and 0-600 mbar (Siemens Sitram P). The length between the pressure probes was 15.78 m (A1 tests) and 13.76 m (A1A and B tests).

3 strain-gauge pressure probes with a measuring range of 0-7 bar (Druck GE, PDCR-4030 series) were attached to the system at different points. The distance between the probes was approximately 8 m (see Figure 3.3).

Six glued-on type shear stress sensors were mounted to the system. 3 hot-films (4, 5, 6) were placed in the test section 1.2 m before the Perspex box and the other three (1, 2, 3) were inside the PIV Perspex box (Dantec). In both

locations they were attached in three different positions over the pipe perimeter (see Figure 3.4). The angle between the sensors was 120°.

The uncertainty of reading was ± 0.5 % in flow measurements, pressure measurements ± 0.08 % and calibrated hot-film measurements ± 3 % (Jorgensen, 2002).

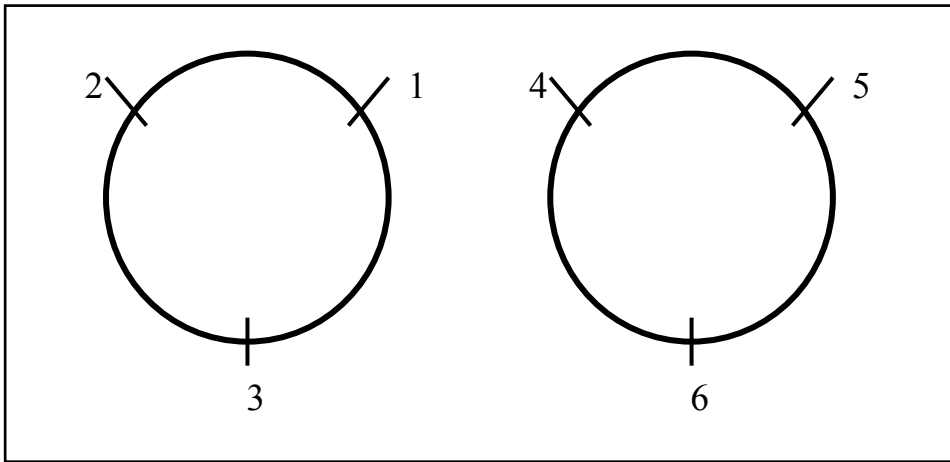


Figure 3. 4 – Positions of the hot-films

In each test the data was stored in 3 different files:

- ◆ With the extension *.set*: a set-up data file giving information about the channels and the calibration file used;
- ◆ With the extension *.raw*: a raw data file as logged by the data logger;
- ◆ With the extension *.dat*: a raw data file converted to engineering units using specified calibration within the program.

3.3 Shear stress sensor calibration and PIV settings

Shear stress sensor calibrations were carried out up to 3 times per day – in the morning, at midday and in the afternoon (depending on the test program). The sensors were calibrated using pressure (gained from differential pressure transducers) and flow measurements for a series of steady flow. Shear stress was directly calculated from pressure using the pressure gradient:

$$\tau_w = \frac{D \cdot \Delta p}{4 \cdot L} \quad (3.1)$$

Shear stress from flow measurements was calculated using Haaland's equation (Haaland, 1983):

$$\tau_w = \frac{1}{2} \frac{\rho \cdot V^2}{\left\{ 3.4735 - 1.5635 \cdot \ln \left[\left(\frac{k}{R} \right)^{1.11} + \frac{63.635}{Re} \right] \right\}^2}, \quad (3.2)$$

where pipe roughness $k = 0.06$ mm was deduced from steady state pressure measurements using Darcy's equation.

Action tables used for hot-films calibration allowed the control valve to open slowly in small steps in between different steady states. The whole process was stored but only a part of the data was used for calibration. Flow and pressure measurements were averaged over the last 30 seconds of a particular steady state while hot-film measurements were averaged at low Reynolds numbers ($Re < 15\ 000$) over the last 5 seconds and at higher Reynolds numbers over the last 30 seconds. This was due to the fact that at low Reynolds numbers the stabilization time for the hot-film probes was longer.

In this study, to calibrate hot-films, shear stress is calculated from flow using Eq. (3.2). The main reason for this was that the shear stress values calculated from three differential pressure probes varied in comparison with Reynolds numbers due to different measurement ranges. Calculated shear stress from the flow rate and differential pressure versus the Reynolds number is depicted in Figure 3.5.

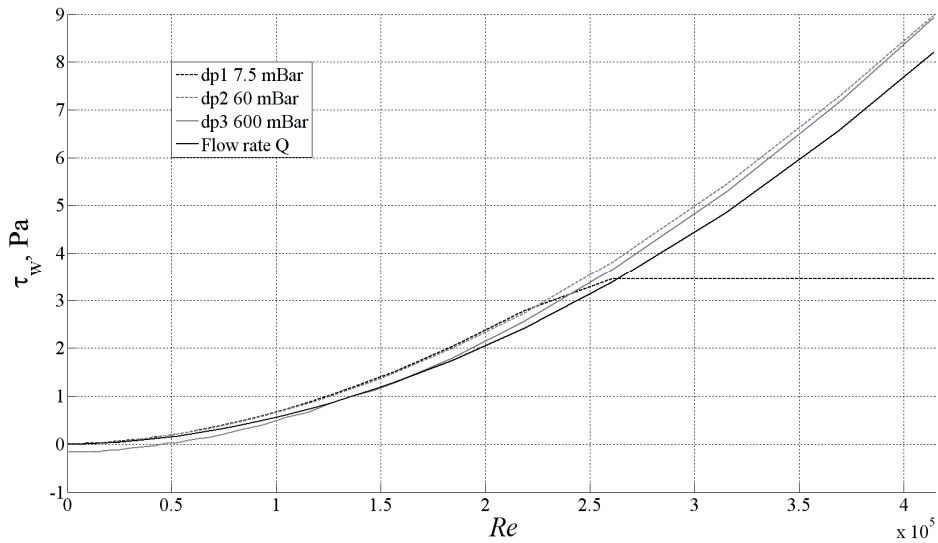


Figure 3. 5 – Calculated shear stress versus the Reynolds number

Calibration curves for hot-films shifted from day to day (sometimes even during a day) so two different approaches were used to calibrate hot-films – individual calibration and group calibration. Individual calibration means that specific calculated calibration curves were used to investigate specific test results (single cases, ensembles that were measured in a short time period). For larger ensembles group calibrations were used. In this case data points gathered from a number of steady state runs were used to calculate calibration curves for hot-films. An example of calibration curves for hot-film 2 is shown in Figure 3.6. Individual calibration from steady state run Group0A020 is used.

In most of the cases it was not possible to use one curve to fit all the data points. Therefore up to three different curves were used to get better results. At low Reynolds numbers shear stress sensors over responded and the stabilization of the output took a long time (about one minute). As a result the averaging of the values could be done over a shorter period of time (~5 seconds). At higher Reynolds numbers the sensors were more stable.

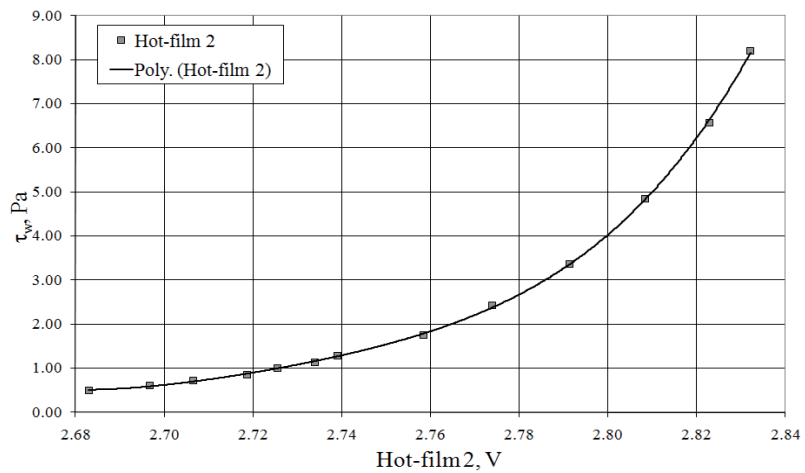
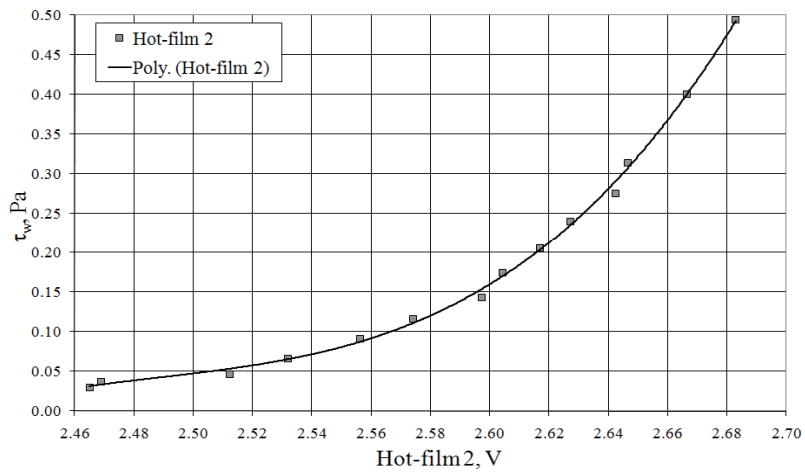
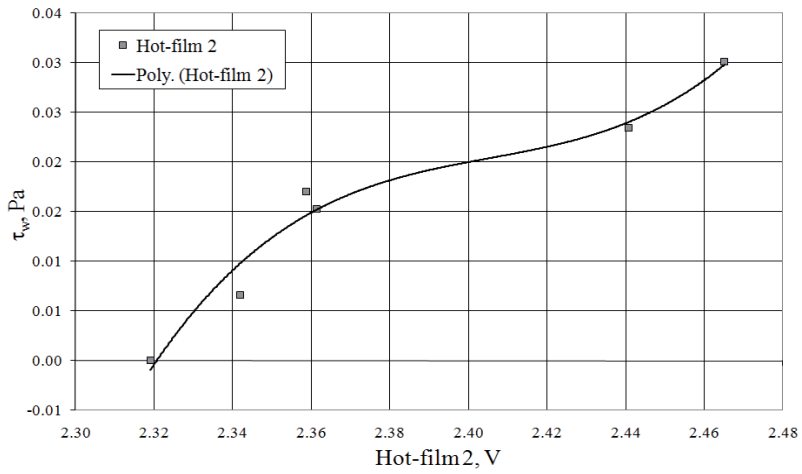


Figure 3. 6 – Calibration curves for hot-film 2, steady state run Group0A020

PIV measurements were carried out using a high-speed camera (HighSpeedStar 3 by LaVision) and a laser for lightening. The camera was adjusted so that it covered nearly the pipe radius (from the top of the pipe to the center). The size of a window used was 256x512 pix. In high Reynolds number cases the camera was set to record at a frequency $f_s = 3000$ Hz ($Re_l = 0$, $Re_f = 400\ 000$), at lower Reynolds number cases $f_s = 2000$ Hz ($Re_l = 0$, $Re_f = 200\ 000$) and $f_s = 1000$ Hz ($Re_l = 0$, $Re_f = 100\ 000$). Diode type laser (LV532 – 1500, produced by DPSS) settings were adjusted accordingly to the test. In high Reynolds number cases the laser was set to the maximum power (1.5 W), in lower Reynolds number cases it was decreased to around 0.9 W. Air bubbles were used for seeding. Therefore multiple electrified wires were inserted into the pipe. Voltage difference between the pipe and wires caused electrolysis and air bubbles were released. The wires were attached inside the pipe just before the Perspex box.

PIV settings in accelerating flow tests were adjusted according to the mean flow ($V_{max}/2$). Acceleration process was recorded for 8 seconds which corresponded to 24 000 images per test. Recording and processing of the data was done using special software DaVis 8.0 (by LaVision). Settings for processing were selected emanated from the particle displacement between frames. The optimal value for particle displacement between continuous frames is about 4 pixels (1/4 of the interrogation area), so the optimal interrogation area should be 16 x 16 or 32 x 32 pixels (Tavoularis, 2005).

The cross-correlation method was used to process the PIV data. As a result, velocity vector fields were calculated taking account of the displacement of the particles between two frames (Figure 3.7). The processing of the data was divided into two groups. At the start of the acceleration process an interrogation window of 32 x 32 pixels with 50% overlap, decreasing size multiple passes (starting from 256 x 256 pixels) and increment of 3 images was used. There was no pre- or post-processing of the images carried out. The same settings were used at higher velocities except that the increment of images was set to 1.

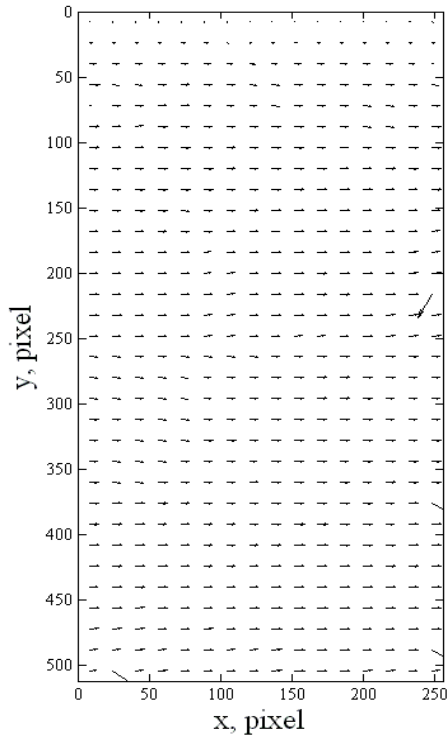


Figure 3. 7 – Calculated velocity vector field, test A1A076, $Re_l = 0$, $Re_f = 400\,000$, $t_v = 2\text{ s}$

A simple reference image with rulers inserted in the pipe was used to calibrate the PIV (shown in Figure 3.8). As a 50 mm camera lens with almost vertical and horizontal lines and a Perspex box was used in the tests, no distortion was taken into account in the calibration. Therefore, a calibration mode “Define scale, no image distortion” was selected. In that mode two points from the reference image and the distance between them measured in mm should be specified. The other option is to enter the pixel / mm ratio directly (LaVision GmbH, 2005). From the calibration image a scale of 1 mm = 5.745 pix was set and used in further calculations.

The post-processing of the calculated vector fields was performed in the Matlab environment using a freeware PIVMat. The PIVMat Toolbox for Matlab contains a set of command-line functions to import, post-process and analyse 2D vector fields from various file formats, including DaVis 8.0 files from LaVision (PIV and Synthetic Schlieren applications). It enables to handle and perform complex operations over a large number of vector fields, and to produce high-quality 2D and 3D outputs based on standard Matlab visualization tools. The

PIVMat Toolbox in itself does not perform any PIV computations (Moisy, 2009).

The calculated vector fields were afterwards cleaned in Matlab from erroneous vectors using simple statistical parameters like range validation and validation by the row median.

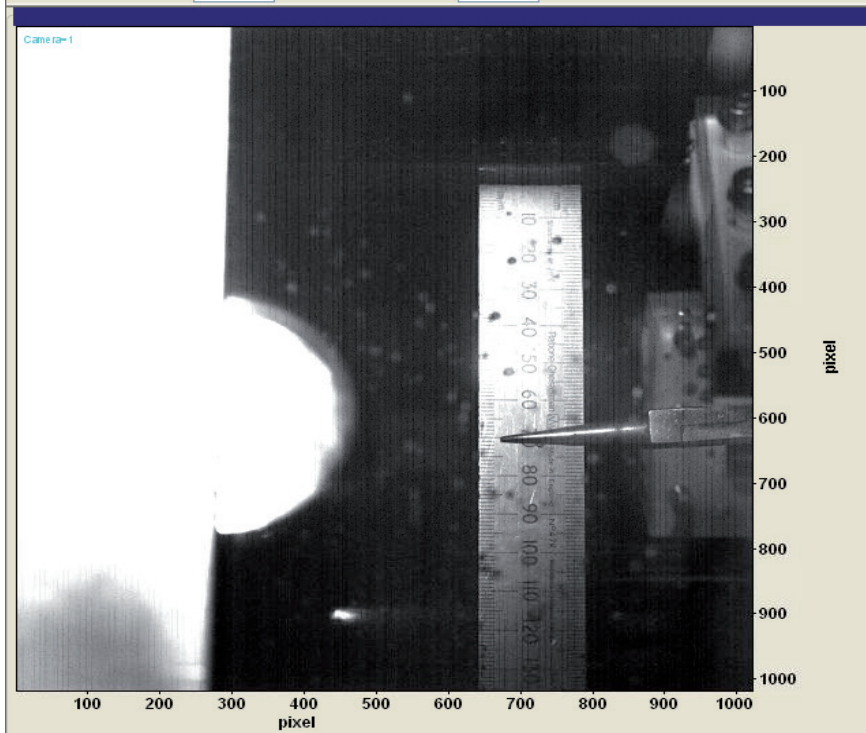


Figure 3. 8 – Image for PIV calibration

Erroneous vectors appeared in the calculated vector fields due to two main reasons – lack of particles in the flow at the start of the accelerating process; bright flashes at the start of the process near the wall region of the pipe (see Figure 3.9). The lack of particles in the flow was caused by the placement of the electrified wires. As they were situated just before the Perspex box where a high-speed camera recorded the flow, there were no visible particles in the pipe just after the start of the process. Therefore, the first moments of the start-up flow could not be visualized. Another major problem was caused by air pockets moving along with the flow and reflecting to the camera as bright flashes. Therefore, some of the data were lost at those images/time steps. This was an issue at the start of the flow when water started to move. In between the tests the electrified rods produced bubbles. As water was not moving, air bubbles accumulated near the top of the pipe. At the start of the test the air pockets moved along with water and as they passed the laser sheet large

reflections were captured. The quality of the vector fields got better as the test proceeded.

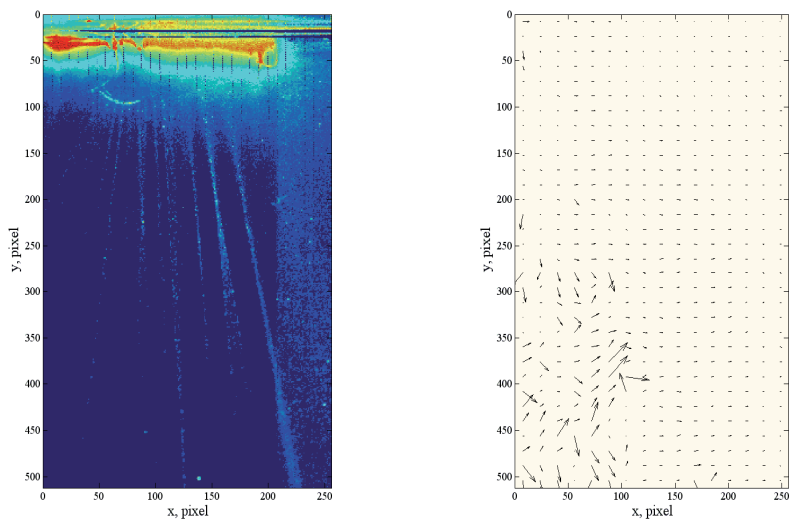


Figure 3. 9 – Example of an air pocket causing erroneous vectors

4. EXPERIMENTAL RESULTS

In this chapter an overview of the experimental procedure and results is given for accelerating from rest tests. A list of test series for all three groups (A1, A1A and B) is shown and analyzed. Furthermore, the test results gained from the present experiments are compared with earlier similar studies and with 1D (presented in Chapter 2) and 2D model calculations. All the hypotheses described in Chapter 1 are discussed in the light of new experimental findings.

4.1 Experimental program

The experimental program presented in this work can be divided into three separate test groups:

- ◆ A1 tests - non-reversing accelerated-from-rest start-up flow is controlled by a butterfly type valve;
- ◆ A1A tests - non-reversing accelerated-from-rest start-up flow is controlled by a globe type valve;
- ◆ B tests - reversing accelerated-from-rest start-up flow is controlled by a pressurized downstream-end tank.

A list of experiments performed in different test groups is given in Table 4.1 – 4.3. The initial condition for all the tests is the same ($Re_I = 0$). In addition to the test number, valve opening time (A1 and A1A tests)/pressure difference (B tests), constant acceleration, the final Reynolds number and whether PIV measurements were performed or not, the presence of one or two flow straighteners is brought forth in Table 4.1. In the middle of the test series A1 the flow straightener positioned just before the control valve was uninstalled from the test rig. In A1A and B test series only the flow straightener on the bend just before the straight test section was installed in the system.

In A1 test series most of the cases were repeated up to three times to check the repeatability of the process. PIV recordings were repeated up to 3 times per test in different cases. Accelerations varied in A1 test series from $A = 0.52 \text{ m/s}^2$ to $A = 2.53 \text{ m/s}^2$.

Table 4.1 – List of experiments in A1 test series

Test no A1	Valve opening time t_v , s	Acceleration A , m/s^2	Re_f	PIV	Flow straightener	
					On the bend	Before the valve
004,005,006	2	2.53	1080000		+	+
010,011,012	2	1.82	695000		+	+
050,051,052	2	1.69	500000	3x	+	
016,017,018	2	1.53	495000		+	+
022,023,024	2	0.95	337000		+	+

027,028,029	2	0.87	215000		+	+
034,035,036	2	0.66	160000		+	+
037,038,039	2	0.53	113000		+	+
040,041,042	2	0.57	68000		+	+
043	2	0.57	68000			
044,045,046	2	0.55	29000		+	+
079,080,081	4	0.83	500000		+	
007,008,009	5	1.09	1080000		+	+
013,014,015	5	0.80	695000		+	+
053	5	0.64	500000		+	
054,055,056	5	0.64	500000	3x	+	
087 - 117	5	0.64	500000		+	
019,020,021	5	0.61	495000		+	+
025,026,030	5	0.55	337000		+	+
031,032,033	5	0.49	215000		+	+
083,084,085	6	0.54	500000		+	
064,065,066	7,5	0.52	500000		+	

In A1A test series most of the experiments were repeated two times. The valve opening time and final Reynolds number were selected to see how different constant acceleration rates in the same Re_f affect the transition to turbulence. One ensemble test series was carried out and 30 repeats of PIV were recorded in the same test as well. Accelerations varied in A1A test series from $A = 0.02 \text{ m/s}^2$ to $A = 0.34 \text{ m/s}^2$.

Table 4. 2 – List of experiments in A1A test series

Test no A1A	Valve opening time t_v , s	Acceleration A , m/s^2	Re_f	PIV
001,012,022	2	0.34	400 000	3x
031,038,044	2	0.34	400 000	3x
052,053,055	2	0.34	400 000	3x
056,058,059	2	0.34	400 000	3x
060,061,062	2	0.34	400 000	3x
063,064,065	2	0.34	400 000	3x
066,067,069	2	0.34	400 000	3x
070,071,072	2	0.34	400 000	3x
073,074,075	2	0.34	400 000	3x
076,077,078	2	0.34	400 000	3x
032	2	0.34	400 000	
002,003	2	0.27	50 000	
004,005	2	0.24	100 000	
082	2	0.24	100 000	1x

006,007	2	0.30	200 000	
080	2	0.30	200 000	1x
008,009	5	0.05	50 000	
010,011	5	0.10	100 000	
013,014	5	0.19	200 000	
015,016	5	0.28	400 000	
017,018,019	7	0.03	50 000	
020,021	7	0.07	100 000	
023,024	7	0.14	200 000	
025,026	7	0.21	400 000	
027,028	10	0.02	50 000	
029,030	10	0.05	100 000	
033,034,035	10	0.10	200 000	
036,037	10	0.16	400 000	
041,042,043	15	0.02	50 000	
046,047	15	0.03	100 000	
048,049	15	0.06	200 000	
050,051	15	0.11	400 000	

In B test series mainly individual tests with no repeats were carried out. Tests were repeated only if concerns about a specific test quality were raised. No PIV measurements were done. As seen in Table 4.3 final steady state velocities in the pipe at higher pressure difference exceeded the upper range of the flow meters (therefore marked as O_of_R in Table 4.3). Accelerations varied in B test series from $A = 0.43 \text{ m/s}^2$ to $A = 4.01 \text{ m/s}^2$.

Table 4. 3 – List of experiments in B test series

Test no B	Pressure difference Δp , bar	Re_f	Test no B	Pressure difference Δp , bar	Re_f
1053	0.05	209 122	1087	1.50	518 796
1054	0.10	226 642	1175	1.50	505 841
1055	0.15	240 583	1176	1.60	537 611
1056	0.20	255 080	1177	1.70	551 490
1057,1058	0.25	272 044	1178	1.80	562 286
1059	0.30	297 644	1179	1.90	569 380
1060,1061	0.35	298 570	1180	2.00	592 513
1062	0.40	309 982	1181	2.10	596 523
1063,1064	0.45	314 917	1182	2.20	614 412
1066,1067	0.50	327 563	1183	2.30	615 954
1068	0.55	342 492	1184	2.40	O_of_R
1069	0.60	355 323	1185	2.50	O_of_R
1070	0.65	362 972	1186	2.60	O_of_R

1071	0.70	375 495	1187	2.70	O of R
1072	0.75	385 303	1188	2.80	O of R
1073	0.80	395 358	1189	2.90	O of R
1074	0.85	400 848	1190	3.00	O of R
1075	0.90	414 296	1191	3.10	O of R
1076	0.95	423 179	1192	3.20	O of R
1077	1.00	432 803	1193	3.30	O of R
1078	1.05	438 910	1194	3.40	O of R
1079	1.10	446 498	1195	3.50	O of R
1080	1.15	458 588	1196	3.60	O of R
1081	1.20	463 832	1197	3.70	O of R
1082	1.25	474 689	1198	3.80	O of R
1083	1.30	486 410	1199	3.90	O of R
1084	1.35	497 513	1200	4.00	O of R
1085	1.40	507 075	1201	4.10	O of R
1086	1.45	511 393	1202	4.20	O of R

4.1.1 Problems that occurred in the test series

The main problem that occurred in the A1 test period was the non-linearity of flow change caused primarily by the control valve. This did not have a major effect on A1 tests with a higher value of accelerations.

Another issue with the control valve was that it opened in steps. This behavior caused pressure waves in the pipe. In some cases (with longer valve opening times) it is noticeable that those pressure waves caused turbulence in the system.

Too few calibration points for hot-film calibrations were gathered. This was noticed in the analyzing process and was caused mainly because of the operation software buildup. Therefore, there is not enough data in the range of low Reynolds numbers to get a good calibration curve.

In A1 series tests with PIV failed. There were problems with the PC software, seeding (not enough bubbles, therefore not enough information) and laser light source. After changing camera lenses and adjusting the light source some tests were recorded but the results were not usable.

In A1A test series most of the problems were cleared and more or less all the tests were repeated. A new laser and seeding system was used to get better results on PIV recordings. The control valve was changed from the butterfly type to the globe type valve. This reduced the problems that affected the linearity of the flow change. The only real issue was that two of the hot-film sensors burned out and therefore could not be recorded. This also affected the B tests as in between the test series the sensors were not replaced with new ones.

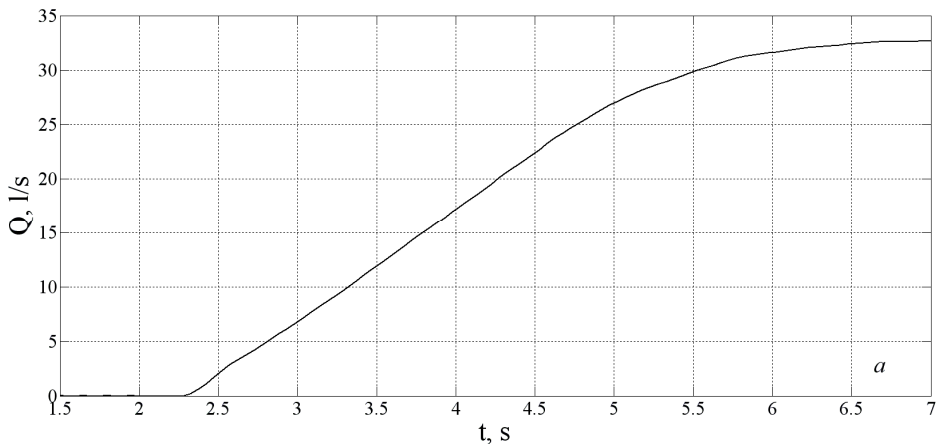
4.2 Experimental results

Experimental results gained from the measurements carried out in Deltares are presented in this section. A 30 repeat ensemble averaged case study is used to describe new findings in the transitional process in accelerating pipe flows. Single cases are used to evaluate different criteria that were proposed in earlier studies by Kurokawa and Morikawa (1986), Lefebvre and White (1991), Koppel and Ainola (2006) and Nakahata et. al. (2007).

The main case study deals with uniformly accelerating flow starting from rest ($Re_f = 0$) and accelerating to $Re_f = 400\,000$. The valve opening time for this case was $t_v = 2$ s. PIV measurements of 30 repeats were carried out to deduce the ensemble averaged velocity vector fields and to describe the evolution of velocity profiles and velocity fluctuations in axial and radial directions in accelerating pipe flow started from rest.

4.2.1 Similarity in transition to turbulence over the pipe length

Earlier experimental studies (Daniel and Koppel (1985), Lefebvre and White (1989, 1991), Koppel and Ainola (2006), Nakahata et. al (2007)) show that at high accelerations transition to turbulence takes place simultaneously over the entire length of the pipe. Lefebvre and White used acceleration rates from 0.2 m/s^2 to 11.8 m/s^2 and concluded that transition times in the test section between different hot-films varied about 3 % or 50 milliseconds. New experimental findings gained in Deltares in a 206.4 mm pipe do not support the hypothesis regarding high and mid-acceleration rates. However, it should be noted that in the test rig hot-films were mounted only at two places over the pipe length and the distance between the sensors was about 1 m. In Figure 4.1 the measured quantities of flow rate and shear stresses are presented for a single start-up accelerating flow. The final Reynolds number for this case is $Re_f = 200\,000$ and the valve opening time $t_v = 2$ s.



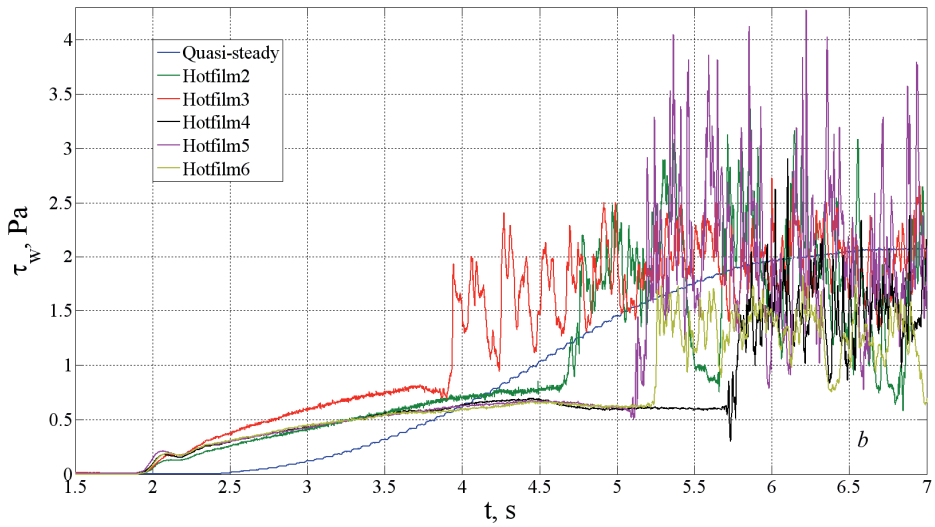


Figure 4. 1 – Case A1A007; a – variation of the flow rate, b – variation of shear stresses

The opening of the control valve causes constant acceleration. Five shear stress sensors located in different axial and radial locations (see Figure 3.4) react to turbulence at different times varying from $t^* = 3.87$ s for hot-film 3 to $t^* = 5.72$ s for hot-film 4. Transition to turbulence takes place at different times over the pipe length and at different radial positions. This tendency is common for all measured cases. The time period of transition to turbulence between the reaction times of the first and last hot-film decreased with the increase of acceleration rates. The selected cases are presented in Figure 4.2 to describe the tendency. The interdependence of the two variables can be described by a power function presented by Eq. (4.1).

$$t = 0.88 \cdot A^{-0.72} . \quad (4.1)$$

The R-squared value or the coefficient of determination for Eq. (4.1) is 0.970.

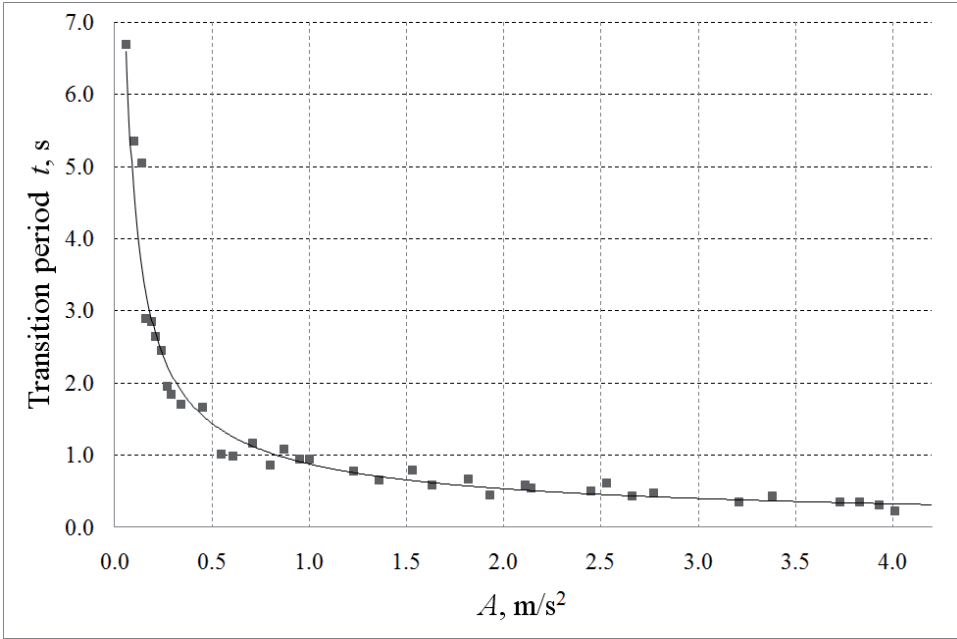


Figure 4. 2 - Dependence between the acceleration rate and transition period

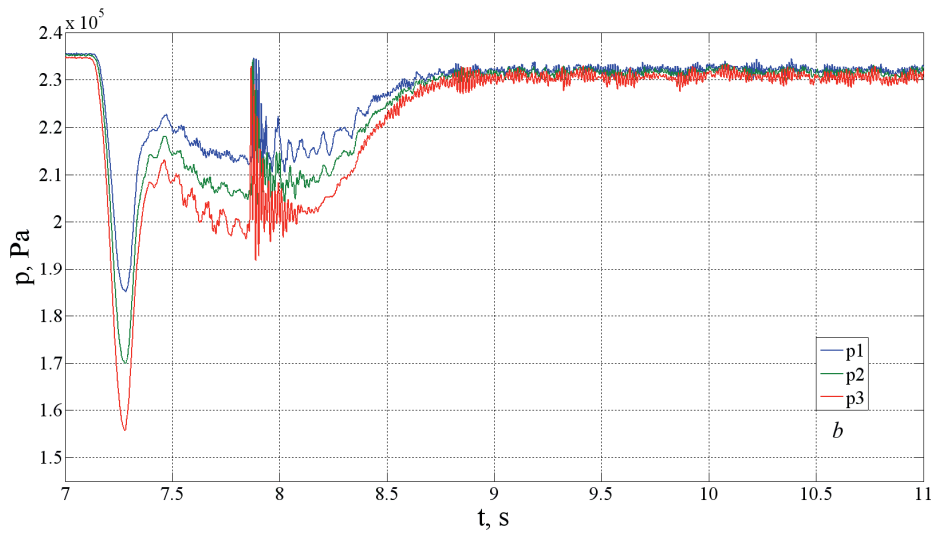
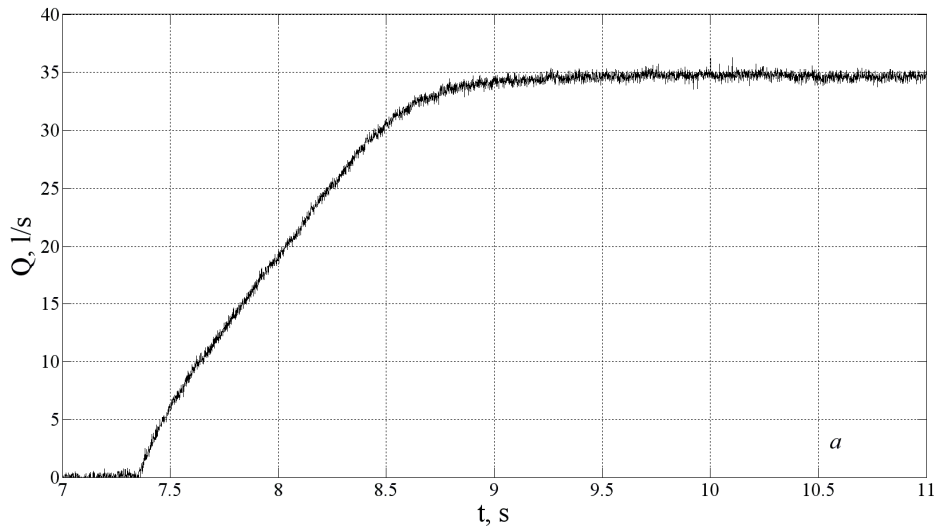
4.2.2 Turbulent slugs

In transition from the laminar to the turbulent state in Hagen-Poiseuille pipe flow two different phases are described – puffs and slugs (Wynanski and Champagne (1973)). In their interpretation slugs are caused by the instability of the boundary layer to small disturbances in the inlet region of the pipe and puffs are generated by large disturbances at the inlet. While slugs are associated with transition from laminar to turbulent flow, puffs represent an incomplete relaminarization process. Puffs can only be seen at $2000 \leq Re \leq 2700$, while slugs occur at any $Re \geq 3200$.

In accelerating pipe flows only turbulent slugs are noticed in some experimental investigations (Moss, 1989; Lefebvre and White, 1991). Lefebvre and White described the appearance of turbulent slugs as an arbitrary process, developing only at definite initial conditions. The slug was a localized, short duration region of turbulence thought to arise from a natural occurrence. The presence of the slug was identified by an abrupt laminar to turbulent transition followed by a brief duration of sustained turbulence and subsequently a reversion to laminar flow (Lefebvre and White (1991)).

Turbulent slugs were noticed in the present study. Figures 4.3 and 4.4 show the appearance of turbulent slugs at two different initial conditions. In A1027 the final Reynolds number was $Re_f = 215\,000$ and the valve opening time $t_v = 2$ s as in A1A014 $Re_f = 200\,000$ and $t_v = 5$ s. A butterfly type control valve

was used in A1027 and for A1A014 flow was controlled by a globe type valve. It should be noticed that linear change in the flow rate could not be obtained with a butterfly valve. However, nonlinearity seems to have practically no influence on the transition process in general (based on all the tests carried out in A1 series).



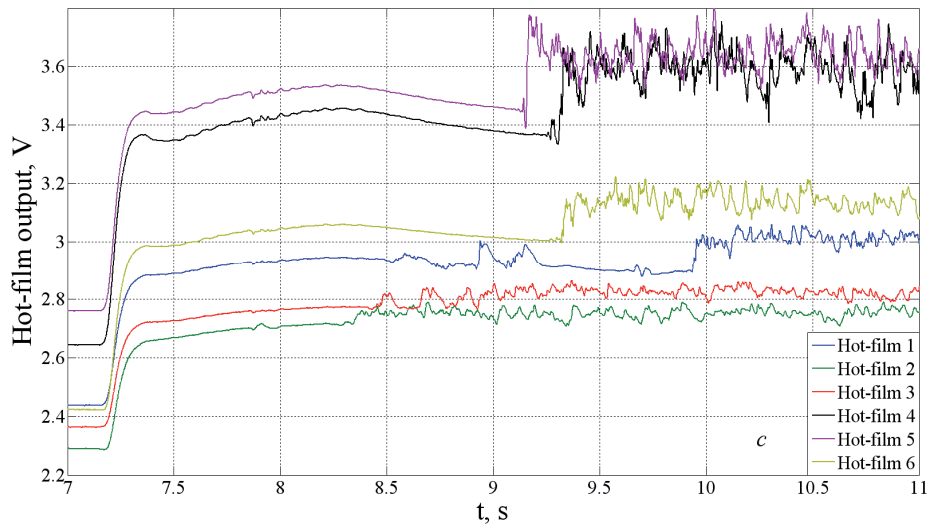
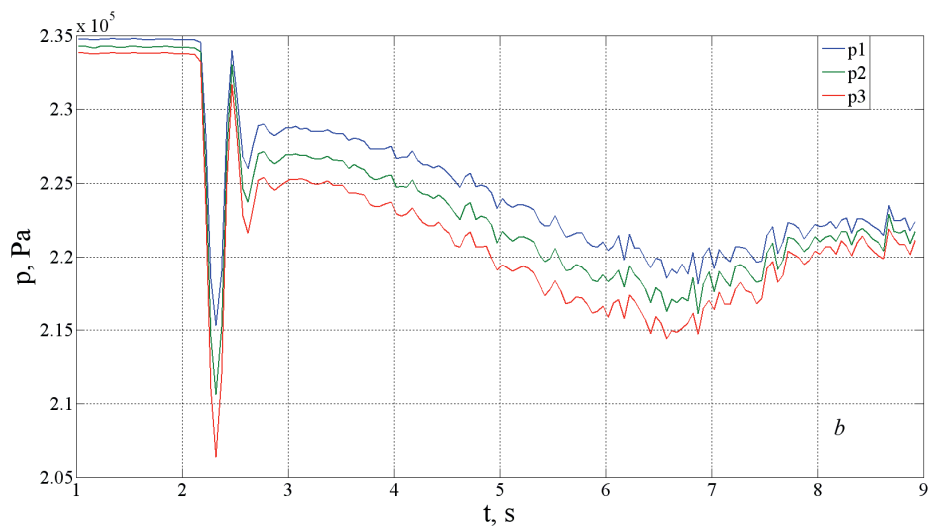
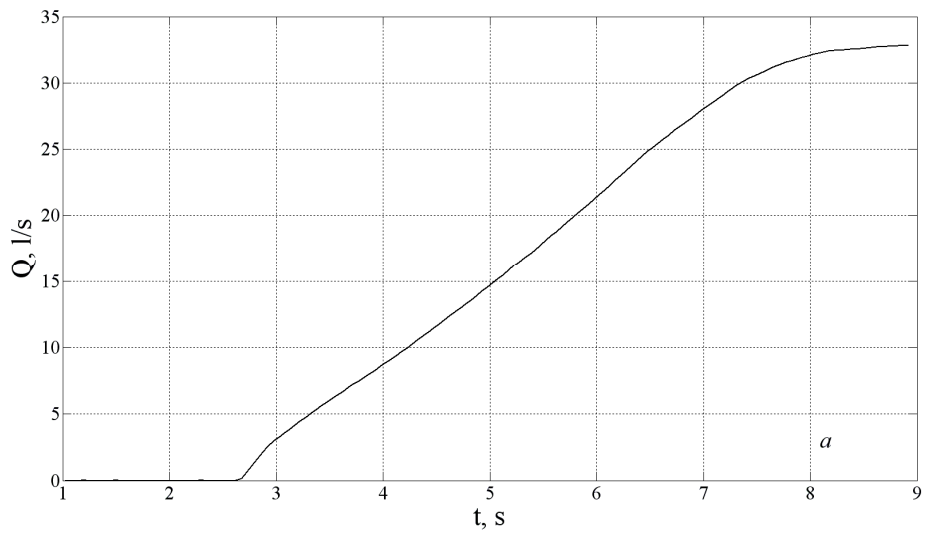


Figure 4. 3 – Case A1027; a – variation of the flow rate, b – variation of pressure, c – variation of hot-film output

As seen in Figure 4.3c a turbulent slug passing hot-film 1 at $t = 8.92$ s causes a short-term increase in its output voltage value. As the slug passes, the output voltage decreases and the transition to turbulence occurs at $t_* = 9.94$ s.



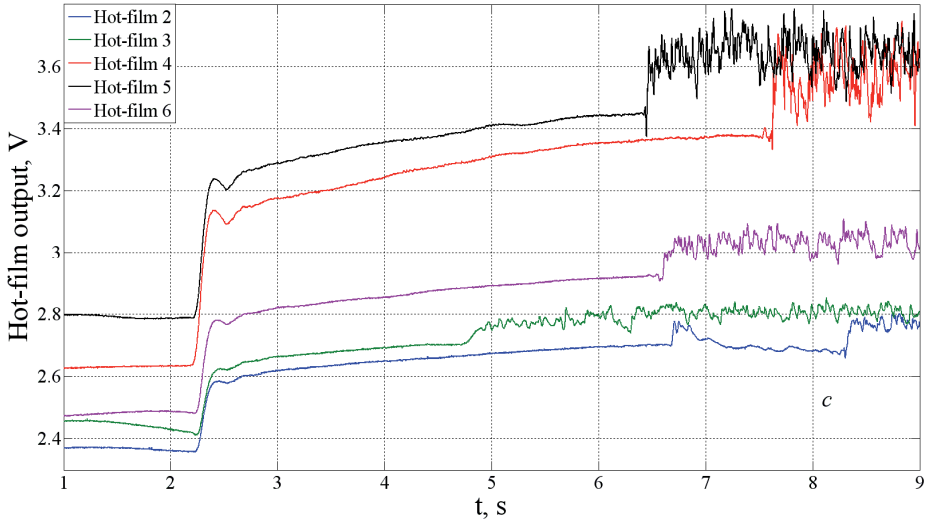


Figure 4. 4 – Case A1A014; a – variation of the flow rate, b – variation of pressure, c – variation of hot-film output

In the present case a turbulent slug is captured by hot-film 2 causing an increase in its output value at $t = 6.68$ s (Figure 4.4c). Other shear stress sensors do not react to the slug indicating that the appearance of the slug is local.

Turbulent slugs were noticed in random test cases and the appearance was arbitrary. Repeated test series carried out at the same initial conditions did not capture the development of turbulent slugs in every repeated run, i.e. the occurrence of turbulent slugs was not repeatable.

4.2.3 Ensemble averaged test results

Time for the experimental study was limited. Therefore, it was feasible to measure only one 30 repeats ensemble test series. This was due to the large amounts of data gathered from PIV measurements – one 30 repeats ensemble measurements need a whole day. Ensemble averaged test results were calculated using Eqs. (4.2) – (4.7). Ensemble averaged shear stresses and RMS values were calculated from hot-film measurements. The time step used in the calculations was set to 1. The ensemble averaged mean shear stress is defined as

$$\langle \tau_w \rangle = \frac{1}{N} \sum_{n=1}^N \tau_{wn} , \quad (4.2)$$

where τ_{wn} represents the shear stress of the n th repeat of the flow transient. N is the total number of repeated runs.

RMS value of shear stress for each individual hot-film is calculated using equation (4.3).

$$\tau_w' = \sqrt{\frac{1}{N} \sum_{n=1}^N (\tau_{wn} - \langle \tau_w \rangle)^2} . \quad (4.3)$$

For accelerating transient flow the instantaneous local velocity can be decomposed into an ensemble averaged mean velocity and a turbulent fluctuating velocity. Axial and radial mean flow and RMS values of the components of velocity fluctuations were calculated from PIV measurements repeated over 30 runs. Time steps varied due to the large amount of data. Ensemble averaged mean velocity is defined as

$$\langle u_z \rangle = \frac{1}{N} \sum_{n=1}^N u_{zn} , \quad (4.4)$$

$$\langle u_r \rangle = \frac{1}{N} \sum_{n=1}^N u_{rn} , \quad (4.5)$$

where u_{zn} represents any component of instantaneous axial and u_{rn} radial velocity of the n th repeat of the flow transient. N is the total number of repeated runs.

The RMS values of components of turbulent fluctuations are defined as

$$u_z' = \sqrt{\frac{1}{N} \sum_{n=1}^N (u_{zn} - \langle u_z \rangle)^2} , \quad (4.6)$$

$$u_r' = \sqrt{\frac{1}{N} \sum_{n=1}^N (u_{rn} - \langle u_r \rangle)^2} . \quad (4.7)$$

It shall be noted that the term “mean” will be used to denote the ensemble averaged unless stated otherwise.

The presented case study deals with uniformly accelerating flow starting from rest ($Re_f = 0$) and accelerating up to $Re_f = 400\,000$. The valve opening time for this case was $t_v = 2$ s. An ensemble average of 30 experiments is used to deduce the mean flow rate, pressure, wall shear stresses and RMS values of wall shear stresses presented in Figures 4.5 – 4.8. The repeatability of measurements is good (the difference in hot-film reaction times to turbulence between single cases varies up to $\pm 2\%$). Hot-films 2 and 5 were used to interpret the results as they were found to be the most stable and reliable during the measurements.

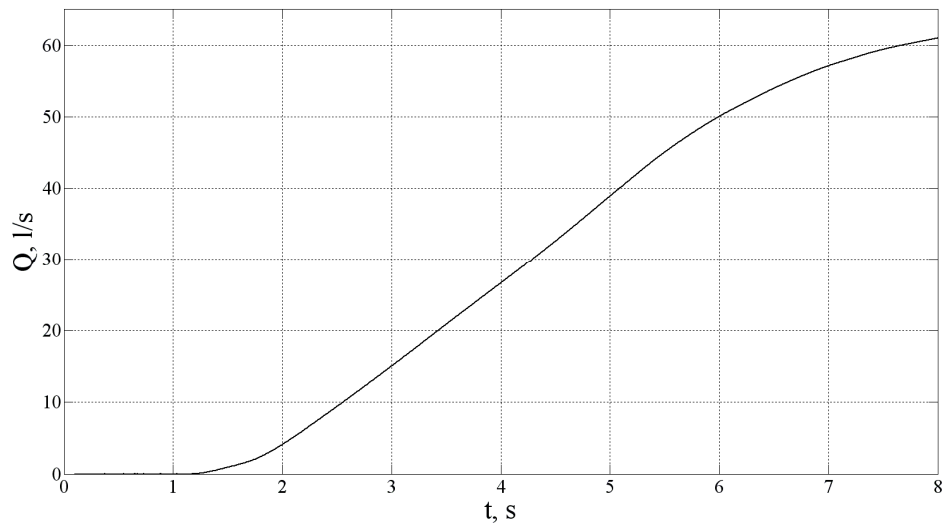


Figure 4. 5 – Variation of the mean flow rate

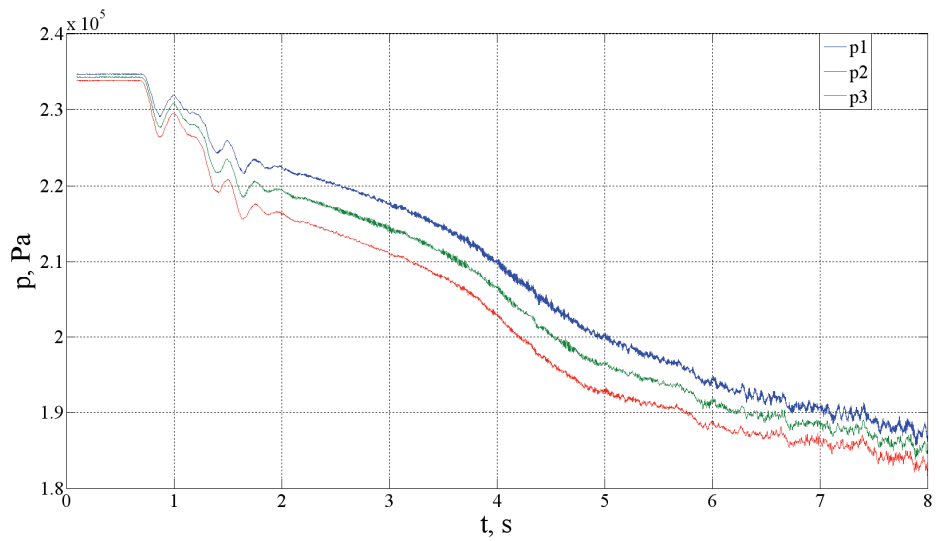


Figure 4. 6 – Variation of mean pressure

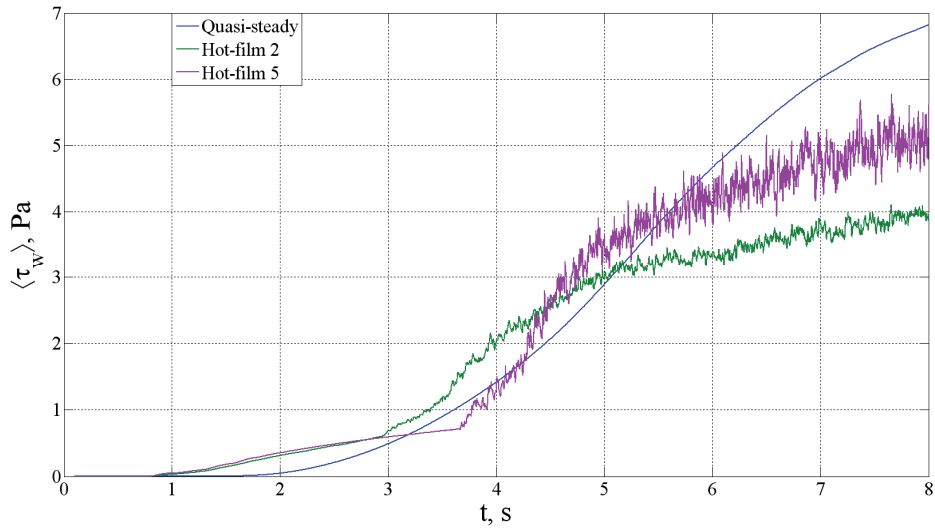


Figure 4. 7 – Variation of mean wall shear stress

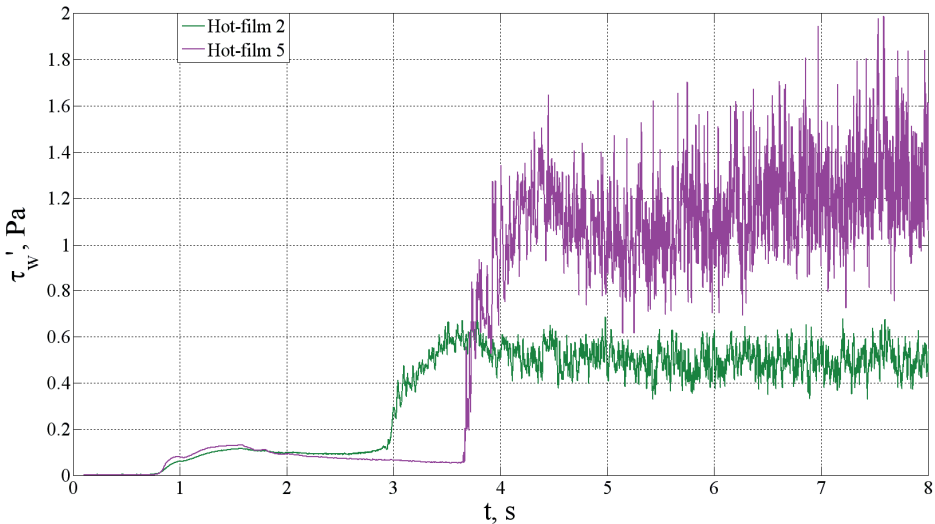


Figure 4. 8 – Variation of RMS of wall shear stress

An abrupt transition from laminar to turbulent flow in pipes is common for start-up flows from rest (Lefebvre & White, 1991, Koppel & Ainola, 2006). The transition to turbulence is delayed up to the supercritical Reynolds number. The quasi-steady value of shear stress presented in Figure 4.7 is calculated for dynamic flow by using the Haaland equation (Haaland, 1983). The examination of shear stress values reveals that the wall shear stress in the accelerated flow initially over-responds compared to the quasi-steady value. Thereafter, the generation of turbulence takes place at different time moments (starting at $t = 3$ s), and the increase in the wall shear stress decreases and it eventually becomes

lower than the quasi-steady value. Later the flow approaches the steady flow condition and the wall shear stress approaches the quasi-steady values. Similar results in a pipe with a smaller diameter were gained by Kurokawa and Morikawa (1986), who stated that in the case of laminar flow the friction coefficient was found to be greater than the corresponding value of the quasi-steady flow. In contrast, it was found to be smaller under the conditions of turbulent flow. The examination of the measured shear stress in the PIV box (hot-film 2) and upstream of the box (hot-film 5) revealed that there was a difference in turbulence generation time. At the same time, all the recorded data in ensemble are similar, repeatability of measurements is very good ($\pm 2\%$).

The difference in turbulence intensity captured by different sensors could have arisen from the hot-film 5 being installed in an old stainless steel pipe and the hot-film 2 in a smooth Perspex pipe. The steel pipe was hydraulically smooth; the roughness over its perimeter varied.

Transition to turbulence seems to have little effect on the mean flow rate. At some acceleration rates it is noticed that at the moment of transition the acceleration of mean flow decreases and starts to increase when the flow is fully turbulent. However, averaging even over two repeated tests smoothes the nonlinearity in flow excursion, indicating that the decrease and increase in flow acceleration could be an arbitrary process. The nonlinearity at the beginning of flow excursion (present in some cases) does not seem to influence the transition process at all.

Changes in pressure are given in Figure 4.6 and can be divided into four parts. At initial stages, because of the opening of the control valve, pressure waves travel through the system and cause remarkable changes in pressure ($t = 0.8 - 1.8$ s). After that the flow is accelerated and pressure in the system starts to drop as pressure difference stays about the same ($t = 1.8 - 3$ s). In the period of transition quick changes in pressure can be seen in different time steps. This usually causes rapid changes in pressure difference as well, depending on the acceleration rate ($t = 3 - 5$ s). After that flow is fully turbulent and reaches a new steady state.

In Figure 4.9 the development of the velocity profile in time is shown. The first time steps in PIV recordings were interrupted with noise (light flashes reflected from air bubbles), and reliable data are not available.

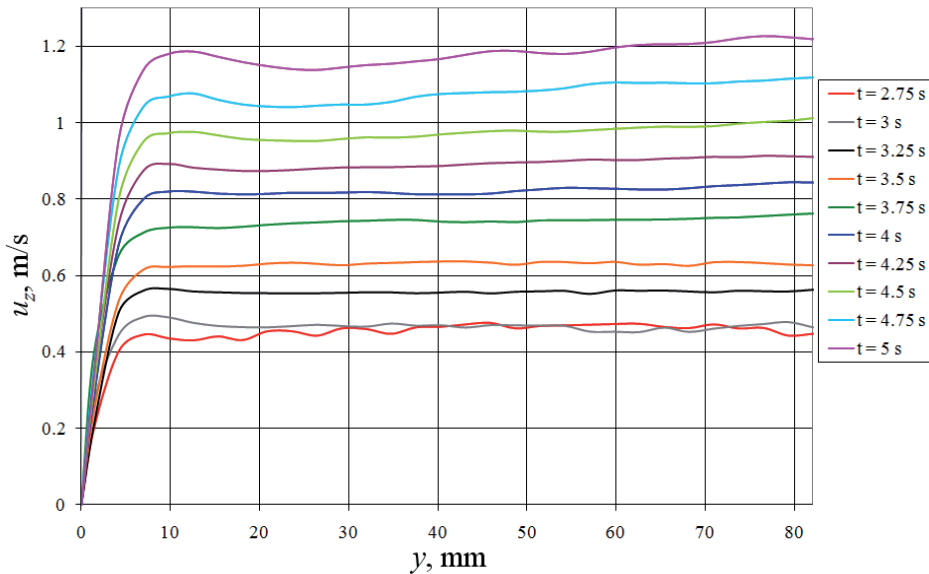


Figure 4.9 – Development of the velocity profile in accelerating flow

It can be deduced from the hot-film measurements that the turbulization process starts in the pipe at $t = 3$ s. It is clearly seen that the shape of the velocity profile in the core remains practically unchanged until the flow is fully turbulent ($t < 4.5$ s). On the other hand, near-wall velocity increases with high velocity gradients evolving immediately. In the turbulent region it can be noticed that flow decelerates near the pipe wall ($r = 10 - 40$ mm) and accelerates in the core region. The initial uniform velocity profile caused by bulk-flow acceleration does not remain equable.

In Figure 4.10 the development of RMS values of axial velocity in time is given. The color bar shows the u_z' values in m/s. The RMS variation of velocity fluctuations in Figure 4.10 indicates a slow increase in the core region of the flow. Near the wall, at $r < 10$ mm, there is a rapid increase which appears to propagate outwards as time progresses. The bulk flow acceleration causes the velocity in the core to increase at a constant rate. However, near the wall the no-slip condition at the wall causes large velocity gradients. With time, the influence of the wall constraint slowly propagates towards the pipe core ($t > 4.1$ s). The imposed acceleration in this particular case is relatively high and therefore little response is observed in turbulence away from the wall region. Turbulence production and propagation delays are considerable here.

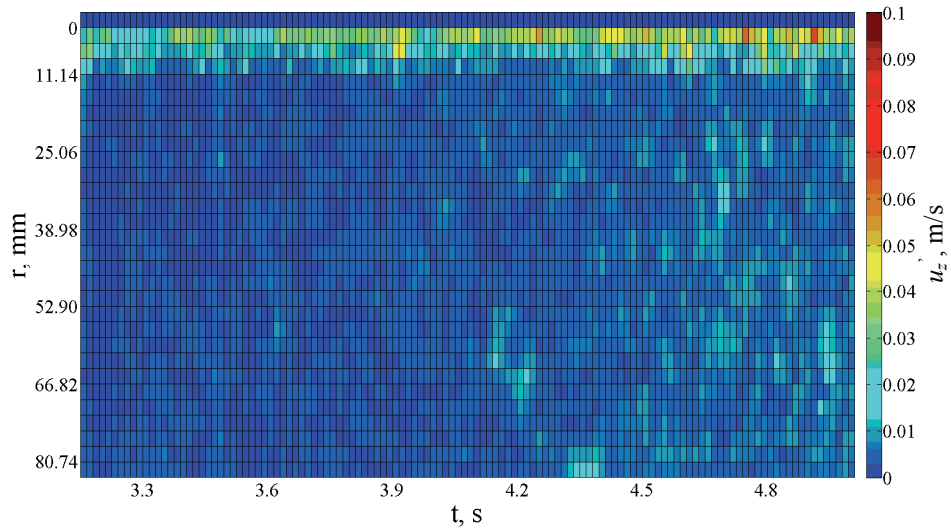


Figure 4. 10 – Development of turbulent intensity in accelerating flow

In Figure 4.11 the variation of axial velocity in three different radial locations is shown compared with turbulent propagation gained from shear stress sensors 2 and 5 and the mean axial velocity calculated from the measured flow rate. It is clearly seen that at the time of transition to turbulence ($t_* = 3$ s) axial velocity near the wall rapidly increases. The fluctuation is seen all over the pipe radius. This is followed by a deceleration near the wall (similar to the findings of Ainola et. al., 1979 and Kurokawa and Morikawa, 1986).

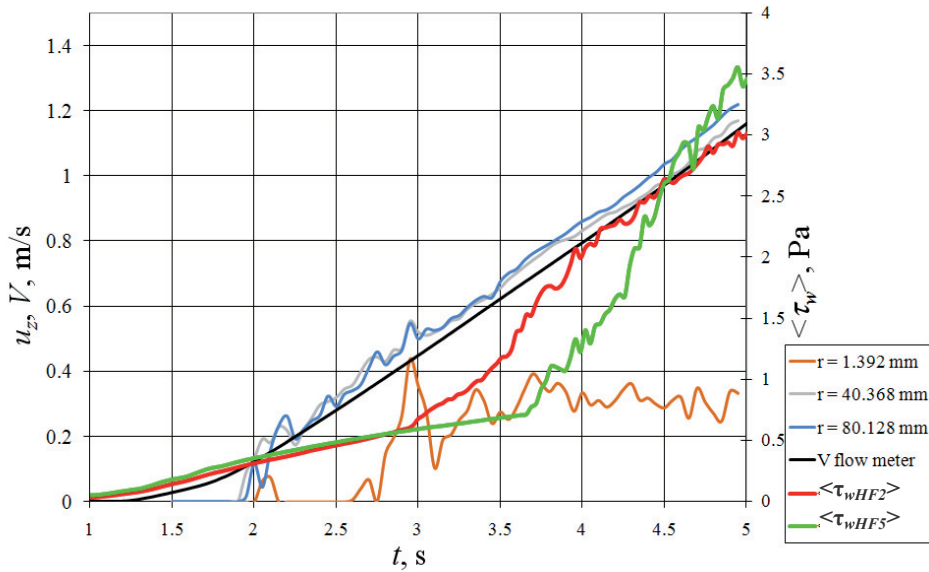


Figure 4. 11 – Variations of axial velocity components in three different radial positions and shear stress at the wall

Afterwards in the core region axial velocity increases linearly and near the wall velocity stabilizes to a constant value. Hot-films show a rapid increase in shear stress as the flow transits into turbulence.

Kurokawa and Morikawa (1986) brought forth in their study that in the fastest acceleration case ($A = 1.7 \text{ m/s}^2$) at the moment of transition flow decelerates at the wall causing a large velocity difference over the pipe radius (similar results were obtained by Ainola et. al., 1979). During the laminar acceleration period velocity difference at each radial position was very small. PIV measurements in the present study give little information about the velocities in the laminar region but it can be seen that after the transition flow starts to decelerate near the wall and accelerate in the core region summarizing similar findings as Kurokawa and Morikawa.

In the next two figures (Figure 4.12 and 4.13) the variation of the radial velocity component is pictured. Compared to axial velocity the radial component is very small and the mean value in steady flow is zero (values of radial velocity fluctuate around zero). Therefore, the main emphasis is placed on the time window where the transition to turbulence is taking place. The color bar shows the values of the radial velocity component u_r in m/s and $r = 0$ corresponds to the top wall of the pipe.

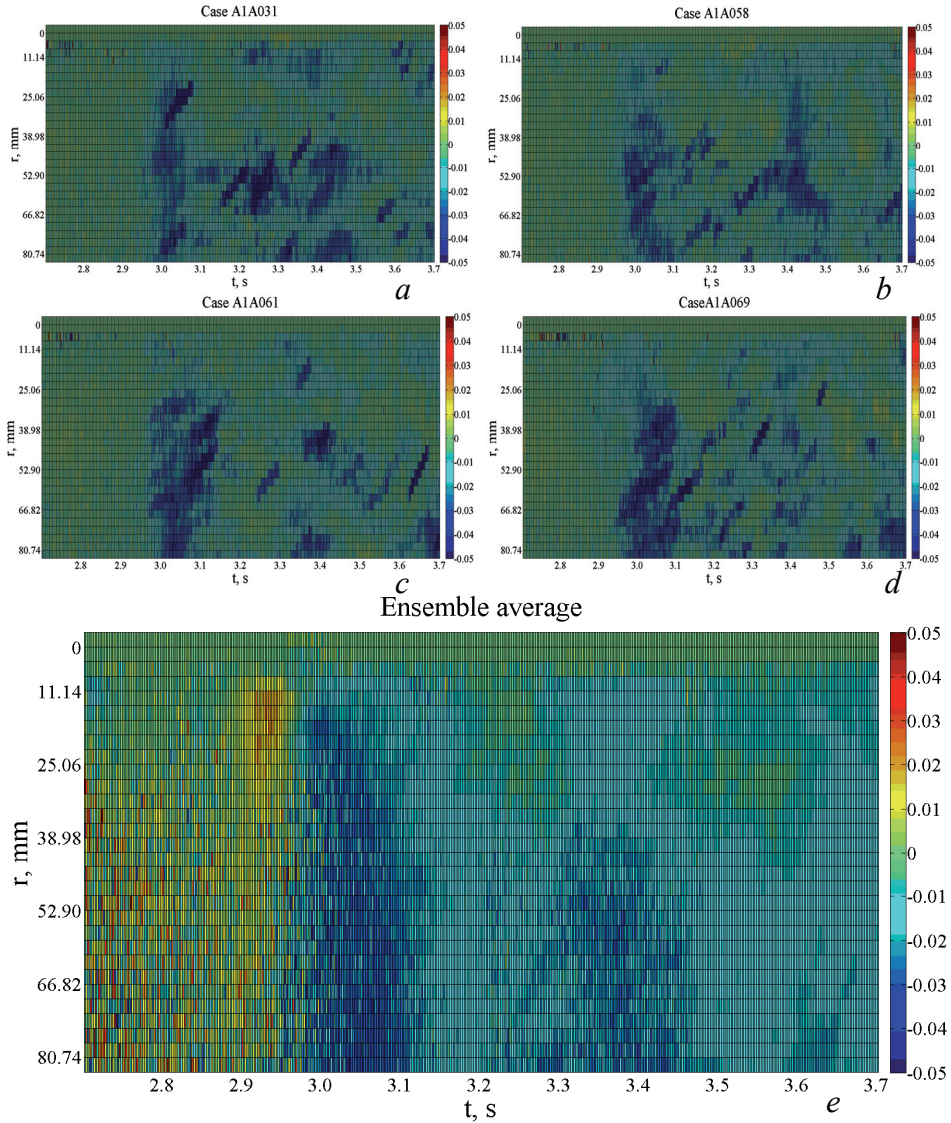


Figure 4.12 – Variation of the radial velocity component in accelerating flow; a – case A1A031; b – case A1A058; c – case A1A061; d – case A1A069; e – ensemble average

Figure 4.12 shows the propagation of the radial velocity component u_r in single measurements and an ensemble averaged value in time in accelerating flows. The negative value of the component corresponds to fluid movement direction from the pipe center to the top. At the moment of transition ($t_* = 3$ s) a progress of radial velocity component towards the pipe top wall is captured by PIV. This structure then settles and appears again in a period $t = 0.35$ s. The increase in radial velocity at the moment of transition is well seen in every single case

measurement as well. The second spike is more arbitrary but well seen in the ensemble averaged figure (Figure 4.12e).

In Figure 4.13 the same movement is given. The propagation of the radial velocity component in different radial locations reveals that a three dimensional wavy structure is developing in the flow at the moment of transition from the laminar to the turbulent state. In every radial position over the pipe radius the velocity is negative, indicating that the fluid is moving from the pipe center towards the top wall. As the movement of the fluid is restricted by the pipe wall, flow direction has to be downwards in another plane, indicating that the developing structure is three-dimensional. The wavy structure is asymmetric allowing the radial velocity to stay negative in between the spikes. PIV measurements indicate that as flow stabilizes in a turbulent steady state, the radial component decreases and fluctuates around zero value ($t > 6$ s, not shown in Figure 4.13).

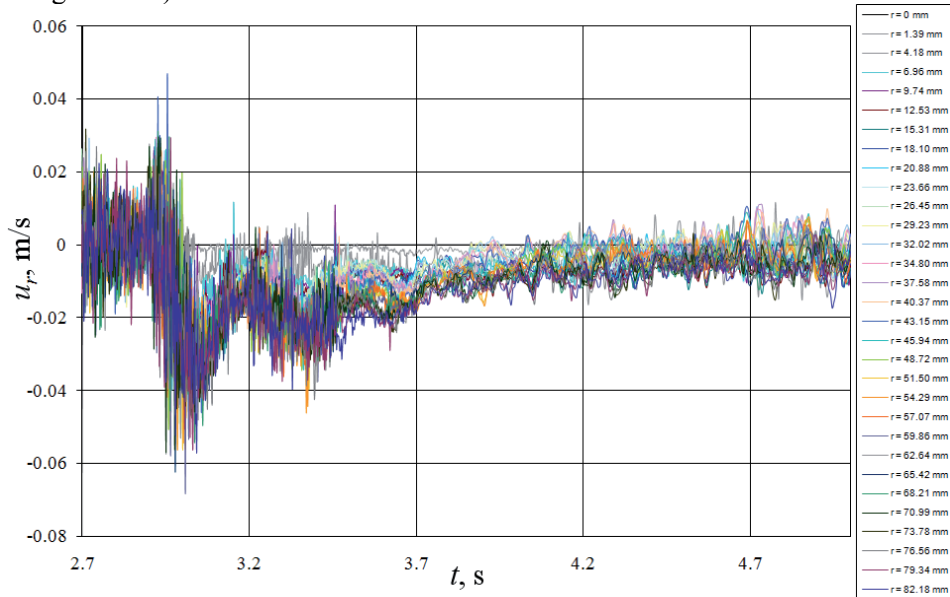


Figure 4. 13 – Propagation of the radial velocity component in time in accelerating flow

Ruubel (1991) showed in his thesis that transition to turbulence in accelerating pipe flow can be described through the equilibrium of forces that influence the flow. Reynolds (1889) stated that in steady flow the transition in flow takes place at the moment when viscous forces overcome inertial forces. In a pipe system the equilibrium of forces is described by Eq. (2.29).

In Figure 4.14 the equilibrium of forces for the ensemble averaged case study is shown. The forces caused by pressure difference are deduced from measurements between pressure probes 1 and 3 using the equation $\frac{1}{\rho} \frac{\partial p}{\partial z}$.

Inertial forces $\frac{\partial V}{\partial t}$ are gained from flow measurements and frictional forces

$\frac{2 \cdot \langle \tau_w \rangle}{\rho \cdot R}$ from the measured values of shear stress sensors 2 and 5.

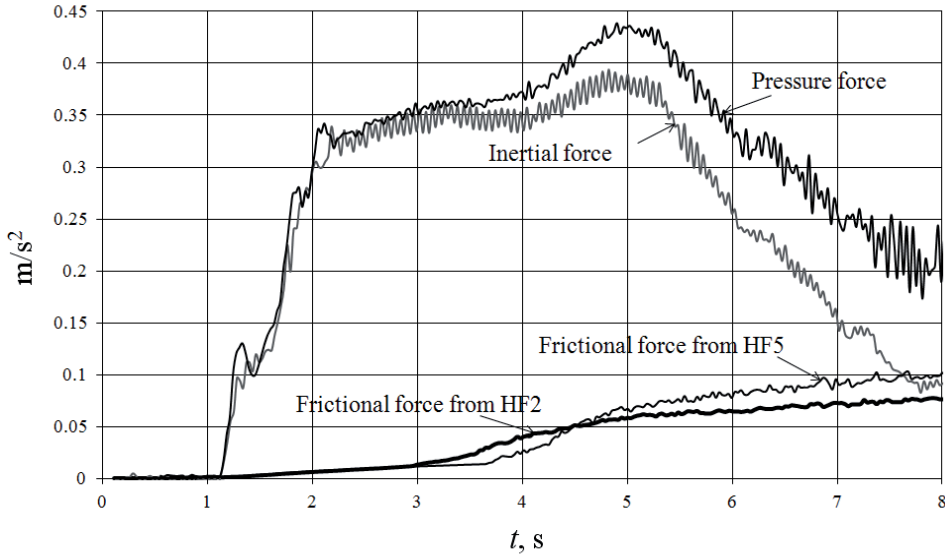


Figure 4. 14 – Equilibrium of forces

At the first stages of the process inertial and pressure forces are almost equal as frictional forces are very small. At the transition ($t^* = 3$ s) frictional forces at the wall start to increase rapidly and inertial forces decrease in comparison to pressure forces. The equilibrium of forces in time is given in Table 4.4. The proportion of each force is given as a percentage of the sum of all the three forces at a given moment. The equilibrium of forces is evaluated in two cases: Case 1 – frictional forces are calculated from hot-film 2 and Case 2 – frictional forces are calculated from hot-film 5.

Table 4. 4 – Variation of forces in time

t, s	Force / %					
	Case 1			Case 2		
	$\frac{1}{\rho} \frac{\partial p}{\partial z}$	$\frac{\partial V}{\partial t}$	$\frac{2 \cdot \langle \tau_w \rangle}{\rho \cdot R}$	$\frac{1}{\rho} \frac{\partial p}{\partial z}$	$\frac{\partial V}{\partial t}$	$\frac{2 \cdot \langle \tau_w \rangle}{\rho \cdot R}$
1.5	70.65	28.65	0.70	70.52	28.60	0.88
2.0	52.50	46.54	0.96	52.43	46.48	1.08
2.5	50.72	47.99	1.29	50.69	47.97	1.35

3.0	49.20	48.92	1.87	49.34	49.06	1.60
3.5	49.12	47.82	3.06	49.76	48.44	1.80
4.0	52.05	42.80	5.15	52.93	43.53	3.54
4.5	51.30	42.56	6.14	51.34	42.59	6.07
5.0	47.94	45.25	6.81	47.46	44.79	7.75
5.5	46.78	44.52	8.71	45.99	43.77	10.24
6.0	48.43	41.12	10.46	47.43	40.27	12.30
6.5	45.46	41.62	12.92	43.89	40.17	15.94
7.0	52.91	31.18	15.91	50.92	30.01	19.07
7.5	52.16	28.61	19.23	49.83	27.34	22.83
8.0	55.53	24.27	20.20	52.00	22.73	25.27

4.3 Analysis of different criteria on transition to turbulence

Experimental results gained on large-scale pipeline carried out in Deltares are compared with previous similar test results using two different criteria describing the transition to turbulence. The first criterion analyzed in Figure 4.15 was introduced by Lefebvre and White (1991) and modified by Nakahata et. al. (2007) to describe the correlation between the transitional Reynolds number and the acceleration rate. Lefebvre and White stated that transition to turbulence in accelerating flow was dependent on the pipe diameter. Emanated from that Nakahata et. al. introduced an empirical formula to calculate the critical Reynolds number in accelerating pipe flow (Eq. (1.1)). Experimental results gained in Deltares are presented in Table A.1 – A.3 (Appendix A).

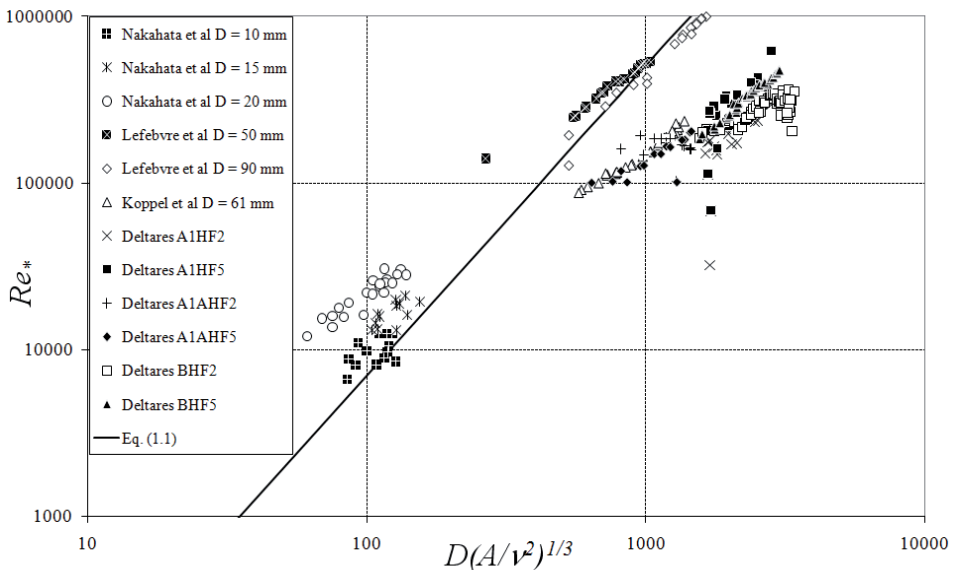


Figure 4. 15 – Correlation of the critical Reynolds number

According to Nakahata et. al. (2007) the empirical equation (Eq. (1.1)) should be valid in the frames of $\pm 40\%$. In the light of the experimental results gained during recent years the diversity of data is distinguishable.

Koppel and Ainola (2006) introduced a criterion to describe transition time through the pressure gradient (acceleration). The variation of dimensionless transition time versus the dimensionless pressure gradient in a start-up flow at high acceleration was proposed. At the early stages of accelerating flow friction forces are very small, so one can assume that inertial forces are equal to pressure forces. Therefore, this criterion is valid as well for flows driven by constant acceleration. In Figure 4.16 the correlation between dimensionless transition time and dimensionless acceleration is given.

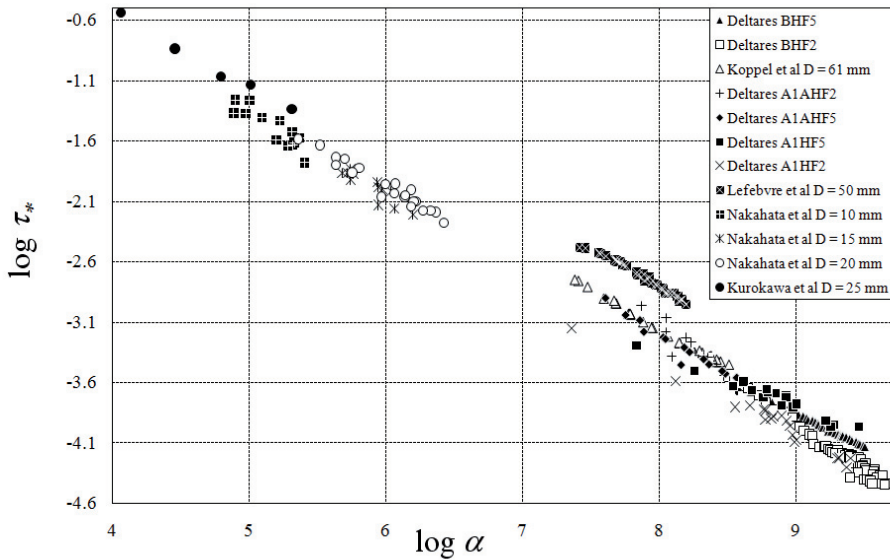


Figure 4. 16 – Variation of dimensionless transition time τ_* versus dimensionless acceleration α

Based on their experimental results Koppel and Ainola (2006) concluded that the dependence between τ_* and α in logarithmic scale is almost linear. Using the least squares matching to their data presented in Figure 4.16, they introduced a function between the two variables:

$$\log \tau_* = 1.80 - 0.62 \log \alpha, \quad (4.8)$$

and for the spring-up turbulence in a pipe

$$\tau_* = 63.1 \alpha^{-0.62}. \quad (4.9)$$

The R-squared value or the coefficient of determination for Eq. (4.8) is 0.995.

Dependence brought forth in Eq. (4.9) is calculated for all the available data and given in Table 4.5.

Table 4. 5 – Dependence between τ_* and α

Test case	Eq. (4.9)
Koppel et. al. D = 61 mm	$\tau_* = 63.1\alpha^{-0.62}$
Lefebvre et. al. D = 50 mm	$\tau_* = 210.93\alpha^{-0.64}$
Nakahata et. al. D = 10 mm	$\tau_* = 300.87\alpha^{-0.77}$
Nakahata et. al. D = 15 mm	$\tau_* = 134.72\alpha^{-0.70}$
Nakahata et. al. D = 20 mm	$\tau_* = 62.376\alpha^{-0.63}$
Kurokawa et. al. D = 25 mm	$\tau_* = 96.206\alpha^{-0.63}$
Deltares BHF5	$\tau_* = 10.201\alpha^{-0.54}$
Deltares A1AHF5	$\tau_* = 98.229\alpha^{-0.65}$
Deltares A1HF5	$\tau_* = 1.2351\alpha^{-0.43}$
Deltares BHF2	$\tau_* = 884.63\alpha^{-0.77}$
Deltares A1AHF2	$\tau_* = 32787\alpha^{-0.95}$
Deltares A1HF2	$\tau_* = 8.4472\alpha^{-0.55}$

At some cases the exponents are close but the coefficients are quite different. In general this dependence does not show a good general correlation between the variables.

Taking into account all the available experimental data shown in Figure 4.16, Eq. (4.8) takes a form

$$\log \tau_* = 2.04 - 0.66 \log \alpha, \quad (4.10)$$

or

$$\tau_* = 108.92\alpha^{-0.66}, \quad (4.11)$$

and the R-squared value for Eq. (4.10) is 0.965. This can be considered as a more universal equation to describe the dependence between dimensionless transition time and dimensionless acceleration in accelerating pipe flows starting from rest.

Kurokawa and Morikawa (1986), Lefebvre and White (1989, 1991) and Nakahata et. al. (2007) analyzed the dependence between the critical Reynolds number and the acceleration rate. In Figure 4.17 and 4.18 the correlation

between the critical Reynolds number (Re_*) and acceleration (A) and the critical Reynolds number (Re_*) and dimensionless acceleration (α) is given in logarithmic scale taking into account all the available experimental data.

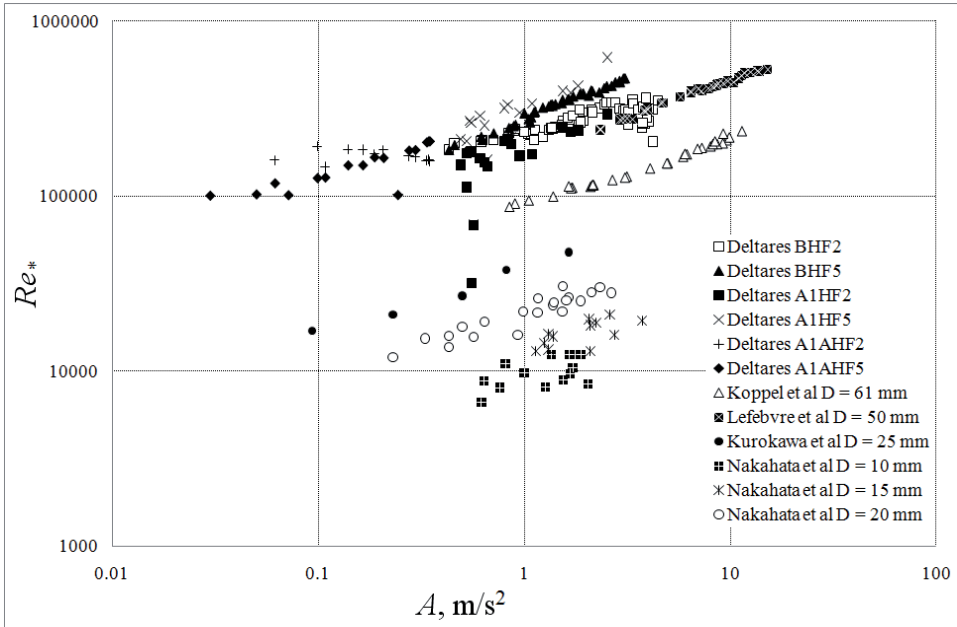


Figure 4.17 – Dependence between the critical Reynolds number and acceleration in logarithmic scale

From Figure 4.17 it is clearly seen that the critical Reynolds number depends on the pipe diameter. At the same acceleration rates Re_* increases as the pipe diameters increase. The only exception here is the test results by Lefebvre and White (1989). Probably the major reason for that is the test rig used in their study. Lefebvre and White used noise and vibration isolators and flow straighteners to reduce the external effects in transition to turbulence. Therefore, at the same acceleration rates transition took place at higher Reynolds numbers compared to other studies (as seen in Figure 4.17).

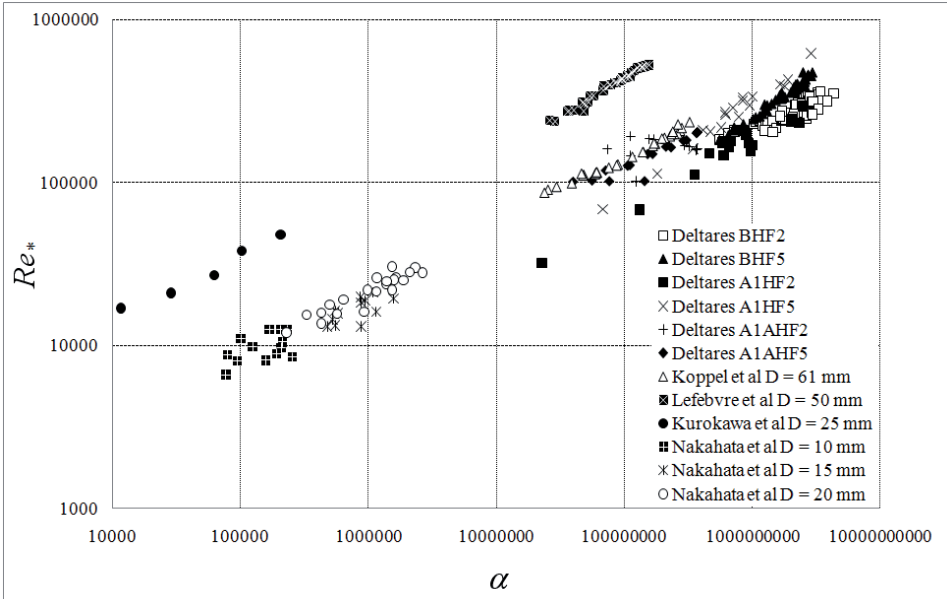


Figure 4.18 – Dependence between the critical Reynolds number and dimensionless acceleration in logarithmic scale

The dependence between the critical Reynolds number and dimensionless acceleration is given in Figure 4.18. It can be concluded that the dependence between Re_* and α in logarithmic scale is almost linear. Using the least squares matching for all the available experimental data presented in Figure 4.18, a function between the two variables becomes:

$$Re_* = 306.94\alpha^{0.33} \quad (4.12)$$

It can be noticed that two test series (Kurokawa and Morikawa (1986) and Lefebvre and White (1991)) fall out from the general trend, therefore the R-squared value or the coefficient of determination for Eq. (4.12) is 0.813. The comparison of all test results confirms the findings of Lefebvre and White (1991) that the critical Reynolds number is proportional to the cube root of dimensionless acceleration.

Kask and Koppel (1987) described the transition to turbulence process as a wavy appearance of the spots of turbulence spreading downstream and enlarging, merging in and filling all the flow (see Figure 1.5). The visualization of the accelerated flow from rest in pipes with $D = 0.036$ m and $D = 0.05$ m showed that the turbulization starts from the bottom of the pipe and propagates downstream in waves eventually filling the whole pipe diameter. Similar wavy structures were noticed in current tests carried out in Deltares. Figure 4.13 shows the propagation of the ensemble averaged radial velocity component in time in accelerating flows (the ensemble averaged case). The wavy structure is moving

downstream with a period of 0.35 s. In Kask and Koppel (1987) the wave periods vary between 0.24 – 0.64 s. The negative value of the radial velocity component corresponds to fluid movement from the pipe center to the top, partly upholding the hypothesis of Kask and Koppel that turbulence generates at the bottom of the pipe and propagates towards the top (PIV measurements were carried out in a single plane). The results from the hot-film sensors indicate that transition to turbulence takes place at different times over the pipe perimeter and in various axial locations turbulence does not always first generate from the pipe bottom (see Table A4 – A6, Appendix A).

According to Ruubel (1991) and Zhao et. al. (2007) the three dimensional wavy structure travels in the pipe downstream, always rotating around the pipe axis in one direction. In Appendix A (Table A.4 – A.6) the sequence in reaction to turbulence is given for each hot-film: 1 corresponds to the first hot-film reacting to turbulence, 2 corresponds to the second hot-film reacting to turbulence etc.

From the present test results it is clearly seen that there is no definite sequence in the occurrence of turbulence in between the hot-films. Hot-film 3 tends to react to turbulence first in almost every test indicating that turbulence starts at the bottom of the pipe and spreads towards the top. Otherwise the sequence in the propagation to turbulence between different hot-films is arbitrary to draw univocal conclusions.

4.4 Comparison between model and experimental results: the development of velocity profiles

In this section the comparison between one- and two-dimensional models and experimental results is brought forth. The correlation between measured (taken from 30 repeats ensemble test case) and theoretical velocity distributions in start-up accelerating pipe flow (1D model) are given in Figure 4.19a and b. Theoretical velocity profiles are calculated using Eq. (2.75) where the convolution integral is calculated using the trapezoidal rule. The main parameters of the experiment are: $Re_1 = 0$ and $Re_f = 400\ 000$, valve opening time $t_v = 2$ s, flow acceleration $A = \text{const} = 0.34$ m/s² (Figure 4.19a) and $A \neq \text{const}$ (Figure 4.19b). Different accelerations are used in the model because flow measurements indicated that due to large inertial forces in the large-scale pipeline system acceleration rate was changing in time just after the opening of the control valve, reaching afterwards to a constant value of $A = 0.34$ m/s². Velocity profiles are deduced from PIV measurements and averaged over 30 repeats. The same ensemble averaged test case is used to compare all the modeled results described in this chapter. ϑ in Figure 4.19a and b indicates the dimensionless distance from the pipe wall ($\vartheta = 1$ corresponds to the pipe axis).

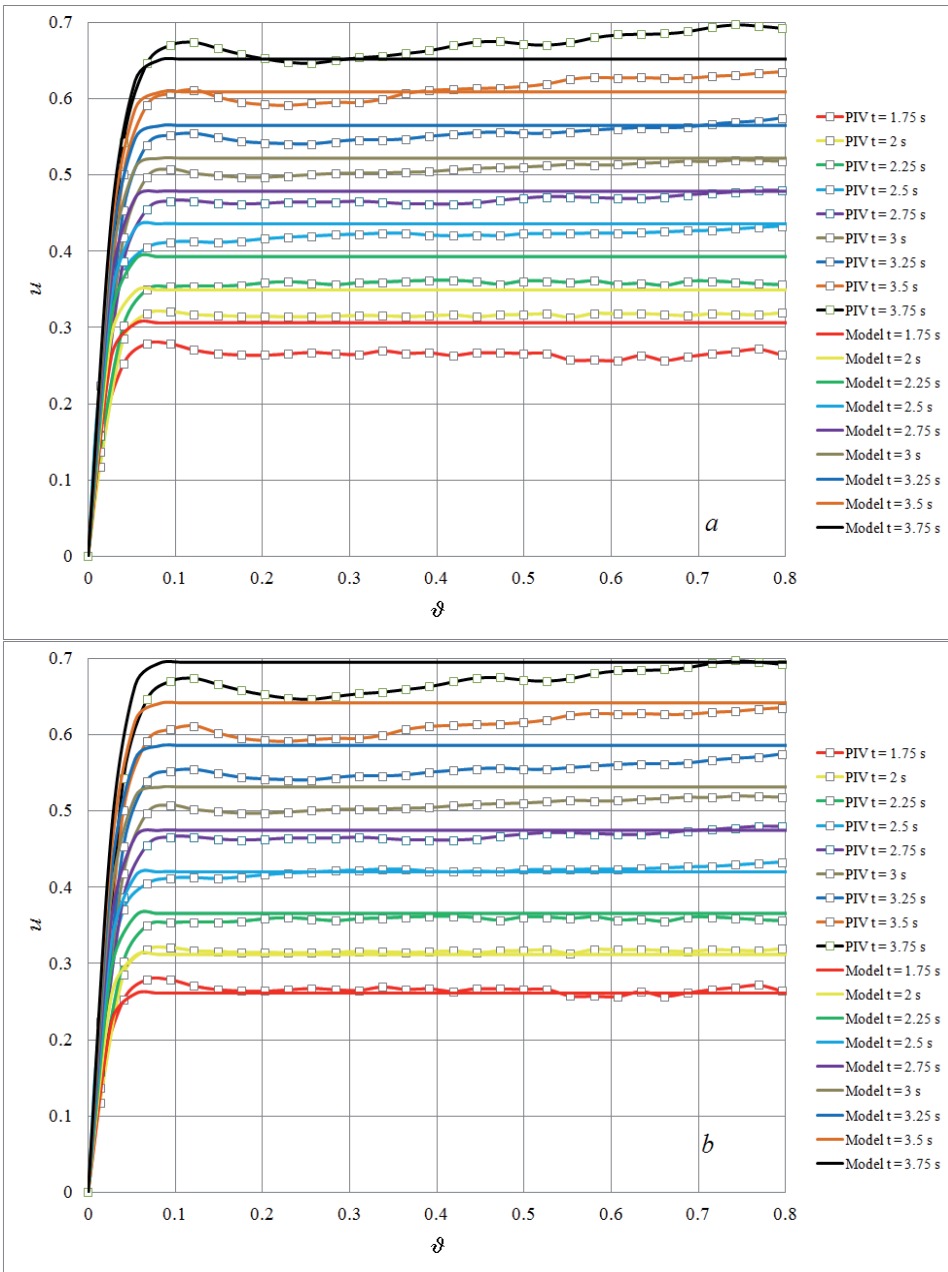


Figure 4.19 – Theoretical and measured ensemble averaged dimensionless velocity profiles, *a* – $A = \text{const}$; *b* – $A \neq \text{const}$

In model calculations the starting time $t = 0$ s is selected based on the start of flow excursion in the ensemble averaged experimental case study (corresponding to $t = 1.25$ s in the experiment, see Figures 4.5 – 4.8). At the first

time steps there is no good PIV data available due to the lack of seeding and appearance of large air bubbles moving downstream and causing reflections in the high-speed camera and therefore lots of erroneous vectors. At first available PIV measurements ($t = 1.75$ s) turbulization process begins in the flow and PIV measurements show good correlation between theoretical values near the pipe wall. In the core region of the pipe the velocity profile is uniform, and the near the wall thickness of the boundary layer is increasing in time. All shear effects are concentrated on the wall region, and the main part of liquid moves like a “solid body”. The bulk flow acceleration causes the increase of velocity in the core and generation of large velocity gradients near the wall. The one-dimensional model (with $A = \text{constant}$, Figure 4.19a) overestimates the velocities at the first timeframes in the core region ($t < 2.5$ s). Afterwards the correlation between measured and modeled velocity profiles is quite good both near the wall and in the core. At $t = 3.75$ s flow is turbulent over the pipe cross-section and the model results start to underestimate the measured velocities. In the case where acceleration is not set to constant (Figure 4.19b), the 1D model shows good correlations between the measured values in the core region until $t \leq 2.75$ s. From this moment forward flow is becoming turbulent over the pipe cross-section and the model results start to overestimate the measured velocities. Turbulence in the flow “breaks the solid body” and the theoretical velocity distributions do not coincide with experimental data as the model is not valid to describe turbulent flow. Correlations between modeled and measured velocities indicate that calculations where acceleration rate is changing in time give better results compared to calculations with fixed acceleration value.

A two-dimensional model (Ainola et. al., 1981) is used to numerically calculate the development of radial and axial velocities in different points over the pipe length and radius and the development of average velocity and pressure. A dimensionless dissipative model based on Eqs. (2.19 – 2.22) describes the development of incipient compressible axisymmetrical flow in circular pipes starting from rest until the transition to turbulence. The dimensionless variables are defined in Eqs. (2.5 – 2.6) and (2.12 – 2.13).

The variation of pressure in different points over the pipe length is given by

$$q(\xi, t) = q_0 + 4 \int_0^t \left(\int_0^\tau \sum_{i=1}^{\infty} \frac{e^{-Dn\lambda_i^2(\tau-\theta)}}{\lambda_i^2} \frac{\partial^2 q(\xi, \theta)}{\partial \xi^2} \right) d\theta d\tau. \quad (4.13)$$

where λ_i is the zeros of the Bessel function of the first kind of order zero J_0 . The initial condition is defined as:

$$q(\xi, t) = q_0, \text{ if } t = 0, \quad (4.14)$$

and border conditions

$$q(\xi, t) = q_0, \text{ if } \xi = 0, \quad (4.15)$$

$$q(\xi, t) = q_3(t), \text{ if } \xi = 1, \quad (4.16)$$

where $q_3(t)$ is the pressure measurement from pressure probe 3 in a dimensionless form ($x/L = 9/10$, see Figure 3.3).

Eq. (4.13) was solved numerically with a finite difference method. The values of the pressure $q(\xi, t)$ were calculated in 50 points over the pipe length (from the water tank to p_3). Total modeling time was selected $t = 6$ s with a time-step of $\Delta t = 0.05$ s.

From a series in Eq. (4.13), 200 first members were taken. The 49 first values of λ_i were hardcoded into a table (British Association for the Advancement of Science, 1937). For $i > 49$ the approximation formula from Abramowitz and Stegun (1979) was used. The series in Eq. (4.13) for $\tau = \theta$ was separately numerically simulated and the result was

$$\sum_{i=1}^{\infty} \frac{1}{\lambda_i^2} = 0.25. \quad (4.17)$$

The second derivative in Eq. (4.13) was approximated with a three-point estimation method (Ainola et. al., 1981) and both integrals were calculated with the trapezoidal rule.

In numerical calculations pressure in the pipe inlet was considered to be constant and at the end of the pipe end decreasing in accordance with the measured data. Comparison between numerical and experimental results is given in Figure 4.20.

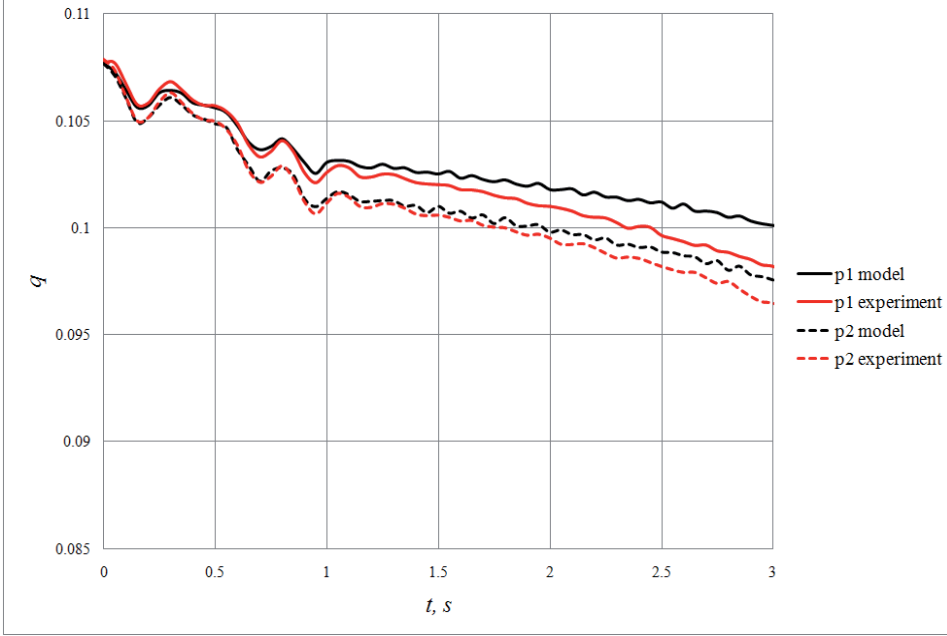


Figure 4. 20 - Comparison between numerical and ensemble averaged dimensionless pressures p_1 and p_2 .

Comparison of pressures shows that there is a good correlation between the measured and calculated values until the transition to turbulence takes place ($t \leq 1.75$ s). After that the divergence between modeled and measured pressures is increasing as the model is not valid to describe the turbulent processes in the pipe system.

Modeled pressures were used to calculate the axial and radial velocities in 50 points over the pipe length (from the water tank to p_3) and 38 points over the pipe radius (from the pipe wall to the pipe centerline) and the mean velocity (Eqs. (4.18 – 4.20) respectively). Total modeling time was selected $t = 6$ s with a time-step of $\Delta t = 0.05$ s.

$$u = \sum_{i=1}^{\infty} \Omega_i(\xi, \tau) J_0(\lambda_i \eta), \quad (4.18)$$

$$v = \sum_{i=1}^{\infty} \frac{1}{\lambda_i} \frac{\partial \Omega_i}{\partial \xi} [J_1(\lambda_i) \eta - J_1(\lambda_i \eta)] \quad (4.19)$$

and

$$U = 2 \sum_{i=1}^{\infty} \frac{J_1(\lambda_i)}{\lambda_i} \Omega_i(\xi, \tau), \quad (4.20)$$

where

$$\Omega_i = -\frac{2}{\lambda_i J_1(\lambda_i)} \int_0^{\tau} e^{-Dn\lambda_i^2(\tau-\theta)} \frac{\partial q(\xi, \theta)}{\partial \xi} d\theta. \quad (4.21)$$

The correlation between measured and modeled velocity distributions in start-up accelerating pipe flow is given in Figure 4.21. The theoretical velocity profiles are calculated from the two-dimensional model using Eq. (4.19). In Figure 4.21 the dimensionless value $\vartheta = 1$ corresponds to the pipe axis, and $\vartheta = 1 - \eta$.

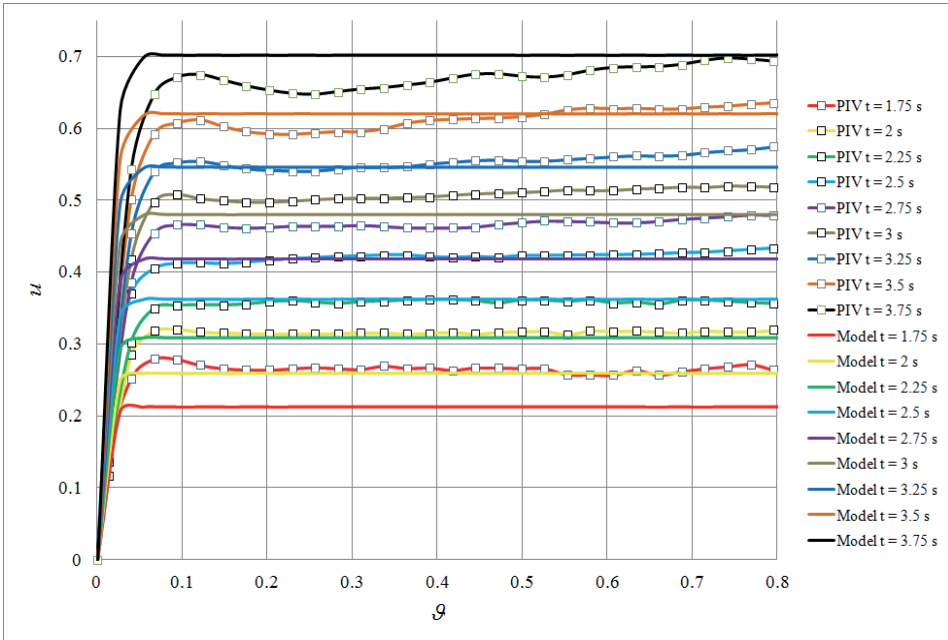


Figure 4. 21 - Modeled and measured ensemble averaged dimensionless velocity profiles

In model calculations time $t = 0$ s is selected based on the start of flow excursion in the ensemble averaged experimental case study corresponding to $t = 1.25$ s in the experiment (see Figures 4.5 – 4.8). On the contrary to the one-dimensional model, the two-dimensional model underestimates the velocities at the first time-steps compared to the experimental results. In the near wall region the difference between the measured and calculated velocity profiles is evident. After the flow is fully turbulent ($t > 3.75$ s) the 2D model starts to overestimate the measured velocities. Similarly to 1D model the theoretical velocity distributions do not

coincide with the experimental data as the two-dimensional model is not valid to describe turbulent flow.

In Figure 4.22 the model result of the development of the radial velocity component in a dimensionless form is given. The radial velocity component is calculated from Eq. (4.19).

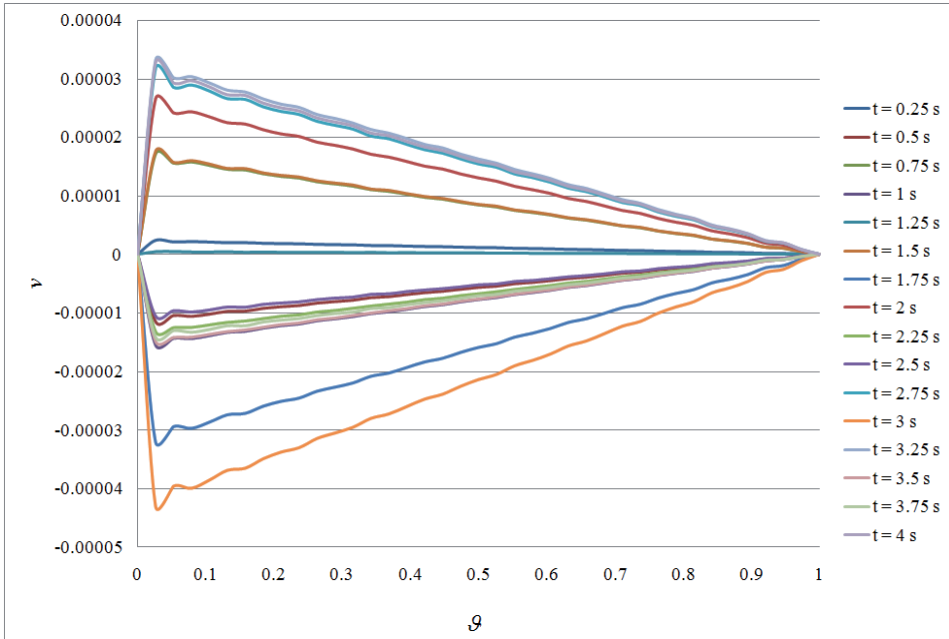


Figure 4. 22 – The development of modeled dimensionless radial velocity over the radius in different time-steps

The two-dimensional model results indicate that in accelerating pipe flow starting from rest the radial velocity component develops near the wall and arbitrarily oscillates around zero value. The magnitude of its value indicates that in the laminar region the value of radial velocity is very small and can be considered to be proportional to zero. This was expected as experimental results showed that it was impossible to measure the development of the radial velocity component in the laminar region with PIV using the settings described earlier in the thesis.

In Figure 4.23 the comparison between the mean dimensionless velocities is presented. Two experimental results gained from flow rate and PIV measurements are compared with the modeled results. The mean velocity for the one-dimensional model is calculated from Eq. (2.75) and for the two-dimensional model from Eq. (4.20).

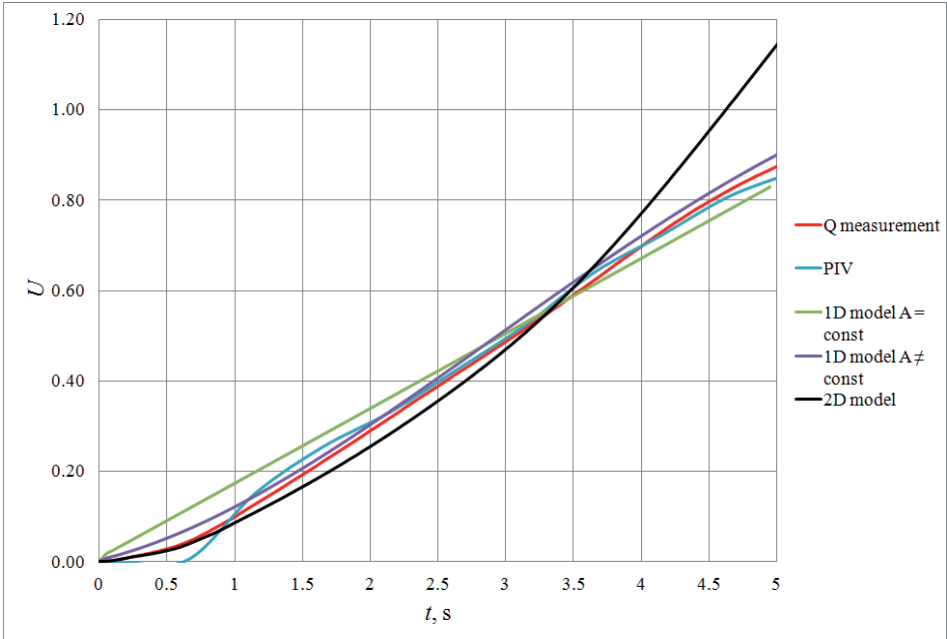


Figure 4. 23 – Comparison between measured and modeled mean velocities

From Figure 4.23 it is clearly seen that the 1D model with $A = \text{const}$ over-responds and the 2D model under-responds at mean velocities compared to the experimental results. The 1D model with $A \neq \text{const}$ shows good correlations with the measured values. The same tendency was noticed in the comparison of the modeled and measured velocity profiles. It is interesting to see that all the curves converge in at $t = 3.3 - 3.5$ s. From the experimental results it can be considered as the time where the flow has become fully turbulent (all the hot-films have reacted to turbulence). The 1D model describes the development of mean velocity compared to the measured values in the turbulent region quite well (both for $A = \text{const}$ and $A \neq \text{const}$). The 2D model is clearly valid only in the laminar region.

4.5 Summary

Chapter 4 gave an overview of the experimental program, results and problems associated with the tests. New experimental findings gained in a large-scale pipeline were analyzed in the light of the hypothesis brought forth in Chapter 1. Over 100 different acceleration rates were used to analyze the transitional process in pipe flow starting from rest.

Single cases were used to describe the emergent of turbulent slugs. Similarly with previous studies the occurrence of turbulent slugs was found to be arbitrary and not repeatable. From a numerous of single cases it was deduced that in large-scale pipelines transition to turbulence does not take place

simultaneously over the entire pipe length. However, it should be noted that the experimental results are gained from a 1 meter long pipe section. The nonlinearity of flow excursion (present in some cases) does not seem to influence the transition process compared to linear flow excursion.

Experimental findings were used to estimate three criteria proposed in earlier studies that described the dependence between different variables at the moment of transition. It was found that the proposed equation (Eq. (1.1)) to calculate the critical Reynolds number is not in good agreement with new measurements. The criteria proposed by Koppel and Ainola (2006) describing the dependence between dimensionless acceleration and dimensionless transition time gave good correlations with all test results available. A more general equation (Eq. (4.14)) was introduced to describe the dependence between the two variables taking into account all the data available. The analysis of the dependence between the critical Reynolds number and dimensionless acceleration confirmed that the critical Reynolds number is proportional to the cube root of dimensionless acceleration.

In addition to single cases, one 30 repeats ensemble test case was measured during the tests series. Furthermore, PIV technique was used to deduce the development of velocity profiles in accelerating flow. Ensemble averaged results apprised the influence of the transitional process to the mean values like flow rate, pressure and friction. Those results were used to describe the equilibrium of forces in accelerating flows. It was found that transition to turbulence takes place when pressure forces become larger than inertial forces. To retain the equilibrium, at the same moment friction forces start to increase.

Ensemble averaged PIV measurements were used to describe the development of axial and radial velocity components. Experimental results were compared with the 1D model described in Chapter 2 and 2D model described in Section 4.4. Model calculations indicated that the 1D model with $A = \text{const}$ overestimates and the 2D model underestimates the development of axial velocities compared to experimental results. The 1D model with $A \neq \text{const}$ correlates well with the measured values until the flow becomes fully turbulent. Correlations between 1D modeled and measured velocity indicate that calculations where acceleration rate is changing in time give better results compared to calculations with fixed acceleration value. The magnitude of the modeled radial velocity component is practically zero. To describe the turbulence intensity axial velocity fluctuations were deduced from the measurements. In accelerating pipe flows the turbulence intensity increases near the wall region and moves towards the core. In the core region the intensity is quite low and increases slowly.

The analysis of the measured radial velocity component implied that at the moment of transition there is evidently a three dimensional structure developing in the flow. In every radial position over the pipe radius the velocity is negative indicating that the fluid is moving from the pipe center towards the top wall. As the movement of the fluid is restricted by the pipe wall, flow

direction has to be downwards in some other plane, indicating that the developing structure is three dimensional. This structure then settles and appears again in a period $t = 0.35$ s. The wavy structure is asymmetric allowing the radial velocity to stay negative in between the spikes. In the turbulent flow region the structure dissipates and the radial velocity component decreases. The analyses of the reaction sequences of different hot-films on transition to turbulence indicated that the rotational direction of the 3-D structure is arbitrary.

5. CONCLUSIONS

5.1 Summary of findings

In this thesis the transition to turbulence in accelerated flows starting from rest is investigated.

In Chapter 1 a historical overview of studies dealing with transitional pipe flow is given. The main emphasis is placed on accelerated flow as a special case of unsteady pipe flow. Over the past half a century a number of experimental investigations have been carried out but some aspects of the transitional process have still remained an enigma. Chapter 1 summarizes the hypotheses brought forth in earlier studies. This thesis analyzes those hypotheses in the light of new experimental findings.

A mathematical model based on Navier-Stokes equations is introduced in Chapter 2 to describe the development of velocity profiles in constant accelerating pipe flows. The Laplace transform method for small times is applied to deduce the equations. Model and experimental velocity profiles are then compared and analyzed in Chapter 4.

In Chapter 3 an overview of the test rig used and the experimental program is given. In addition to the description of instruments used, hot-film and PIV calibration methods are introduced. The experimental results revealed that mounting plays an important role in the data quality gained from the hot-film measurements. Very small disturbances in pipe wall roughness seem to incur local transition to turbulence. A clear indicator to this statement is hot-film 3 that reacted first to turbulence in almost all test cases.

PIV measurements failed in the first time steps of acceleration from rest tests. It was due to the fact that oxygen particles used for seeding were produced upstream from the camera position. This caused a lack of particles (and therefore lack of data) at the first time steps of flow excursion. PIV measurements were carried out only with one camera position and similar settings because of the tight time schedule during the measurements. Because of a large capture area, data near the wall region were lost and the similar settings turned out to be not suitable at a wide range of Reynolds numbers.

Experimental results are described in Chapter 4. Subsequently the main findings are brought forth:

- ◆ In large-scale pipelines transition to turbulence does not take place simultaneously over the pipe length. It was found that the transition period decreases with the increase of acceleration rate.
- ◆ Turbulent slugs, preceding the transition process in accelerating pipe flow in a large diameter pipeline, were noticed in several cases. Slugs occurred in random test cases, were not repeatable and their appearance was arbitrary.
- ◆ The influence of the transition to turbulence on the mean flow rate and pressure is hardly noticeable. At some initial conditions the

transition process seems to cause a decrease in acceleration in constantly accelerated flow excursion. After the transition flow acceleration increases. At the same initial conditions repeated cases indicate that the nonlinearity in the flow excursion is arbitrary and not caused by the transition process. Changes in pressure are more dependent on initial conditions than the transition process. Although it can be noted that at the moment of transition pressure difference in the system increases.

- ◆ In accelerating pipe flow starting from rest shear stresses at the initial time steps over-respond compared to quasi-steady values. After the transition to turbulence it has a reverse tendency.
- ◆ At the moment of transition axial velocity fluctuations show a small increase in the core region. Near the wall there is a rapid generation which appears to propagate outwards as time progresses. At the transition flow decelerates near the wall region but accelerates in the core breaking the bulk-flow profile.
- ◆ The analyses of the equilibrium of forces show that transition to turbulence takes place when pressure forces become larger than inertial forces. In constantly accelerating flow inertial forces remain constant while friction forces and pressure forces increase.
- ◆ Three criteria were analyzed in the light of new experimental findings. The empirical formula (Eq. (1.1)) presented by Nakahata et al. (2007) does not correlate well with all the data available. From the obtained experimental results it follows that the logarithm of transition time is the linear function of the logarithm of acceleration. Taking into account all the data available a new empirical formula is suggested that describes the dependence between dimensionless transition time and dimensionless acceleration in accelerating pipe flows starting from rest.
- ◆ The critical Reynolds number is proportional to the cube root of dimensionless acceleration.
- ◆ Ensemble averaged PIV measurements were used to describe the development of axial and radial velocity components. Experimental results were compared with 1D and 2D model results. Model calculations indicated that the 1D model with $A = \text{const}$ overestimates and the 2D model underestimates the development of axial velocities compared to measurements. The 1D model with $A \neq \text{const}$ shows good correlations with the PIV measurements until the flow becomes fully turbulent. Correlations between 1D modeled and measured velocity indicate that calculations where acceleration rate is changing in time give better results compared to calculations with fixed acceleration value. The comparison of pressures shows that there is a good correlation between the measured and

calculated (2D model) values until the transition to turbulence takes place.

- ◆ There is an increase in the radial velocity component at the moment of transition. It can be noticed that a wavy structure develops in the flow moving from the pipe center to the top and travels downstream with a period of 0.35 s. It indicates that the transition process is a three-dimensional problem. The analysis of the sequences of hot-films reactions to turbulence indicates that the rotational direction of that structure is arbitrary.

5.2 Recommendation for future research

Investigations of transitional processes in accelerating pipe flow have been a subject of active research for the last half a decade. Despite numerous studies many aspects of transition to turbulence have still remained an enigma. This thesis concentrates on transitional processes in a large-scale pipeline system. Therefore the main recommendations for future research are as follows:

- ◆ In the thesis transition to turbulence was investigated at different acceleration rates up to $A = 4.20 \text{ m/s}^2$. In previous studies carried out in small-scale pipelines the highest acceleration rates used were about 11 m/s^2 . It might be interesting to study the transitional processes in large-scale pipelines at the same high acceleration rates. Still, one has to take into account the rise of forces in the system. Some test cases done in Deltares showed that at high accelerating rates and high Reynolds numbers the stability of the test rig (vibrations etc) became a real problem. Therefore, the transition to turbulence might be incurred by external factors rather than by the hydrodynamics of the process itself.
- ◆ PIV measurements showed that for transitional processes and flows starting from rest LDV might give better results. Extra measurements are needed in the pipe wall area, especially in the boundary layer.
- ◆ Transition to turbulence is a three-dimensional problem. Therefore, 3D PIV or LDV measurements are needed to be carried out to have a better overview of the structures developing at the moment of transition.

BIBLIOGRAPHY

Papers presented by the candidate

Annus, I., Koppel, T. 2011. "Transition to Turbulence in Accelerating Pipe Flow." *ASME, J. Fluids Eng.* 133(7), pp. 071202-1-071202-9. [DOI: 10.1115/1.4004365]

Laanearu, J., Annus, I., Koppel, T., Bergant, A., Vučkovič, S., Hou, Q., Tijsseling, A. S., Anderson, A., van't Westende, J. M. C. 2011. "Emptying of Large-Scale Pipeline by Pressurized Air." *ASCE, J. Hydr. Eng. Submitted.*

Annus, I., Koppel, T., Vardy, A. 2010. "Transition to Turbulence in Acceleration Flow." *Proceedings of the Hydralab III joint transnational access user meeting, Hannover, (Eds.) Joachim Grüne, Mark Klein Breteler*, pp. 9 – 12.

Vardy, A., Bergant, A., He, S., Ariyaratne, C., Koppel, T., Annus, I., Tijsseling, A., Hou, Q. 2009. "Unsteady Skin Friction Experimentation in a Large Diameter Pipe." *Proceedings of the 3rd IAHR International Meeting of the Workgroup on Cavitation and Dynamic Problems in Hydraulic Machinery and Systems, Brno, Czech Republic, (Eds.) P. Rudolf*, pp. 593 - 602.

Laanearu, J., Annus, I., Koppel, T. 2009. "On Long-Wave Dependent Flow Transitions in Partially Filled Large-Scale Pipeline." *Proceedings of Water Engineering for a Sustainable Environment: 33RD IAHR Congress, Vancouver, British Columbia, Canada*, pp. 6553 - 6560.

List of references

1. Abramowitz, M., Stegun, I. A. 1979. "Handbook of Mathematical Functions with Formulas, Graphs and Mathematical Tables". *Nauka, Moskow*. 830 pp.
2. Achard, J.L., Lespirand, G.H. 1981. "Structure of the Transient Wall-friction Law in One-dimensional Models of Laminar Pipe Flow". *J. Fluid Mech.* 113, pp. 263-293.
3. Adamkowski, A., Lewandowski, M. 2006. "Experimental Examination of Unsteady Friction Models for Transient Pipe Flow Simulation". *J. Fluids Eng.* 128, pp. 1351-1363.
4. Ainola, L., Koppel, T., Lamp, J., Liiv, U. 1979. "An Investigation of Local Velocities in the Pipe at Starting from Rest Unsteady Liquid Flow". *Trans. Tallinn Polyt. Inst.* 472, pp. 35-45 (in Russian).
5. Ainola, L., Koppel, T., Lamp, J., Liiv, U. 1981. "On the Criteria of the Transition from Laminar to Turbulent in Starting Pipe Flow". *Trans. Tallinn Polyt. Inst.* 505, pp. 17-29 (in Russian).
6. Ainola, L., Lamp, J., Liiv, U., Sarv, L. 1979. "A Theoretical Investigation of the Unsteady Liquid Flow in Round Pipes Using a Dissipation Model". *Trans. Tallinn Polyt. Inst.* 472, pp. 25-34 (in Russian).
7. Ainola, L., Lamp, J., Sarv, L., Liiv, U. 1981. "Study of Transition Process of Compressible Fluid in Pipes Using a Numerical Method". *Hydro technical Buildings.* 1, pp. 22-25 (in Russian).
8. Ainola, L., Liiv, U. 1985. "Mathematical Models for Unsteady Flows in Pipes". *Trans. Tallinn Polyt. Inst.* 593, pp. 85-94 (in Russian).
9. Annus, I., Koppel, T. 2011. "Transition to Turbulence in Accelerating Pipe Flow." *ASME, J. Fluids Eng.* 133(7), 9 pages.
10. Annus, I., Koppel, T., Vardy, A. 2010. "Transition to turbulence in accelerating flow". *Proceedings of the Hydralab III Joint Transnational Access User Meeting, Hannover, FZK*, pp. 9-12.
11. Akhavan, R., Kamm, R. D., Shapiro, A. H. 1991. "An Investigation of Transition to Turbulence in Bounded Oscillatory Stokes Flows Part 1. Experiments". *J. Fluid Mech.* 225, pp. 395-422.
12. Ben-Dov, G., Cohen, J. 2007. "Critical Reynolds Number for a Natural Transition to Turbulence in Pipe Flows". *Phys. Rev. Lett.* 98(6), pp. 064503-1-064503-4.
13. Ben-Dov, G., Cohen, J. 2007. "Instability of Optimal Non-axisymmetric Base-flow Deviations in Pipe Poiseuille Flow". *J. Fluid Mech.* 558, pp. 189-215.

14. Bergant, A., Simpson, A.R., and Vitkovsky, J. 2001. "Developments in Unsteady Pipe Flow Friction Modelling". *J. Hydr. Res.* 39(3), pp. 249-257.
15. Biau, D., Soueid, H., Bottaro, A. 2008. "Transition to Turbulence in Duct Flow". *J. Fluid Mech.* 596, pp. 133-142.
16. Bradshaw, P. 1982. "Shear Layer Studies – Past, Present, Future." *Recent Contributions to Fluid Mechanics, W. Haase, Ed., Springer.* pp. 1-9.
17. Brereton, G.J. 2000. "The Interdependence of Friction, Pressure Gradient, and Flow Rate in Unsteady Laminar Parallel Flows". *Phys. Fluids.* 12(3), pp. 518-530.
18. Brereton, G.J., Jiang, Y. 2005. "Exact Solutions for Some Fully Developed Laminar Pipe Flows Undergoing Arbitrary Unsteadiness". *Phys. Fluids.* 17, 118104.
19. British Association for the Advancement of Science. 1937. "Mathematical Tables Volume VI. Bessel Functions Part I". *Cambridge University Press.* 287 pp.
20. Brown, F.T. 1962. "The Transient Response of Fluid Lines". *ASME J. Basic Eng.* 84(3), pp. 547-553.
21. Brunone, B., Golia, U.M., and Greco, M. 1991. "Some Remarks on the Momentum Equation for Fast Transients". *Int. Meeting on Hydraulic Transient with Column Separation, 9th Round Table, IAHR, Valencia, Spain,* pp.140-148.
22. Brunone, B., Karney, B. W., Micarelli, M., Ferrante, M. (2000). "Velocity Profiles and Unsteady Pipe Friction in Transient Flow." *J. Water Resour. Plng. and Mgmt.* 126(4), pp. 236-244.
23. Carstens, M. R. 1956. "Transition from Laminar to Turbulent Flow during Unsteady Flow in a Smooth Pipe". *Proc., Int. Congress of Applied Mechanics.* 3, pp. 370-377.
24. D'Souza, A.F., Oldenburger, R. 1964. "Dynamic Response of Fluid Lines". *ASME J. Basic Eng.* 86(3), pp. 586-589.
25. Daniel, E., Liiv, U., Ruubel, R. Sarv, L. 1985. "Analysis of an Experimental Investigation of the Reynolds Shear Stresses in Accelerated Pipe Flow". *Trans. Tallinn Polyt. Inst.* 593, pp. 73-84 (in Russian).
26. Daniel, E., Koppel, T. 1985. "The Turbulization of the Accelerated Pipe Flow". *Trans. Tallinn Polyt. Inst.* 593, pp. 109-122 (in Russian).
27. Darbyshire, A. G., Mullin, T. 1995. "Transition to Turbulence in Constant-mass-flux Pipe Flow". *J. Fluid Mech.* 289, pp. 83-114.
28. Das, D., Arakeri, J. H. 1998. "Transition of Unsteady Velocity Profiles with Reverse Flow". *J. Fluid Mech.* 374, pp. 251-283.

29. Davidson, P. A. 2006. "Turbulence. An Introduction for Scientists and Engineers". *Oxford University Press Inc., New York*.
30. Eckmann, D. M., Grothberg, J. B. 1991. "Experiments on Transition to Turbulence in Oscillatory Pipe Flow". *J. Fluid Mech.* 222, pp. 329-350.
31. Eliahou, S., Tumin, A., Wygnanski, I. 1998. "Laminar-turbulent Transition in Poiseuille Pipe Flow Subjected to Periodic Perturbation Emanating from the Wall". *J. Fluid Mech.* 361, pp. 333-349.
32. Eckhardt, B., Schneider, T. M., Hof, B., Westerweel, J. 2007. "Turbulence Transition in Pipe Flow". *Annu. Rev. Fluid Mech.* 39, pp. 447-468.
33. Faisst, H., Eckhardt, B. 2003. "Traveling Waves in Pipe Flow". *Phys. Rev. Lett.* 91(22), pp. 224502-1- 224502-4.
34. Ferrante, M., Brunone, B. 2003. "Pipe System Diagnosis and Leak Detection by Unsteady-state Tests. 1. Harmonic Analysis". *Adv. Water Resources.* 26, pp. 95-105.
35. Ghidaoui, M. S. 2004. "On the Fundamental Equations of Water Hammer". *Urban Water J.* 1(4), pp. 71-83.
36. Ghidaoui, M. S., Kolyshkin, A. A. 2001. "Stability Analysis of Velocity Profiles in Water-Hammer Flows." *J. Hydr. Eng.* 127(6), pp. 499-512.
37. Ghidaoui, M. S., Zhao, M. and McInnis, D. A., Axworthy, D. H. 2005. "A Review of Water Hammer Theory and Practice". *Appl. Mech. Rev.* 58(1), pp. 49-76.
38. Greenblatt, D., Moss, E. A. 1999. "Pipe-flow Relaminarization by Temporal Acceleration". *Phys. of Fluids.* 11(11), pp. 3478-3481.
39. Greenblatt, D., Moss, E. A. 2003. "Rapid Transition to Turbulence in Pipe Flows Accelerated From Rest". *ASME J. Fluids Eng.* 125, pp. 1072-1075.
40. Haaland, S. E. 1983. "Simple and Explicit Formulas for the Friction Factor in Turbulent Pipe Flow". *ASME, J. Fluids Eng.* 105, pp. 89-90.
41. Han, G., Tumin, A., Wygnanski, I. 2000. "Laminar-turbulent Transition in Poiseuille Pipe Flow Subjected to Periodic Perturbation Emanating from the Wall. Part 2. Late Stage of Transition". *J. Fluid Mech.* 419, pp. 1-27.
42. He, S., Ariyaratne, C., Vardy, A. E. 2008. "A Computational Study of Wall Friction and Turbulence Dynamics in Accelerating Pipe Flows". *Computers and Fluids.* 37, pp. 674-689.
43. He, S., Jackson, J. D. 2000. "A Study of Turbulence under Conditions of Transient Flow in a Pipe". *J. Fluid Mech.* 40, pp. 1-38.

44. Hino, M., Sawamoto, M., Takasu, S. 1976. "Experiments on Transition to Turbulence in an Oscillatory Pipe Flow". *J. Fluid Mech.* 75, pp. 193-207.
45. Hof, B., van Doorne, C. W. H., Westerweel, J., Nieuwstadt, F. T. M., Faisst, H., Eckhardt, B., Wedin, H., Kerswell, R. R., Waleffe, F. 2004. "Experimental Observation of Nonlinear Traveling Waves in Turbulent Pipe Flow". *Science.* 305, pp. 1594-1598.
46. Holmboe, E.I., Rouleau, W.T. 1967. "The Effect of Viscous Shear on Transients in Liquid Lines". *ASME J. Basic Eng.* 89(1), pp. 174-180.
47. Iguchi, M., Nishihara, K., Nakahata, Y., Knisely, C. W. 2010. "Effect of Initial Constant Acceleration on the Transition to Turbulence in Transient Circular Pipe Flow". *J. Fluids Eng.* 132, pp. 111203-1-111203-9.
48. Jorgensen, F., E. 2002. "How to Measure Turbulence with Hot-Wire Anemometers – a Practical Guide". *DantecDynamics.* pp. 73.
49. Kask, E. 1980. "An Experimental Investigation of the Velocity Distribution in the Cross-section during Starting Period of the Liquid in the Pipe". *Trans. Tallinn Polytech. Inst.* 485, pp. 17-22 (in Russian).
50. Kask, E., Koppel, T. 1987. "Analysis of Generation and Development of Turbulence at Accelerated Fluid Flow in Circular Pipe". *Trans. Tallinn Polytech. Inst.* 637, pp. 42-46 (in Russian).
51. Kask, E., Koppel, T. 1987. "The Visualization of the Boundary Layer at the Accelerated Fluid Flows in Pipes". *Trans. Tallinn Polytech. Inst.* 632, pp. 117-122 (in Russian).
52. Kapelan, Z., Savic, D.A., and Walters, G.A. 2004. "Incorporation of Prior Information in Inverse Analysis for Leak Determination and Roughness Calibration". *Urban Water J.* 1(2), pp. 129-141.
53. Kerswell, R. R. 2005. "Recent Progress in Understanding the Transition to Turbulence in a Pipe." *Nonlinearity.* 18, pp. R17-R44.
54. Koppel, T., Ainola, L. 2006. "Identification of Transition to Turbulence in a Highly Accelerated Start-up Pipe Flow". *ASME, J. Fluids Eng.* 128(4), pp. 680-686.
55. Koppel, T. A., Liiv, U. R. 1977. "Experimental Investigation of the Development of Motion of Liquid in Conduits". *Fluid Dyn.* 12(6), pp. 881-887.
56. Kovasnay, L. S. G., Komoda, H., Vesudeva, B. R. 1962. "Detailed flow Field in Transition". *Proc. Heat Trans. And Fluid Mech. Inst.* pp. 1-26.
57. Kurokawa, J., Morikawa, M. 1986. Accelerated and decelerated flows in circular pipe (1st report, velocity profiles and friction coefficient). *Bull. JSME.* 29, pp. 758-765.

58. Lam, K. W., Leutheusser, H. J. 2002. "Flow Establishment in Elastic Pipes". *J. Eng. Mech.* 128, pp. 1169-1173.
59. Lamp, J. 1983. "Transition in Accelerated Fluid Flows". *Trans. Tallinn Polyt. Inst.* 544, pp. 63-67 (in Russian).
60. Lamp, J., Liiv, U. 1983. "An Investigation of Universal Velocity Distribution Law during Unsteady Starting Pipe Flow". *Trans. Tallinn Polyt. Inst.* 544, pp. 69-76 (in Russian).
61. LaVision GmbH. 2005. "DaVis 7.1 - Perspective Calibration Wizard Manual for DaVis 7.1". *LaVision GmbH, Göttingen.* pp. 5-18.
62. Lefebvre, P.J., White, F.M. 1989. "Experiments on Transition to Turbulence in a Constant-acceleration Pipe Flow". *ASME, J. Fluids Eng.* 111, pp. 223-227.
63. Lefebvre, P. J., White, F. M. 1991. "Further Experiments on Transition to Turbulence in Constant-acceleration Pipe Flow". *ASME, J. Fluids Eng.* 113, pp. 428-432.
64. Letelier, S. M., Leutheusser, H. J. 1976. "Skin Friction in Unsteady Laminar Pipe Flow". *ASCE J. Hydr. Div.* 102(1), pp. 41-56.
65. Leutheusser, H. J., Lam, K. W. 1977. "Flow Instability in Accelerated Fluid Motion". *Proc. Sixth Can. Congr. App. Mech.* pp. 679-680.
66. Leutheusser, H. J., Lam, K. W. 1977. "Laminar-to-Turbulent Transition in Accelerated Motion". *Proc. 17th Cong. IAHR.* Part A118, pp. 343-350.
67. Lindgren, E. R. 1969. "Propagation Velocity of Turbulent Slugs and Streaks in Transition Pipe Flow". *Phys. Fluids.* 12, pp. 418-425.
68. Maruyama, T., Kuribayashi, T., Mizushina, T. 1976. "The Structure of the Turbulence in Transient Pipe Flows". *J. Chem. Eng. Jap.* 9(6), pp. 431-439.
69. Maruyama, T., Kato, Y., Mizushina, T. 1978. "Transition to Turbulence in Starting Pipe Flows". *J. Chem. Eng. Jap.* 11(5), pp. 346-353.
70. Merkli, P., Thomann, H. 1975. "Transition to Turbulence in Oscillating Pipe Flow". *J. Fluid Mech.* 68, pp. 567-575.
71. Moisy, F. 09.12.2009. "PIVMat". <http://www.fast.u-psud.fr/pivmat/>.
72. Moss, E. A. 1989. "The Identification of Two Distinct Laminar to Turbulent Transition Modes in Pipe Flows Accelerated from Rest". *Experiments in Fluids.* 7, pp. 271-274.
73. Mullin, T., Peixinho, J. 2006. "Recent Observations of the Transition to Turbulence in a Pipe". *Sixth IUTAM Symp. on Laminar-Turbulent Trans.* pp. 45-55.
74. Mullin, T., Peixinho, J. 2006. "Transition to Turbulence in Pipe Flow". *J. of Low Temp. Phys.* 145, pp. 75-88.

75. Nakahata, Y., Knisely, C.W., Nishihara, K., Sasaki, Y., Iguchi, M. 2007. "Critical Reynolds number in constant-acceleration pipe flow". *J. of the Japanese Society for Experimental Mechanics*. 7(2), pp. 142-147 (in Japanese).
76. Nakahata, Y., Knisely, C.W., Nishihara, K., Sasaki, Y., Iguchi, M. 2007. "Propagation of Turbulence in Constant-Acceleration Pipe Flow". *J. of the Japanese Society for Experimental Mechanics*. 7(2), pp. 148-154 (in Japanese).
77. Nakahata, Y., Knisely, C.W., Nishihara, K., Sasaki, Y., Iguchi, M. 2007. "Wavelet Analysis of Transition to Turbulence in Constant-Acceleration Pipe Flow". *J. of the Japanese Society for Experimental Mechanics*. 7(2), pp. 155-161 (in Japanese).
78. Nishihara, K., Knisely, C.W., Nakahata, Y., Iguchi, M. 2008. "Comparison of analytical solutions and measured values of accelerating laminar pipe flow". *J. of the Japanese Society for Experimental Mechanics*. 8(1), pp. 32-37 (in Japanese).
79. Nishihara, K., Knisely, C.W., Nakahata, Y., Wada, I., Iguchi, M. 2009. "Transition to Turbulence in Constant Velocity Pipe Flow after Initial Constant-Acceleration". *J. of JSEM*. 9, pp. 30-35.
80. Ohmi, M., Iguchi, M., Kakehashi, K., Masuda, T. 1982. "Transition to Turbulence and Velocity Distribution in an Oscillating Pipe Flow". *Bulletin of the JSME*. 25 (201), pp. 365-371.
81. Pezzinga, G. 2000. "Evaluation of Unsteady Flow Resistances by Quasi-2D or 1D Models". *J. of Hydr. Engrg., ASCE*. 126(10), pp. 778-785.
82. Reynolds, O. 1883. "An Experimental Investigation of the Circumstances Which Determine Whether the Motion of Water Shall Be Direct or Sinuous, and of the Law of Resistance in Parallel Channels". *Phil. Trans. R. Soc. Lond.* 174, pp. 935-982.
83. Reuter, J., Rempfer, D. 2005. "Analysis of Pipe Flow Transition. Part II. Energy Transfer". *Theoret. Comput. Fluid Dynamics*. 19, pp. 39-64.
84. Rotta, J. 1956. "An Experimental Contribution to the Transition from Laminar to Turbulent flow in a Pipe". *Proc., Int. Congress of Applied Mechanics*. 3, pp. 350-359.
85. Rubin, Y., Wygnanski, I, J., Haritonidis, J. H. 1979. "Further Observations on Transition in a Pipe". *In Laminar-turbulent Transition. Proc. IUTAM Symp.* pp. 17-26.
86. Ruubel, R. 1991. "The Characteristics of Turbulence in Accelerating Flow of Fluid in Pipe". *PhD Thesis*, St. Petersburg State Polytechnical University, 167 pp. (in Russian).

87. Sato, H. 1980. "A Life History of Turbulence". *Third International Symposium on Stochastic Hydraulics, August 5 – 7, Tokyo, Japan.* pp. GL-1-1-GL-1-9.
88. Schneider, T. M., Eckhardt, B., Yorke, J. A. 2007. "Turbulence Transition and the Edge of Chaos in Pipe Flow". *Phys. Rev. Lett.* 99(3), pp. 034502-1-034502-4.
89. Shuy, E.B. 1995. "Approximate Wall Shear Equation for Unsteady Laminar Pipe Flows". *J. Hydr. Res.* 33(4), pp. 457-469.
90. Shuy, E.B. 1996. "Wall Shear Stress in Accelerating and Decelerating Turbulent Pipe Flows". *J. Hydr. Res.* 34(2), pp. 173-183.
91. Swinney, H. L., Gollub, J. P. 1978. "The Transition to Turbulence". *Physics today.* 31(8), pp. 41-49.
92. Tavoularis, S. 2005. "Measurement in Fluid Mechanics". *Cambridge University Press.* pp. 279.
93. Taylor, G. I. 1923. "Experiments on the Motion of Solid Bodies in Rotating Fluids". *Proc. R. Soc. Lond. A.* 104, pp. 213-218.
94. Tritton, D. J. 1977. "Physical Fluid Dynamics". *Van Nostrand Company Ltd, England.* pp. 233.
95. Vardy, A., Bergant, A., He, S., Ariyaratne, C., Koppel, T., Annus, I., Tijsseling, A., and Hou, Q. 2009. "Unsteady Skin Friction Experimentation in a Large Diameter Pipe". *Proceedings of the 3rd IAHR International Meeting of the Workgroup on Cavitation and Dynamic Problems in Hydraulic Machinery and Systems, Brno, Czech Republic, (Eds.) P. Rudolf,* pp. 593 - 602.
96. Vardy, A.E., Brown, J.M.B. 1995. "Transient, Turbulent, Smooth Pipe Friction". *J. Hydr. Res.* 33(4), pp. 435-456.
97. Vardy, A., Brown, J. 2003. "Transient Turbulent Friction in Smooth Pipe Flows". *J. Sound Vibr.* 259(5), pp. 1011-1036.
98. Vardy, A.E., Hwang, K.L. 1991. "A Characteristic Model of Transient Friction in Pipes". *J. Hydr. Res.* 29(5), pp. 669-685.
99. Viola, J.P., Letelier, S. M., Leutheusser, H. J. 1984. "Characteristics of Unsteady Turbulent Pipe Flow". *Forum of Unsteady Flow. Annu. Meet. ASME. New-York.* pp. 21-22.
100. Viola, J. P., Leutheusser, H. J. 2004. "Experiments on Unsteady Turbulent Pipe Flow". *J. Eng. Mech.* 130(2), pp. 240-244.
101. Viswanath, D., Cvitanović, P. 2009. "Stable Manifolds and the Transition to Turbulence in Pipe Flow". *J. Fluid Mech.* 627, pp. 215-233.
102. Wedin, H., Kerswell, R. R. 2004. "Exact Coherent Structures in Pipe Flow: Travelling Wave Solutions". *J. Fluid Mech.* 508, pp. 333-371.

103. Willis, A. P., Kerswell, R. R. 2009. "Turbulent Dynamics of Pipe Flow Captured in a Reduced Model: Puff Relaminarisation and Localised "Edge" States". *J. Fluid Mech.* 619, pp. 213-233.
104. Wygnanski, I. J., Champagne, F. H. 1973, "On Transition in a Pipe. Part 1. The Origin of Puffs and Slugs and the Flow in a Turbulent Slug". *J. Fluid Mech.* 59(2), pp. 281-335.
105. Wygnanski, I. J., Sokolov, M., Friedman, D. 1975, "On Transition in a Pipe. Part 2. The Equilibrium Puff". *J. Fluid Mech.* 69(2), pp. 283-304.
106. Zhao, M., Ghidaoui, M. S., Kolyshkin, A. A. 2007. "Perturbation Dynamics in Unsteady Pipe Flows". *J. Fluid Mech.* 570, pp. 129-154.
107. Zielke, W. 1968. "Frequency Dependent Friction in Transient Pipe Flow". *ASME J. Basic Eng.* 90(1), pp.109-115.

ABSTRACT

This thesis studies some aspects of flow development and transition to turbulence in start-up accelerating flows in large diameter pipes. Earlier experimental studies have been carried out mainly in small diameter pipe systems. The thesis focuses on the hypotheses brought forth in those studies and analyzes them in the light of new experimental findings.

The thesis gives an historical overview of experimental and theoretical investigations that deal with transition to turbulence in pipes. The main emphasis is placed on flow development and transitional processes in accelerating pipe flows. The novelty of this thesis lies in the new experimental data that is used to analyze the hypotheses brought forth in earlier investigations and to describe new findings in accelerating pipe flow starting from rest.

In this thesis a thorough overview of the test rig, specification of instrumentation and test procedure is given. The calibration processes of hot-films and PIV system have been described exhaustively.

A 1D mathematical model brought forth in the thesis is deduced to describe the development of velocity profiles in constantly accelerating start-up pipe flow. Model results are compared with experimental data in two cases – acceleration rate is fixed to a constant value and acceleration rate is changing in time. It is found that in laminar flow (before the transition to turbulence) the model results with $A \neq \text{const}$ correlate well with the experimental findings in the near wall region and in the core, but with $A = \text{const}$ the 1D model is overestimating the velocities in the core. The 2D model on the contrary underestimates the velocities in the laminar region compared to experimental results. Modeling of the radial velocity component confirmed that in the laminar phase it is practically zero.

It is shown in the thesis that transition to turbulence in accelerating pipe flow is dependent on the pipe diameter. In pipes with a large diameter transition to turbulence does not take place simultaneously over the pipe length. Transition to turbulence is accompanied with the rise of the radial velocity component. Its periodic change gives an indication of wavy structures developing in the flow. The criterion characterizing transition to turbulence and describing the dependence between dimensionless acceleration and dimensionless transition time is specified taking into account all the data available.

KOKKUVÕTE

Käesolevas doktoritöös uuritakse suure läbimõõduga torudes voolu arengut ja turbulentsile voolule üleminekuprotsessi mõningaid aspekte paigalseisust algavas kiirenevas voolus. Varasemad eksperimentaalsed tööd on läbi viidud peamiselt väikese läbimõõduga torudes. Doktoritöö keskendub eelnimetatud uurimustes välja toodud hüpoteesidele ning analüüsib neid uute katseandmete valguses.

Doktoritöö annab ajaloolise ülevaate eksperimetaalsetest ja teoreetilistest tööd, mis on seotud turbulentsile ülemineku torudes. Peamine rõhk on pandud voolu arengule ja üleminekuprotsessidele kiirenevas voolus. Töö uudsus väljendub uutes katseandmetes, mille abil on analüüsitud varasemates uuringutes välja toodud hüpoteese ning kirjeldatud uusi nüansse turbulentsile ülemineku protsessis.

Töös on ära toodud põhjalik katseseadme kirjeldus koos mõõteriistade spetsifikatsioonide ning katseprotseduuridega. Pikemalt on kirjeldatud termomanomeetrite ja PIV tehnika kalibreerimisprotsesse.

Doktoritöös ära toodud ühemõõtmeline matemaatiline mudel on tuletatud kirjeldamaks kiirusprofiili muutust paigalseisust konstantselt kiirenevas voolus. Mudeli tulemusi on kõrvutatud katseandmetega kahel juhul – kui kiirendus on konstantne ning kui kiirendus ajas muutub. Töös on leitud, et laminaarses voolurežiimis (enne üleminekut turbulentsile voolule) kirjeldab mudel (kui $A \neq$ konstantne) hästi kiiruse kasvu nii seinäärse piirkonnas kui ka tuumas, kuid ülehindab mõõdetud kiirust kui $A =$ konstant. Kahemõõtmeline mudel vastupidiselt alahindab laminaarses režiimis katseandmetest saadud kiirusi. Toru radiaalsuunalise kiiruskomponendi mudelarvutus kinnitas, et laminaarses faasis see puudub.

Töös on näidatud, et üleminek turbulentsile kiirenevas voolus on sõltuv toru diameetrist. Suurte torude puhul ei toimu üleminek samaaegselt kogu toru pikkusel. Turbulentsile üleminekuuga kaasneb radiaalkiiruskomponendi kasv, mille perioodiline muutus annab aimu laineliste struktuuride tekkest voolus. Kõigi olemasolevate katseandmete põhjal on täpsustatud ülemineku protsessi iseloomustavat kriteeriumit, mis seob dimensioonitu kiirenduse dimensioonitu turbulentsile ülemineku ajaga.

CURRICULUM VITAE

1. Personal data

Name: Ivar Annus

Date and place of birth: 04.02.1983, Tallinn, Estonia

Nationality: Estonian

2. Contact information

Address: Ehitajate tee 147-27, Tallinn, Estonia

Phone: +3725298810

E-mail: ivar.annus@gmail.com

3. Education

Educational institution	Graduation year	Education (field of study/degree)
Tallinn University of Technology	2007	Product Development/MSc
Tallinn University of Technology	2005	Product Development/BSc
Tallinn Väike-Õismäe High School	2001	Secondary/gold medal

4. Language competence/skills (fluent; average, basic skills)

Language	Level
Estonian	Native language
English	Fluent
Finnish	Average
Russian	Basic skills

5. Professional Employment

Period	Organisation	Position
2006-...	Tallinn University of Technology	Assistant
2005-2006	AS Infodepot	Project manager

6. Scientific work

Laanearu, J., Annus, I., Raidmaa, M., Koppel, T. 2011. "Transient Flow during Filling of Horizontal Pipe Containing Water." *In: Proceedings of 11th International Conference on Computing and Control for the Water Industry 2011, CCWI2011, Exeter, UK, 5-7 September 2011. (Eds.) Dragan Savič, Zoran Kapelan, David Butler.* pp. 913-918.

Annus, I., Koppel, T. 2011. "Transition to Turbulence in Accelerating Pipe Flow." *ASME, J. Fluids Eng.* 133(7), pp. 071202-1-071202-9. [DOI: 10.1115/1.4004365]

Laanearu, J., Annus, I., Koppel, T., Bergant, A., Vučkovič, S., Hou, Q., Tijsseling, A. S., Anderson, A., van't Westende, J. M. C. 2011. "Emptying of Large-Scale Pipeline by Pressurized Air." *ASCE, J. Hydr. Eng. Submitted.*

Annus, I., Koppel, T., Vardy, A. 2010. "Transition to Turbulence in Acceleration Flow." *Proceedings of the Hydralab III joint transnational access user meeting, Hannover, 2-4 February 2010. (Eds.) Joachim Grüne, Mark Klein Breteler.* pp. 9 – 12.

Laanearu, J., Annus, I., Vassiljev, A., Koppel, T. 2009. "On Determination of Flow Routes in a Stormwater Network Using the Least Squares Method." *In: Integrating Water Systems: Computing and Control in the Water Industry 2009, CCWI2009, Sheffield, UK, 1-3 September 2009. (Eds.) Joby Boxall, Cedo Maksimovic.* Leiden: Taylor & Francis, 2009, pp. 731 - 734.

Laanearu, J., Bergant, A., Annus, I., Koppel, T., Van't Westende, J. 2009. "Some Aspects of Fluid Elasticity Related to Filling and Emptying of Large-Scale Pipeline." *In: Proceedings of the 3rd IAHR International Meeting of the Workgroup on Cavitation and Dynamic Problems in Hydraulic Machinery and Systems: 3rd IAHR International Meeting of the Workgroup on Cavitation and Dynamic Problems in Hydraulic Machinery and Systems in Brno, Czech Republic, 14.-16.10.2009. (Eds.) P. Rudolf.* Brno, Czech Republic: Brno Technical University, 2009, pp. 465 - 474.

Vardy, A., Bergant, A., He, S., Ariyaratne, C., Koppel, T., Annus, I., Tijsseling, A., Hou, Q. 2009. "Unsteady Skin Friction Experimentation in a Large Diameter Pipe." *In: Proceedings of the 3rd IAHR International Meeting of the Workgroup on Cavitation and Dynamic Problems in Hydraulic Machinery and Systems: 3rd IAHR International Meeting of the Workgroup on Cavitation and Dynamic Problems in Hydraulic Machinery and Systems in Brno, Czech Republic, 14-16.10.2009. (Eds.) P. Rudolf.* Brno, Czech Republic: Brno Technical University, 2009, pp. 593 - 602.

Laanearu, J., Annus, I., Koppel, T. 2009. "On Long-Wave Dependent Flow Transitions in Partially Filled Large-Scale Pipeline." *In: Water Engineering for a Sustainable Environment: 33RD IAHR Congress, Vancouver, British Columbia, Canada, 9-14 August, 2009.* Madrid: International Association of Hydraulic Engineering and Research (IAHR), 2009, pp. 6553 - 6560.

Koppel, T., Vassiljev, A., Lukjanov, D., Annus, I. 2008. "Use of Pressure Dynamics for Calibration of Water Distribution System and Leakage Detection." *In: Proceedings of WDSA 2008: Water Distribution Systems Analysis, 17-20 August 2008, Kruger National Park, South Africa. (Eds.) van Zyl, J.E.; Illembada, A.A, Jacobs, H.E.* South Africa: University of Johannesburg, 2008, pp. 704 - 715.

7. Defended theses

Water hammer analysis in pressure pipes of Narva town, Master's degree

Modifying the frame of Bestnet Ltd's trailer 1336 2T, Bachelor's degree

8. Honours and awards

DoRa scholarship for young researchers to participate in international conferences, 2011

DoRa scholarship for young researchers to participate in international conferences, 2009

AS Tallinna Vesi doctoral studies scholarship of TUT development foundation, 2009

Scholarship of Jaan Poska, 2008

9. Main areas of scientific work/Current research topics

Transitional Accelerating Pipe Flow

Dynamics of Liquid Flow in Pressure Pipes

Mechanics of Fluid-Structure Interaction

10. Other research projects

Two-phase Flow in Pipes

ELULOOKIRJELDUS

1. Isikuandmed

Ees- ja perekonnanimi: Ivar Annus
Sünniaeg ja -koht: 04.02.1983, Tallinn, Eesti
Kodakondsus: Eestlane

2. Kontaktandmed

Aadress: Ehitajate tee 147-27, Tallinn, Eesti
Telefon: 5298810
E-posti aadress: ivar.annus@gmail.com

3. Hariduskäik

Õppeasutus (nimetus lõpetamise ajal)	Lõpetamise aeg	Haridus (eriala/kraad)
Tallinna Tehnikaülikool	2007	Tootearendus/ Tehnikateaduste magister
Tallinna Tehnikaülikool	2005	Tootearendus/ Tehnikateaduste bakalaureus
Tallinna Väike-Õismäe Keskool	2001	Keskharidus/ kuldmedal

4. Keelteoskus (alg-, kesk- või kõrgtase)

Keel	Tase
Eesti	Emakeel
Inglise	Kõrgtase
Soome	Keskstase
Vene	Algtase

5. Teenistuskäik

Töötamise aeg	Tööandja nimetus	Ametikoht
2006-...	Tallinna Tehnikaülikool	Assistent
2005-2006	AS Infodepot	Projektijuht

6. Teadustegevus

Avaldatud artiklid ja konverentsi ettekanded on ära toodud inglise keelses elulookirjelduses.

7. Kaitstud lõputööd

Hüdraulilise löögi analüüs Narva linna survetorudes, magistritöö

AS Bestnet treileri 1336 2T raami modifitseerimine, bakalaureusetöö

8. Teaduspreemiad- ja tunnustused

DoRa stipendium Noorteadlaste osalemine rahvusvahelises teadmisteringluses, 2011

DoRa stipendium Noorteadlaste osalemine rahvusvahelises teadmisteringluses, 2009

TTÜ Arengufondi AS Tallinna Vesi doktoriõppe stipendium, 2009

Jaan Poska nimeline stipendium, 2008

9. Teadustöö põhisuunad

Üleminekuprotsessid torus kiirenevas voolus

Vedeliku voolamise dünaamika survetorudes

Vedeliku ja konstruktsiooni koostoime mehaanika

10. Teised uurimisprojektid

Kahefaasiline voolamine torudes

APPENDIX A

Table A. 1 – Experimental results, A1 test series

Test no	t_v , s	Re_f	A , m/s^2	Hot-film 2		Hot-film 5	
				$\tau_* \times 10^3$	Re_*	$\tau_* \times 10^3$	Re_*
A1005	2	1080000	2.53	0.0592	294436.6	0.1080	620704.3
A1012	2	695000	1.82	0.0592	237498.7	0.1127	428052.8
A1051	2	500000	1.69	0.0498	231946.7	0.1089	388757.5
A1017	2	495000	1.53	0.0601	247553.8	0.1221	400416.6
A1023	2	337000	0.95	0.0845	169950.3	0.1577	299803.5
A1028	2	215000	0.87	0.1099	197586.5	0.1906	218683.8
A1035	2	160000	0.66	0.1239	147619.3	0.2338	161437.4
A1038	2	113000	0.53	0.1577	112395.5	0.3126	113135.7
A1042	2	68000	0.57	0.2582	68165.2	0.5061	68720.39
A1045	2	29000	0.55	0.7042	32016.1		
A1080	4	500000	0.83	0.1343	211219.6	0.1972	332559.8
A1008	5	1080000	1.09	0.0930	173960.1	0.1671	337063
A1014	5	695000	0.80	0.1221	206901.4	0.1887	318309.9
A1055	5	500000	0.64	0.0807	156193.9	0.1615	253969.3
A1020	5	495000	0.61	0.1258	164953.6	0.2038	288267.8
A1026	5	337000	0.55	0.1324	180067.2	0.2113	261495.3
A1031	5	215000	0.49	0.1634	150642	0.2563	211404.6
A1084	6	500000	0.54	0.1493	178278.2	0.2216	270748.5
A1065	7.5	500000	0.52	0.1512	175749	0.2178	205852.7

Table A. 2 – Experimental results, A1A test series

Test no	t_v , s	Re_f	A , m/s^2	Hot-film 2		Hot-film 5	
				$\tau_* \times 10^3$	Re_*	$\tau_* \times 10^3$	Re_*
A1A022	2	400 000	0.34	0.2178	161807.5	0.2761	204927.4
A1A031	2	400 000	0.34	0.2216	160142	0.2770	202274.8
A1A052	2	400 000	0.35	0.2160	158291.3	0.2770	205050.8
A1A007	2	200 000	0.30	0.2573	166989.3	0.2995	182843.1
A1A005	2	100 000	0.24	0.4131	102155.3	0.3530	101785.1
A1A003	2	50 000	0.27				
A1A016	5	400 000	0.28	0.2864	169580.2	0.3145	181732.7
A1A014	5	200 000	0.19	0.4131	173713.3	0.3944	166495.8
A1A011	5	100 000	0.10				
A1A009	5	50 000	0.05				
A1A026	7	400 000	0.21	0.4037	183768.4	0.3568	165015.3
A1A024	7	200 000	0.14	0.5915	185249	0.4929	149901.7

A1A021	7	100 000	0.07			0.6620	101600.1
A1A019	7	50 000	0.03				
A1A037	10	400 000	0.16	0.5399	184755.4	0.4507	150025.1
A1A035	10	200 000	0.10	0.8591	192713.2	0.5962	126953.8
A1A030	10	100 000	0.05			0.9108	102648.8
A1A028	10	50 000	0.02				
A1A051	15	400 000	0.11	0.6573	147064.1	0.5775	127940.8
A1A049	15	200 000	0.06	1.0835	160388.7	0.8253	118564.3
A1A047	15	100 000	0.03	0.2178		1.2582	100921.5
A1A043	15	50 000	0.02	0.2216		0.2761	

Table A. 3 – Experimental results, B test series

Test no	Δp , bar	Re_f	A , m/s^2	Hot-film 2		Hot-film 5	
				$\tau^* \times 10^3$	Re^*	$\tau^* \times 10^3$	Re^*
B1053	0.05	209122.2	0.43	0.2376	185063.9	0.2319	182473
B1054	0.1	226641.6	0.46	0.2253	200300.8	0.2103	195180.7
B1055	0.15	240583.1	0.62	0.1962	209214.7	0.1953	209060.5
B1056	0.2	255079.7	0.62	0.1718	204989.1	0.1878	218005.3
B1057	0.25	272043.9	0.71	0.1512	209060.5	0.1718	228035.7
B1061	0.3	297644.4	0.84	0.1343	229621.1	0.1559	244654.5
B1060	0.35	298569.7	0.89	0.1408	237128.5	0.1577	251193.4
B1062	0.4	309982	0.91	0.1286	241804.5	0.1502	255326.5
B1064	0.45	314917	1.07	0.1108	224914.3	0.1484	263777.7
B1067	0.5	327563.1	1.05	0.1070	227856.8	0.1418	275806.9
B1068	0.55	342491.6	1.08	0.0995	226055.5	0.1361	282160.7
B1069	0.6	355322.7	1.00	0.0939	233242.2	0.1324	297150.9
B1070	0.65	362972	1.13	0.0911	239596	0.1277	303689.8
B1071	0.7	375494.6	1.11	0.0779	208690.4	0.1230	300642.5
B1072	0.75	385303	1.23	0.0732	216987.4	0.1221	320900.8
B1073	0.8	395358.2	1.31	0.0742	239349.3	0.1183	326088.7
B1074	0.85	400848.4	1.34	0.0751	246246	0.1155	332973.1
B1075	0.9	414296.4	1.37	0.0704	242045.1	0.1127	328031.9
B1076	0.95	423179.4	1.42	0.0695	248109	0.1099	335866.3
B1077	1	432802.7	1.36	0.0667	244777.8	0.1070	334472.1
B1078	1.05	438909.9	1.53	0.0667	267664.1	0.1070	355951.9
B1079	1.1	446497.5	1.66	0.0685	274912.4	0.1042	355353.5
B1080	1.15	458588.3	1.52	0.0657	255708.9	0.0995	340492.9
B1081	1.2	463831.8	1.63	0.0648	279742.6	0.0995	358573.6
B1082	1.25	474688.9	2.06	0.0638	299902.2	0.0967	375297.2
B1083	1.3	486409.6	1.73	0.0629	288156.8	0.0967	372533.6
B1084	1.35	497513.4	1.86	0.0638	311795.6	0.0939	381503
B1085	1.4	507075.1	2.31	0.0629	319093.3	0.0930	392489.7

B1086	1.45	511393.2	1.93	0.0554	268589.4	0.0911	387122.8
B1087	1.5	518795.8	1.87	0.0545	263969	0.0901	384895.9
B1175	1.5	505841.3	2.11	0.0610	310734.6	0.0911	402143.8
B1176	1.6	537610.6	2.14	0.0610	302227.8	0.0911	399152
B1177	1.7	551490.4	2.45	0.0601	333750.4	0.0892	415005.8
B1178	1.8	562285.8	2.52	0.0601	341695.8	0.0864	426572.3
B1179	1.9	569379.9	2.66	0.0582	344280.5	0.0836	428028.1
B1180	2	592512.9	2.77	0.0535	341689.6	0.0817	449396.8
B1181	2.1	596522.6	2.92	0.0507	299371.7	0.0789	449705.2
B1182	2.2	614412.1	2.90	0.0516	317538.8	0.0779	457188
B1183	2.3	615954.3	3.03	0.0507	307878.5	0.0761	472647
B1184	2.4	O_of_R	3.09	0.0488	310278.1	0.0742	473208.4
B1185	2.5	O_of_R	3.36	0.0479	357358.4	0.0742	O_of_R
B1186	2.6	O_of_R	3.21	0.0469	304183.3	0.0723	O_of_R
B1187	2.7	O_of_R	3.38	0.0460	338666.9	0.0714	O_of_R
B1188	2.8	O_of_R	3.20	0.0451	254789.8	0.0704	O_of_R
B1189	2.9	O_of_R	3.56	0.0432	312887.5	0.0685	O_of_R
B1190	3	O_of_R	3.90	0.0423	345082.5	0.0685	O_of_R
B1191	3.1	O_of_R	3.78	0.0413	322844	0.0667	O_of_R
B1192	3.2	O_of_R	3.91	0.0423	363928.1	0.0667	O_of_R
B1193	3.3	O_of_R	4.22	0.0413	204773.2	0.0667	O_of_R
B1194	3.4	O_of_R	3.73	0.0394	246135	0.0657	O_of_R
B1195	3.5	O_of_R	3.77	0.0394	259397.9	0.0657	O_of_R
B1196	3.6	O_of_R	4.20	0.0366	313806.7	0.0620	O_of_R
B1197	3.7	O_of_R	3.83	0.0394	258102.4	0.0648	O_of_R
B1198	3.8	O_of_R	4.04	0.0385	267849.1	0.0648	O_of_R
B1199	3.9	O_of_R	3.93	0.0366	281852.3	0.0601	O_of_R
B1200	4	O_of_R	4.46	0.0366	352361.6	0.0563	O_of_R
B1201	4.1	O_of_R	3.75	0.0366	262975.8	0.0554	O_of_R
B1202	4.2	O_of_R	4.01	0.0357	316952.8	0.0526	O_of_R

Blank spaces in the tables indicate that a certain hot-film did not react to turbulence in the given case in the recording timeframe. O_of_R stands for the flow meter being out of the measuring range.

Table A. 4 – Sequence in reaction to turbulence, A1 test series

Test no	t_v , s	Re_f	A , m/s^2	Sequence in reaction to turbulence					
				HF1	HF2	HF3	HF4	HF5	HF6
A1005	2	1080000	2.53	2	1	3	5	4	6
A1012	2	695000	1.82	2	1	3	5	4	6
A1051	2	500000	1.69		1	2	4	3	5
A1017	2	495000	1.53	2	1	3	5	4	6

A1023	2	337000	0.95	2	1	3	5	4	6
A1028	2	215000	0.87	2	1	3	5	4	6
A1035	2	160000	0.66	6	1	2	4	3	5
A1038	2	113000	0.53	6	1	5	4	2	3
A1042	2	68000	0.57	6	1	5	4	2	3
A1045	2	29000	0.55		1				
A1080	4	500000	0.83		2	1	4	3	5
A1008	5	1080000	1.09	2	1	3	5	4	6
A1014	5	695000	0.80	3	1	2	5	4	6
A1055	5	500000	0.64		1	2	3	3	5
A1020	5	495000	0.61	3	1	2	5	4	5
A1026	5	337000	0.55	3	1	2	6	4	5
A1031	5	215000	0.49	6	1	2	5	3	4
A1084	6	500000	0.54		1	2	4	3	5
A1065	7.5	500000	0.52		1	1	4	3	5

Table A. 5 – Sequence in reaction to turbulence, A1A test series

Test no	t_v , s	Re_f	A_s , m/s ²	Sequence in reaction to turbulence				
				HF2	HF3	HF4	HF5	HF6
A1A022	2	400 000	0.34	2	1	5	3	4
A1A031	2	400 000	0.34	2	1	5	3	4
A1A052	2	400 000	0.35	2	1	5	3	4
A1A007	2	200 000	0.30	2	1	5	3	4
A1A005	2	100 000	0.24	3	1	5	2	3
A1A003	2	50 000	0.27		1			
A1A016	5	400 000	0.28	2	1	5	3	4
A1A014	5	200 000	0.19	4	1	5	2	3
A1A011	5	100 000	0.10		1			
A1A009	5	50 000	0.05		1			
A1A026	7	400 000	0.21	4	1	5	2	3
A1A024	7	200 000	0.14	4	1	4	3	2
A1A021	7	100 000	0.07		1	4	2	2
A1A019	7	50 000	0.03		1			
A1A037	10	400 000	0.16	4	1	5	2	3
A1A035	10	200 000	0.10	5	1	4	2	3
A1A030	10	100 000	0.05		1		3	2
A1A028	10	50 000	0.02		1			2
A1A051	15	400 000	0.11	4	1	5	2	3
A1A049	15	200 000	0.06	5	1	4	3	2
A1A047	15	100 000	0.03		1	4	3	2
A1A043	15	50 000	0.02		1			

Table A. 6 – Sequence in reaction to turbulence, B test series

Test no	Δp , bar	Re_f	A , m/s^2	Sequence in reaction to turbulence			
				HF2	HF3	HF4	HF5
B1053	0.05	209122.2	0.43	4	1	2	2
B1054	0.1	226641.6	0.46	4	1	2	3
B1055	0.15	240583.1	0.62	4	1	2	3
B1056	0.2	255079.7	0.62	2	1	3	4
B1057	0.25	272043.9	0.71	2	1	4	3
B1061	0.3	297644.4	0.84	2	1	4	3
B1060	0.35	298569.7	0.89	2	1	4	3
B1062	0.4	309982	0.91	2	1	4	3
B1064	0.45	314917	1.07	2	1	4	3
B1067	0.5	327563.1	1.05	2	1	4	3
B1068	0.55	342491.6	1.08	2	1	4	3
B1069	0.6	355322.7	1.00	2	1	4	3
B1070	0.65	362972	1.13	2	1	3	3
B1071	0.7	375494.6	1.11	2	1	4	3
B1072	0.75	385303	1.23	2	1	3	4
B1073	0.8	395358.2	1.31	2	1	4	3
B1074	0.85	400848.4	1.34	2	1	4	3
B1075	0.9	414296.4	1.37	2	1	3	3
B1076	0.95	423179.4	1.42	2	1	4	3
B1077	1	432802.7	1.36	2	1	4	3
B1078	1.05	438909.9	1.53	2	1	3	3
B1079	1.1	446497.5	1.66	2	1	4	3
B1080	1.15	458588.3	1.52	2	1	4	3
B1081	1.2	463831.8	1.63	2	1	4	3
B1082	1.25	474688.9	2.06	2	1	4	3
B1083	1.3	486409.6	1.73	2	1	4	3
B1084	1.35	497513.4	1.86	2	1	4	3
B1085	1.4	507075.1	2.31	2	1	4	3
B1086	1.45	511393.2	1.93	2	1	4	3
B1087	1.5	518795.8	1.87	2	1	4	3
B1175	1.5	505841.3	2.11	2	1	4	3
B1176	1.6	537610.6	2.14	2	1	4	3
B1177	1.7	551490.4	2.45	2	1	4	3
B1178	1.8	562285.8	2.52	2	1	4	3
B1179	1.9	569379.9	2.66	3	1	2	4
B1180	2	592512.9	2.77	3	1	2	4
B1181	2.1	596522.6	2.92	3	1	2	4
B1182	2.2	614412.1	2.90	3	1	2	4
B1183	2.3	615954.3	3.03	3	1	2	4

B1184	2.4	O of R	3.09	3	1	2	4
B1185	2.5	O of R	3.36	3	1	2	4
B1186	2.6	O of R	3.21	3	1	1	4
B1187	2.7	O of R	3.38	3	1	2	4
B1188	2.8	O of R	3.20	3	1	2	4
B1189	2.9	O of R	3.56	3	1	2	4
B1190	3	O of R	3.90	3	1	2	4
B1191	3.1	O of R	3.78	3	1	2	4
B1192	3.2	O of R	3.91	3	1	2	4
B1193	3.3	O of R	4.22	3	1	2	4
B1194	3.4	O of R	3.73	3	1	2	4
B1195	3.5	O of R	3.77	3	1	2	4
B1196	3.6	O of R	4.20	3	1	2	4
B1197	3.7	O of R	3.83	3	1	2	4
B1198	3.8	O of R	4.04	3	1	2	4
B1199	3.9	O of R	3.93	3	1	2	4
B1200	4	O of R	4.46	3	1	2	4
B1201	4.1	O of R	3.75	3	1	2	4
B1202	4.2	O of R	4.01	3	1	1	4

**DISSERTATIONS DEFENDED AT
TALLINN UNIVERSITY OF TECHNOLOGY ON
CIVIL ENGINEERING**

1. **Heino Mölder**. Cycle of Investigations to Improve the Efficiency and Reliability of Activated Sludge Process in Sewage Treatment Plants. 1992.
2. **Stellian Grabko**. Structure and Properties of Oil-Shale Portland Cement Concrete. 1993.
3. **Kent Arvidsson**. Analysis of Interacting Systems of Shear Walls, Coupled Shear Walls and Frames in Multi-Storey Buildings. 1996.
4. **Andrus Aavik**. Methodical Basis for the Evaluation of Pavement Structural Strength in Estonian Pavement Management System (EPMS). 2003.
5. **Priit Vilba**. Unstiffened Welded Thin-Walled Metal Girder under Uniform Loading. 2003.
6. **Irene Lill**. Evaluation of Labour Management Strategies in Construction. 2004.
7. **Juhan Idnurm**. Discrete Analysis of Cable-Supported Bridges. 2004.
8. **Arvo Iital**. Monitoring of Surface Water Quality in Small Agricultural Watersheds. Methodology and Optimization of monitoring Network. 2005.
9. **Liis Sipelgas**. Application of Satellite Data for Monitoring the Marine Environment. 2006.
10. **Ott Koppel**. Infrastruktuuri arvestus vertikaalselt integreeritud raudtee-ettevõtja korral: hinnakujunduse aspekt (Eesti peamise raudtee-ettevõtja näitel). 2006.
11. **Targo Kalamees**. Hygrothermal Criteria for Design and Simulation of Buildings. 2006.
12. **Raido Puust**. Probabilistic Leak Detection in Pipe Networks Using the SCEM-UA Algorithm. 2007.
13. **Sergei Zub**. Combined Treatment of Sulfate-Rich Molasses Wastewater from Yeast Industry. Technology Optimization. 2007.
14. **Alvina Reihan**. Analysis of Long-Term River Runoff Trends and Climate Change Impact on Water Resources in Estonia. 2008.
15. **Ain Valdmann**. On the Coastal Zone Management of the City of Tallinn under Natural and Anthropogenic Pressure. 2008.

16. **Ira Didenkulova**. Long Wave Dynamics in the Coastal Zone. 2008.
17. **Alvar Toode**. DHW Consumption, Consumption Profiles and Their Influence on Dimensioning of a District Heating Network. 2008.
18. **Annely Kuu**. Biological Diversity of Agricultural Soils in Estonia. 2008.
19. **Andres Tolli**. Hiina konteinerveod läbi Eesti Venemaale ja Hiinasse tagasisaadetavate tühjade konteinerite arvu vähendamise võimalused. 2008.
20. **Heiki Onton**. Investigation of the Causes of Deterioration of Old Reinforced Concrete Constructions and Possibilities of Their Restoration. 2008.
21. **Harri Moora**. Life Cycle Assessment as a Decision Support Tool for System optimisation – the Case of Waste Management in Estonia. 2009.
22. **Andres Kask**. Lithohydrodynamic Processes in the Tallinn Bay Area. 2009.
23. **Loreta Kelpšaitė**. Changing Properties of Wind Waves and Vessel Wakes on the Eastern Coast of the Baltic Sea. 2009.
24. **Dmitry Kurennoy**. Analysis of the Properties of Fast Ferry Wakes in the Context of Coastal Management. 2009.
25. **Egon Kivi**. Structural Behavior of Cable-Stayed Suspension Bridge Structure. 2009.
26. **Madis Ratassepp**. Wave Scattering at Discontinuities in Plates and Pipes. 2010.
27. **Tiia Pedusaar**. Management of Lake Ülemiste, a Drinking Water Reservoir. 2010.
28. **Karin Pachel**. Water Resources, Sustainable Use and Integrated Management in Estonia. 2010.
29. **Andrus Räämet**. Spatio-Temporal Variability of the Baltic Sea Wave Fields. 2010.
30. **Alar Just**. Structural Fire Design of Timber Frame Assemblies Insulated by Glass Wool and Covered by Gypsum Plasterboards. 2010.
31. **Toomas Liiv**. Experimental Analysis of Boundary Layer Dynamics in Plunging Breaking Wave. 2011.
32. **Martti Kiisa**. Discrete Analysis of Single-Pylon Suspension Bridges. 2011.